

Dissertation

submitted to the
Combined Faculties for the Natural Sciences and for Mathematics
of the Ruperto-Carola University of Heidelberg, Germany
for the degree of
Doctor of Natural Sciences

presented by
Dipl-Biol. Jan-Marek Weislogel
born in: Heidelberg
Oral-examination:.....

Title

Visualisation of nuclear localised calcium signals
using recombinant calcium indicators in
in vivo model systems

Referees:

Prof. Dr. Hilmar Bading

Dr. Jochen Wittbrodt

Danksagung

Ich möchte mich bei Prof. Dr. Hilmar Bading bedanken, dass er mir ermöglicht hat am Institut der Neurobiologie meine Doktorarbeit anzufertigen. Für das Vertrauen, die Unterstützung und die wissenschaftlichen Diskussionen, die Grundlagen meiner Doktorarbeit waren. Mein Dank gilt Dr. Jochem Wittbrodt, der als Zweitgutachter diese Arbeit unterstützt hat.

Obwohl mein Dank der gesamten Arbeitsgruppe von Prof. Dr. Hilmar Bading gilt, die mir immer hilfsbereit und unterstützend zur Seite stand, möchte ich dennoch einige Mitglieder namentlich nennen. Mein besonderer Dank gilt Dr. Anja Eder, Dr. Peter Bengtson, Dr. Bettina Buchthal, Simon Wiegert und Jana Schlüter.

Weiter möchte ich mich bei Prof. Dr. Christoph Schuster, Dr. Andre Fiala (Neurobiologie, Universität Würzburg), Thomas Völler (Neurobiologie, Universität Würzburg), Dr. Peter Bengtson, Dr. Carla Margulies, Mareike Bongers, Jana Schlüter und Dr. Matthias Knirr bedanken ohne deren Unterstützung und Hilfe die Forschung an der Fruchtfliege nicht so erfolgreich verlaufen wäre.

Mein Dank gilt Dr. Peter Bengtson, Desiree Ditzel, Eckehard Freitag für die hervorragende Zusammenarbeit am Projekt der Kernkalziumindikatoren in juvenilen und adulten Ratten.

Ich möchte mich bei Prof. Dr. Thomas Hohstein (Zoologie, Universität Heidelberg), Dr. Yukio Nakamura (Zoologie, Universität Heidelberg), Dr. Sven Poppelreuther (Zeiss Application Center), Dr. Ulrike Engels (Nikon Imaging Center) und ganz besonders bei Jana Schlüter ohne deren Hilfe die Forschung an dem Süßwasserpoly Hydra nicht möglich gewesen wäre.

Ich möchte mich zuletzt sehr herzlich bei meiner Familie bedanken, die mich während der ganzen Zeit immer unterstützt hat. Besonders gilt dies für meinen Brüdern Lars-Robin und Peer-Matti, die mir besonders in der letzten Phase meiner Arbeit sehr geholfen haben den nötigen Abstand zu gewinnen, um wenigstens einen klugen Gedanken zu fassen.

Table of contents

1	Summary	7
2	Zusammenfassung.....	8
3	Introduction	9
3.1	Nuclear Calcium signalling	9
3.1.1	Nuclear calcium signals induce CREB mediated gene expression.....	9
3.1.2	Calcium induced Calcium release.....	10
3.2	Visualisation of Ca ²⁺ signals using recombinant Ca ²⁺ -indicators	12
3.2.1	FRET based Ca ²⁺ -indicator.....	12
3.2.2	Circularly permuted recombinant Ca ²⁺ -indicator.....	14
3.3	Fruit fly: Odour avoidance assay and nuclear Ca ²⁺ -imaging.....	17
3.3.1	Odour avoidance assay.....	17
3.3.2	Memory phases	18
3.3.3	The functional anatomy of the olfactory system	18
3.3.4	The role of mushroom bodies in long-term memory	20
3.3.5	The molecular mechanism of long-term memory.....	21
3.4	Hippocampal neurons.....	22
3.4.1	Organization and role of the hippocampus in long term memory	22
3.4.2	Long-term potentiation (LTP)	23
3.4.3	Molecular mechanism of LTP	24
3.4.4	DNA delivering system based on recombinant adeno-associated virus (rAAV).....	26
3.5	Freshwater polyp: nuclear and cytoplasmic Ca ²⁺ -imaging.....	30
3.5.1	The freshwater polyp <i>H. vulgaris</i>	30
3.5.2	Molecular mechanism involved in head regeneration	31
4	Material and Method.....	33
4.1	Material: media, buffer and antibodies	33
4.1.1	Fruit fly: preparation of larval muscle cells	33
4.1.2	Fruit fly: preparation and <i>in vivo</i> imaging of adult flies	33
4.1.3	Fruit fly: immunohistochemistry (IHC).....	33
4.1.4	Hippocampal neurons: media for dissociated cells.....	34
4.1.5	Hippocampal neurons: media for cultured brain slice	34
4.1.6	Hippocampal neurons: anaesthesia for <i>in vivo</i> injection	34
4.1.7	Hippocampal neurons: media for acute brain slice.....	35
4.1.8	Hippocampal neurons: western blot (WB) and immunohistochemistry (IHC).....	35
4.1.9	Freshwater polyps: hydra medium.....	37
4.2	DNA Plasmids and transgenic flies	37
4.2.1	Following DNA plasmids were obtained.....	37
4.2.2	Following transgenic flies expressing the Ca ²⁺ -indicators were obtained	38
4.3	Cloning of Ca ²⁺ -indicators and Ca ²⁺ /CaM buffer (hippocampal neurons).....	38

4.3.1	Nuclear Ca ²⁺ -indicator: pN1 GCaMP NLS	38
4.3.2	Nuclear localized EYFP: rAAV EYFP-Nuc	39
4.3.3	Nuclear Ca ²⁺ -indicator: rAAV GCaMP NLS	39
4.3.4	Nuclear Ca ²⁺ -indicator: rAAV Inverse Pericam NLS (rAAV IP NLS)	39
4.3.5	Nuclear Ca ²⁺ -indicator: rAAV GCaMP 1.6 NLS	40
4.3.6	Nuclear Ca ²⁺ -indicator: rAAV GCaMP 2.0 NLS	40
4.3.7	Nuclear localized EYFP: rAAV EYFP Cherry Nuc	40
4.3.8	Nuclear localized EYFP: rAAV EYFP-Nuc Cherry	40
4.3.9	Nuclear Ca ²⁺ -indicator: rAAV GCaMP2 NLS Cherry	41
4.3.10	Nuclear Ca ²⁺ /CaM buffer: pM13 NLS VP16 and p2xM13 NLS VP16	41
4.3.11	Nuclear Ca ²⁺ /CaM buffer: rAAV (2x) M13 NLS VP16 myc	41
4.3.12	Nuclear Ca ²⁺ /CaM buffer: rAAV (2x) M13 NLS myc	41
4.4	Cloning of Ca ²⁺ -indicators and Ca ²⁺ /CaM buffer (transgenic flies)	41
4.4.1	Nuclear Ca ²⁺ -indicator: UAS GCaMP NLS	42
4.4.2	Nuclear Ca ²⁺ -indicator: UAS GCaMP2 NLS Cherry	42
4.4.3	Nuclear Ca ²⁺ /CaM buffer: UAS 2xM13 NLS myc	42
4.4.4	Nuclear Ca ²⁺ /CaM buffer positive control: UAS CaMBP4 myc	42
4.4.5	Nuclear Ca ²⁺ /CaM buffer negative control: UAS mM13 NLS myc	43
4.5	Cloning of Ca ²⁺ -indicators (transgenic hydra)	43
4.5.1	Nuclear/ cytoplasmic Ca ²⁺ -indicator: hyGCaMP and hyGCaMP NLS	43
4.5.2	Nuclear Ca ²⁺ -indicator: hyGCaMP NLS mars	44
4.5.3	Cytoplasmic Ca ²⁺ -indicator: hyGCaMP mars	44
4.6	Fruit fly: culture, <i>in vivo</i> imaging and behaviour assay	44
4.6.1	Fruit fly: culture and genetics	44
4.6.2	Fruit fly: immunostaining and live imaging of 3 rd instar larvae	45
4.6.3	Fruit fly: behaviour assay	46
4.6.4	Fruit fly: <i>in vivo</i> imaging	47
4.6.5	Fruit fly: whole mount immunostaining of adult brains	48
4.7	Hippocampal neurons: culture and <i>in vitro</i> , <i>in vivo</i> imaging	49
4.7.1	Hippocampal neurons: culture and stimulation of primary	49
4.7.2	Hippocampal neurons: immunostaining of dissociated cells	49
4.7.3	Hippocampal neurons: western blot analysis of dissociated cells	50
4.7.4	Hippocampal neurons: preparation and infection of cultured brain slice	50
4.7.5	Hippocampal neurons: <i>in vivo</i> injection and slice preparation of juvenile rats	51
4.7.6	Hippocampal neurons: <i>in vivo</i> injection and slice preparation of adult rats	51
4.7.7	Hippocampal neurons: patch-clamp recording and Ca ²⁺ -imaging of young rats	52
4.8	Freshwater polyp: culture, microinjection and <i>in vivo</i> imaging	53
4.8.1	Freshwater polyp: embryo microinjection	54
4.8.2	Freshwater poly: <i>in vivo</i> imaging	54
5	Results	56
5.1	Visualisation of nuclear Ca ²⁺ signals in hippocampal neurons	56

5.2	Blocking nuclear Ca ²⁺ /CaM signalling pathway in hippocampal neurons	58
5.3	Visualisation of Ca ²⁺ signals in 3rd larvae of <i>D. melanogaster</i>	60
5.4	Blocking nuclear Ca ²⁺ /CaM signalling pathway in adult flies	63
5.5	Visualisation of Ca ²⁺ signals in mushroom bodies of adult flies	66
5.6	Visualisation of nuclear Ca ²⁺ signals in organotypic slices.....	70
5.7	Visualisation of nuclear Ca ²⁺ signals using rAAV GCaMP2 NLS Cherry.....	73
5.8	Visualisation of nuclear Ca ²⁺ signals in brain slices	75
5.9	Visualisation of Ca ²⁺ signals in freshwater polyps using hyGCaMP.....	79
5.10	Visualisation of nuclear Ca ²⁺ signals in freshwater polyps using hyGCaMP NLS.....	82
6	Discussion.....	84
6.1	Nuclear Ca ²⁺ -indicator pN1 GCaMP NLS	84
6.2	Nuclear Ca ²⁺ /CaM inhibitor: rAAV 2xM13 NLS myc	85
6.3	Visualisation of nuclear Ca ²⁺ signals in 3 rd instar larvae.....	86
6.4	Blocking nuclear Ca ²⁺ /CaM signalling pathway in adult flies	87
6.5	Visualisation of Ca ²⁺ signals in mushroom bodies of adult flies	87
6.6	Visualisation of nuclear Ca ²⁺ signals in brain slices.....	89
6.7	Visualisation of nuclear Ca ²⁺ signals using rAAV GCaMP2 NLS Cherry.....	90
6.8	Visualisation of nuclear Ca ²⁺ signals in brain slices	92
6.9	Visualisation of Ca ²⁺ signals in freshwater polyps using hyGCaMP.....	92
6.10	Visualisation of nuclear Ca ²⁺ signals in freshwater polyps using hyGCaMP NLS.....	95
7	References	97

1 Summary

The generation of calcium signals following synaptic activity is a fundamental property of neurons that controls many neuronal processes including cell survival, learning and memory. In cultured neurons, increases in nuclear calcium concentrations are known to be critical for the activation of gene expression mediated by the transcription factor CREB. CREB has been implicated in transcription-dependent plasticity (late phase LTP). It is still unclear whether nuclear calcium signals are also responsible for CREB mediated gene transcription *in vivo*.

The goal of the study was to visualise nuclear calcium signals *in vivo*. Investigating the importance of nuclear Ca^{2+} signalling in the intact brain is impeded by the restrictions and complexities of *in vivo* experimentation. However, *D. melanogaster* provides an excellent system to explore the role nuclear Ca^{2+} in an intact behaving animal. Since Ca^{2+} signalling of the nucleus is of particular interest transgenic flies expressing the nuclear localised Ca^{2+} indicator UAS GCaMP NLS to visualise nuclear Ca^{2+} signals and the nuclear Ca^{2+} /CaM inhibitor UAS 2xM13 myc to interfere with nuclear Ca^{2+} signalling were generated. Using these flies, it could be shown that nuclear Ca^{2+} signalling could play a role in LTM.

Further, using rAAV-mediated gene transfer the nuclear Ca^{2+} indicator rAAV GCaMP 2.0 NLS was expressed in CA1 pyramidal neurons of juvenile rats two weeks after *in vivo* injection. In acute slices from these juvenile rats an increase in nuclear Ca^{2+} concentration was visualised evoked by LTP inducing electrical stimulation. Using this method a correlation between LTP and increase in nuclear Ca^{2+} concentration could be shown. It is still unclear whether nuclear Ca^{2+} signals are necessary to induce LTP in acute slice.

The major challenge of Ca^{2+} imaging *in vivo* either in flies or in rodents based on difficulties to detect signals through the intransparent skulls. The freshwater polyp *H. vulgaris* is completely transparent. Therefore, Ca^{2+} imaging of transgenic hydras expressing the Ca^{2+} -indicators hyGCaMP or hyGCaMP NLS was done. Increase in nuclear Ca^{2+} signals was observed in ectodermal cells expressing hyGCaMP NLS. At the moment, the role of Ca^{2+} signals, especially of nuclear Ca^{2+} signals in hydra is unknown.

2 Zusammenfassung

Mit Hilfe des Botenstoffs Kalzium koordinieren und steuern Nervenzellen intrazelluläre Vorgänge wie z.B. Zellwachstum, Zelldifferenzierung, Lern- und Erinnerungsprozesse. In kultivierten Nervenzellen konnte gezeigt werden, dass ein Anstieg der Kalziumkonzentration im Zellkern entscheidend für Gentranskription ist, die von dem Transkriptionsfaktor CREB reguliert wird. Der CREB-regulierten Gentranskription kommt eine zentrale Bedeutung in der transkriptionsabhängigen Phase von Langzeitpotenzierung zu. Es ist noch unklar, ob Kernkalziumsignale auch *in vivo* an der CREB vermittelten Gentranskription beteiligt sind. Das Ziel dieser Arbeit war, Veränderungen der Kernkalziumkonzentration *in vivo* darzustellen.

Die Fruchtfliege *D. melanogaster* ist für diese Fragestellung ein geeigneter Modellorganismus. Für diese Arbeit wurden daher mehrere transgene Fliegenlinien generiert. Eine transgene Fliegenlinie expremiert den Kernkalziumindikator (UAS GCaMP NLS), um Kernkalziumsignale darzustellen, während eine weitere transgene Fliegenlinie einen Inhibitor des Kernkalziumsignalwegs (UAS 2xM13 NLS myc) expremiert. Mit Hilfe dieser Fliegenlinien konnte gezeigt werden, dass Kernkalziumsignale eine Rolle in Lern- und Erinnerungsprozesse spielen.

Mit Hilfe eines virusbasierenden Gentransfersystems wurde der Kernkalziumindikator (rAAV GCaMP 2.0 NLS) in CA1 Pyramidenzellen des Hippokampus von Ratten expremiert. In Gehirnschnitten wurden Veränderungen der Kernkalziumkonzentration in Abhängigkeit von LTP-induzierenden Stimulationen dargestellt. Damit wurde gezeigt, dass ein Anstieg der Kernkalziumkonzentration mit LTP zeitlich korreliert, jedoch ist dabei unklar, ob der Anstieg der Kernkalziumkonzentration notwendig für Langzeitpotenzierung ist.

Da der Süßwasserpolyp *H. vulgaris* vollständig transparent ist, sind Veränderungen von Kalziumsignalen leichter darzustellen als in anderen Modellorganismen. Für diese Arbeit wurden transgene Hydralinien (hyGCaMP und hyGCaMP NLS) generiert. Ein Anstieg in der Kernkalziumkonzentration konnte gezeigt werden, dennoch ist im Moment die Rolle von Kalziumsignalen, speziell von Kernkalziumsignalen in Hydra, völlig unbekannt.

3 Introduction

3.1 Nuclear Calcium signalling

3.1.1 Nuclear calcium signals induce CREB mediated gene expression

Calcium (Ca^{2+}) acts as an intracellular second messenger responsible for controlling several cellular mechanisms such as proliferation, development, learning and memory. In the nervous system, the Ca^{2+} dependent mechanisms of learning and memory are based on physiological changes in synaptic transmission. Coincident activation of pre- and postsynaptic neurons leads to modifications of synaptic efficacy between two those cells, thereby creating associative links between them (Lamprecht and LeDoux, 2004). Such associative links underlie learning in behaving animals, as well as in an in vitro model of memory termed long- term potentiation (LTP). LTP occurs in two phases, first as a temporary, reversible change in synaptic efficacy that can be prolonged into a more permanent change (Andersen et al., 1971; Bliss and Collingridge, 1993; Nicoll and Malenka, 1999). The early phase of LTP is independent of gene transcription and involves Ca^{2+} influx into the dendrite activating kinases, which modulate the activity of their substrate leading for example to morphological alteration in the cytoskeleton (Engert and Bonhoeffer, 1999; Fukazawa et al., 2003). The late, more permanent phase of LTP is transcription dependent, but again Ca^{2+} influx into the dendrite is crucial. It is generally accepted that influx of Ca^{2+} into postsynaptic neurons through L-type voltage operated Ca^{2+} channels (VOCC) but mostly through NMDA receptors stimulates mechanisms mediating long- term potentiation (LTP) (Nicoll and Malenka, 1999). The role of Ca^{2+} as a regulator of the different phases of LTP and including genetic (transcriptional) responses, raises the issue of specificity: what mechanism allows neurons to use a single second messenger to convert a range of electrical stimuli into distinct responses?

It seems that the amplitude and the duration of Ca^{2+} signals evoked by synaptic activity at the site of Ca^{2+} entry are extremely important in modulating the genetic response. The Ca^{2+} signal is represented by a Ca^{2+} code, which communicates specific firing patterns to the nucleus where the nuclear Ca^{2+} pool could decode this impulse

pattern to determine the transcriptional response (Bading, 2000; Hardingham et al., 2001). The two major pathways for synapse to nucleus communication are: the MAP kinase/ extracellular signal-regulated kinase (ERK1/2) cascade (Bading and Greenberg, 1991; Ginty et al., 1994; Xing et al., 1996; Chawla et al., 1998; Impey et al., 1998) and the Ca^{2+} /calmodulin (CaM) dependent protein kinases, especially, the nuclear CaM kinase IV (Sheng et al., 1991; Cruzalegui and Means, 1993; Matthews et al., 1994; Sun et al., 1994; Bito et al., 1996; Chawla et al., 1998). Both pathways trigger the phosphorylation of the transcription factor CREB (cAMP response element binding protein) at serine 133. However, this phosphorylation event is not sufficient to induce CREB mediated gene transcription. Activation of coactivator CREB-binding protein (CBP) is a second regulatory step necessary for gene expression. The CREB/ CBP complex stimulates transcription of genes by binding to the DNA regulatory element, CRE (cAMP response element) (Sheng et al., 1988; Bading et al., 1993; Bading et al., 1995). So CaM kinase IV and Ca^{2+} act directly in the nucleus by controlling the activity of CBP, but the ERK1/2 cascade cannot control the activity of CBP (Chawla et al., 1998; Hardingham and Bading, 1998; Hu et al., 1999). Therefore, the change in the nuclear Ca^{2+} concentration following synaptic activity triggers CREB mediated gene transcription. It seems that the activation of the transcription factor CREB is involved in changes in synaptic efficacy and may be critical for LTP and memory formation (Bourtchuladze et al., 1994; Segal and Murphy, 1998). Despite this knowledge, it is still unclear how the Ca^{2+} signal in neurons is conveyed from the synapse to the nucleus.

3.1.2 Calcium induced Calcium release

To understand the role of nuclear Ca^{2+} signalling, it is important to understand the dynamics of Ca^{2+} signalling across the nuclear pore complex in hippocampal neurons. The nuclear pore is unlikely to cause a diffusion barrier for Ca^{2+} ions. It seems that Ca^{2+} ions can move freely into the nucleus with no apparent impediment at the nuclear envelop (Eder and Bading, 2007), suggesting that fast Ca^{2+} waves (10-30 $\mu\text{m/s}$) might facilitate the transfer of information from synapses to the nucleus. These waves may be mediated by Ca^{2+} induced Ca^{2+} release (CICR), a reaction diffusion mechanism in which Ca^{2+} ions diffuse along the outer wall of the endoplasmic reticulum (ER), and induce the further release of Ca^{2+} from ER in a regenerative manner. Calcium stored within the ER of

neurons represents an important source. The Ca^{2+} concentration within the ER is $\sim 100\mu\text{M}$ whereas the cytoplasmic Ca^{2+} concentration is ten times lower at resting conditions ($[\text{Ca}^{2+}]_c \approx 100\text{nM}$) compared to excited conditions ($[\text{Ca}^{2+}]_c \approx 1000\text{nM}$) (Berridge et al., 2000). Both internal and external sources of Ca^{2+} can contribute to the intracellular Ca^{2+} concentration in neurons. Increases in intracellular Ca^{2+} concentration caused by Ca^{2+} influx from the extracellular space involve ligand and/or voltage gated ion channels. These activity-induced increases can be amplified by Ca^{2+} release from intracellular Ca^{2+} stores regulated predominantly by ryanodine receptors (RYRs) and by inositol-1,4,5-trisphosphate receptors (InsP_3Rs). Ca^{2+} directly activates the RYR to evoke CICR (see above) but the activation of the InsP_3R is more complex and involves stimulation with the receptor agonist, InsP_3 . InsP_3Rs have a bell-shaped Ca^{2+} dependence when treated with low concentrations of InsP_3 : low concentrations of Ca^{2+} (100-300nM) stimulate further Ca^{2+} release but at concentrations above 300nM, Ca^{2+} becomes inhibitory and switches off the channel thus inhibiting Ca^{2+} release (Bootman and Lipp, 1999). InsP_3 is a part of the phosphoinositide pathway, which is widely expressed in the brain (Fisher et al., 1992; Furuichi and Mikoshiba, 1995). The InsP_3 pathway is initiated at the plasma membrane by the interaction of a ligand (for example hormones) with a cell surface receptor. This interaction results in the activation of heterotrimeric G-proteins consisting of three subunits. The α subunit of the G-protein can activate phospholipase C (PLC), which stimulates the hydrolysis of phosphatidylinositol 4, 5-bisphosphate (PIP_2) to form the second messenger diacylglycerol (DAG) and InsP_3 (Furuichi and Mikoshiba, 1995; Seymour-Laurent and Barish, 1995). InsP_3 diffuses from the plasma membrane to the endoplasmic reticulum to bind InsP_3Rs and evoke the release of Ca^{2+} from the InsP_3R -gated store. The process of Ca^{2+} -induced Ca^{2+} -release (CICR) enables the InsP_3Rs and RYR to communicate with each other to establish coordinated Ca^{2+} signals, often organized into waves propagating through the neuron (Berridge, 1993; Clapham, 1995). Despite the complex mechanism of Ca^{2+} signalling within a single neuron, the main focus of this work was the visualisation of nuclear Ca^{2+} signals in complex interaction between neurons *in vivo*.

Calcium imaging is traditionally done using chemically synthesized Ca^{2+} -indicators that are entering the cells as acetoxymethyl esters. The use of Ca^{2+} indicators

such as Fluo-3 and fluorescence microscopy makes it possible to visualise Ca^{2+} events. Confocal microscopy has proven a vital tool in localising distinct Ca^{2+} signals *in vitro*. The Ca^{2+} indicator Fluo-3 is chemically similar to BAPTA and was developed by Minta *et al.* (Minta and Tsien, 1989) for use with visible-light excitation sources in flow cytometry and confocal laser scanning microscopy. An insuperable disadvantage is that one cannot target them to specific intracellular locations. An alternative to the synthetic indicators is protein based Ca^{2+} probes, which becoming more and more an attractive tool for studying Ca^{2+} dynamics *in vivo*.

3.2 Visualisation of Ca^{2+} signals using recombinant Ca^{2+} -indicators

3.2.1 FRET based Ca^{2+} -indicator

The first genetic encoded Ca^{2+} -indicator made use of the Ca^{2+} -sensitive photoprotein “aequorin” from the jellyfish *Aequorea victoria* (Blinks *et al.*, 1976). However, a major disadvantage of this protein is that it needs a cofactor “coelenterazine” to generate light in a Ca^{2+} -dependent and irreversible reaction. The most used genetically encoded indicators are usually based on fluorescent proteins, which are spontaneously fluorescent without enzymes or cofactors required. Fluorescent proteins are most commonly used as reporter gene to monitor gene transcription in cells, tissues or whole animals. Fluorescent proteins are also used as fusion proteins to monitor the location, interaction, aggregation, etc. Mutagenesis of the green fluorescent proteins (GFP) (Tsien, 1998) led to the creation of several variants that absorb and emit light of different wavelength, these makes it possible to be used for FRET (Fluorescence resonance energy transfer) (Heim and Tsien, 1996).

The first FRET based Ca^{2+} indicator was pioneered by the development of “cameleons” more than 10 years ago by Atsushi Miyawaki and Roger Tsien (Miyawaki *et al.*, 1997). Cameleons are tandem repeats of two different GFP variants with overlapping emission and excitation spectra linked together by Ca^{2+} sensor based on calmodulin (CaM) and the CaM binding peptide of myosin light chain kinase M13 (Ikura *et al.*, 1992). Miyawaki *et al.* demonstrated that the binding of Ca^{2+} resulted in a globular condensation of calmodulin around the M13 peptide, which leads to a Ca^{2+} -dependent increase in FRET between donor and acceptor. The reversible changes in FRET can be

detected as changes in the yellow over cyan emission fluorescents, and the probes function as ratiometric emission Ca^{2+} indicator. The idea of FRET based Ca^{2+} -indicator has been modified in different ways within the last decade including a decrease in pH sensitivity of the acceptor in the yellow cameleons (Miyawaki et al., 1999; Griesbeck et al., 2001; Nagai et al., 2002; Evanko and Haydon, 2005) and a shift to longer wavelength donor and acceptor pairs in the red cameleons (Mizuno et al., 2001) as well as changing the Ca^{2+} -detector molecule from calmodulin to troponin C (Heim and Griesbeck, 2004; Mank et al., 2006) or optimizing the donor/ acceptor interactions through redesign the calmodulin -M13 interaction (Palmer et al., 2006).

Despite these modifications, FRET based genetic encoded Ca^{2+} -indicators have some disadvantages which makes it sometimes more complicated to work with as with single fluorophore Ca^{2+} -indicators. The FRET based genetic encoded Ca^{2+} -indicators have shown lower signal strength *in vivo* even the improved molecules have shown a smaller dynamic range when expressed *in vivo*. An obvious difference in biophysical properties seems to be characteristic for most of those indicators compared to the results monitored in more simple assays. A comparative *in vivo* analysis by Reiff et al. who expressed of 10 different genetically encoded Ca^{2+} -indicators in transgenic flies (Reiff et al., 2005), demonstrated that the fold change fluorescence ratio ($\Delta R/R_0$), where R is the ratio of fluorescence at the acceptor and donor emission wavelengths, and ΔR is the change in ratio over the background R_0 , for a maximum physiological stimulus was between 5.8% and 11.6% (TN-L15 (Heim and Griesbeck, 2004) and YC2.0 (Miyawaki et al., 1999), respectively) of the change observed *in vitro*. This decrease *in vivo* has been observed and is almost explicable by the more complex interactions with other biological molecules *in vivo* compared to *in vitro*. For example, calmodulin is involved in several signalling pathways and recognises multiple cellular targets in its Ca^{2+} -bound form, therefore interaction with endogenous binding partners are likely. While these would also be relevant for non-FRET based genetic encoded Ca^{2+} -indicators that used also calmodulin as sensor, the decreased FRET signal seems to be also depending on the orientation between the donor and acceptor fluorophores which may allow an enhanced vulnerability to interaction of this sort (Kotlikoff, 2007). This phenomenon was also observed at non-calmodulin FRET based genetic encoded Ca^{2+} -indicators (TN-L15

(Heim and Griesbeck, 2004)), which displayed the lowest relative dynamic range in flies relative to its *in vitro* results (Reiff et al., 2005). This cannot be explained by endogenous calmodulin interaction, but may depend on troponin C interaction with troponin 1 (Kotlikoff, 2007).

3.2.2 Circularly permuted recombinant Ca²⁺-indicator

Alternatively, one can use genetic encoded Ca²⁺-indicators based on a single GFP molecule. The GFP molecule is an 11-stranded β -barrel that forms a nearly perfect shell around a chromophore spontaneously generated by an unusual multi-step pathway involving cyclization and oxidation of residues 65–67 (Tsien, 1998). Baird et al. could show that despite a complex maturation process the GFP molecule tolerate major transposition and insertion which were the basis to develop a single chromophore Ca²⁺-indicators (Baird et al., 1999). The GFP molecule is still fluorescent after a variety of circular permutations (Heinemann and Hahn, 1995) and insertion of different proteins e.g. calmodulin. Conformational changes of calmodulin following Ca²⁺ binding increased around 7-fold the fluorescence intensity of the GFP-CaM molecule, named Camgaroo (Baird et al., 1999). In 2001, two laboratories independently developed based on the idea of circularly permutations of enhanced GFP (resp. YFP) genetic encoded Ca²⁺-indicators in which calmodulin and a target peptide were incorporated within cpEGFP (pN1 GCaMP (Nakai et al., 2001)) or cpEYFP (Pericams (Nagai et al., 2001)). Nagai et al. designed four different genetic encoded Ca²⁺-indicators all based on single YFP (Inverse Pericam, Flash Pericam, Ratiometric Pericam and Split Pericam (Nagai et al., 2001)). In this work only Inverse Pericam were used to visualise Ca²⁺ signals within neurons.

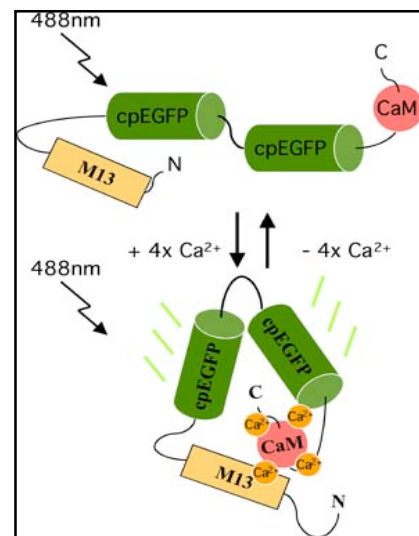


Fig 2. Schematic representation of recombinant Ca²⁺ probes. pN1 GCaMP consists of three different domains (M13, calmodulin and cpEGFP). The N-terminus of cpEGFP is connected to the C-terminus of M13, a peptide of the myosin light chain kinase. M13 is a target sequence of calmodulin (CaM). The N-terminus of CaM is fused to C-terminus of cpEGFP.

Both genetic encoded Ca²⁺-indicators are similarly designed containing three different domains. The polypeptides of the green fluorescent protein (pN1 GCaMP) or the yellow fluorescent protein (Inverse Pericam) were flipped around a central site. The

N-terminus of the circularly permuted fluorescence proteins (amino acid 145- 238) is connected to the M13 fragment of the myosin light chain kinase (Rhoads and Friedberg, 1997; Romoser et al., 1997), which is the target sequence of calmodulin (Mori et al., 2000). The C-terminus of the circularly permuted fluorescence proteins (amino acid 1-144) is connected to calmodulin. Binding of Ca^{2+} to calmodulin induces a conformation change due to Ca^{2+} -calmodulin-M13 interaction that leads to a more compact conformational in the circularly permuted fluorescence proteins. The reversible conformation change alters the spectral properties relative to the Ca^{2+} concentration (Nagai et al., 2001). So, pN1 GCaMP becomes brighter when it binds Ca^{2+} , whereas Inverse Pericam gets dimmer. Despite these characteristic optical properties of pN1 GCaMP and Inverse Pericam, differences similar as reported for FRET based genetic encoded Ca^{2+} -indicators have been shown. Pologruto et al. measured K_D values for both indicators in cultured hippocampal slices and compared that data set with reported K_D values measured in vitro. The reported discrepancy between the K_D in vitro and in the cell cytoplasm is not likely attributable to an error in calibration of the reference synthetic indicator (X-Rhod-5F) it may arise from differences in the biochemical milieu (Pologruto et al., 2004). This study reflects the difficulty to extrapolated results from simple cell culture system to a high complex cellular network. Further, pN1 GCaMP is significant less bright than native fluorescent protein and display variable stability above 30°C. The quantum yield of pN1 GCaMP and Inverse Pericam are 0.05 and 0.44 whereas EGFP and EYFP are above 0.6. The extinction coefficients are also significantly lower than the parent proteins, with pN1 GCaMP absorption being less than 3% of EGFP (Kotlikoff, 2007). Nevertheless, the temporal resolution of pN1 GCaMP in vitro is a promising aspect, which makes the probe more suitable for monitoring intracellular Ca^{2+} concentration ($[\text{Ca}^{2+}]_i$) in excitable cells. The dissociation time constant ($\tau \sim 200\text{ms}$) is independent of the $[\text{Ca}^{2+}]_i$, whereas the association time constant is faster at high $[\text{Ca}^{2+}]_i$ ($\tau < 10\text{ms}$ for $[\text{Ca}^{2+}]_i > 500\text{mM}$) (Nakai et al., 2001). This measurement was performed at room temperature indicate in vitro kinetics significantly faster than *in vivo* (Reiff et al., 2005). As mention before, interactions between genetic encoded Ca^{2+} indicators and endogenous proteins can markedly decrease the sensor properties and might explain again the obviously differences between *in vitro* and *in vivo*.

The temperature-sensitivity of pN1 GCaMP makes it useless for in vivo imaging in mammalian cells and allows only in vivo imaging in lower organisms e.g. *D. melanogaster* (Wang et al., 2003), *C. elegans* (Kahn-Kirby et al., 2004) and *H. vulgaris* (data are shown in result part). To overcome that disadvantages pN1 GCaMP was improved leading to GCaMP 1.6 (Ohkura et al., 2005) by the replacements of Val-163 with Ala (V163A) and Ser-175 with Gly (S175G), which were known to provide a more efficient chromophore formation of GFP (Tsien, 1998). V163A/S175G mutations of GCaMP 1.6 markedly improve the brightness of the probes as well as decrease the pH sensitivity (Ohkura et al., 2005). But also GCaMP 1.6 stays only bright at 37°C, once the probe was briefly exposed at lower temperature such at 28°C. Expressed in transgenic flies indicated that GCaMP 1.6 reported the largest and most rapid signals reflecting neuronal activity, although photobleaching was a consisting finding (Reiff et al., 2005).

Recently, GCaMP 1.6 was further modified by A206K mutation to prevent dimerisation (Zacharias et al., 2002) and a plasmid leader sequence (RSET) attached to the N-terminus for protein purification. GCaMP 1.6 cDNA was subjected to random mutagenesis by low fidelity PCR amplification and bacterial colonies displaying the brightest fluorescence at 37°C were isolated and sequenced. This process identified two new mutations (D180Y and V93I). So the resulting genetic encoded Ca²⁺-indicator, GCaMP 2.0, is brighter than wild-type GFP, maintains a 5-fold dynamic range, displays the reduced pH sensitivity of GCaMP 1.6 and is fully functional at 37°C. Interestingly, the addition of a polyHis linker was critical for thermal stability, because removal of the sequence led to loss of fluorescence at 37°C (Tallini et al., 2006).

As the question about in vivo imaging of nuclear calcium signals has been asked the first time, the improved indicators (GCaMP 1.6 and GCaMP 2.0) were not available, but Wang et al. has shown that pN1 GCaMP can be used to visualize Ca²⁺ signals in fly antennal lobes (Wang et al., 2003). Therefore, a transgenic fly was made in the lab expressing a nuclear Ca²⁺ indicator (UAS GCaMP NLS) to visualize nuclear Ca²⁺ signals during odour avoidance assay.

3.3 Fruit fly: Odour avoidance assay and nuclear Ca^{2+} -imaging

3.3.1 Odour avoidance assay

Classical conditioning is one form of learning whereby a conditioned stimulus (CS) becomes predictive of an unconditioned stimulus (US) when the two stimuli are paired in an appropriate way. The prototypic example of classical conditioning stems from studies on dogs conducted by Ivan Pavlov in which a tone cues (CS) paired with a food reward (US) became predictive of the food reward, shown by the dog's salivation upon hearing the tone cue after conditioning.

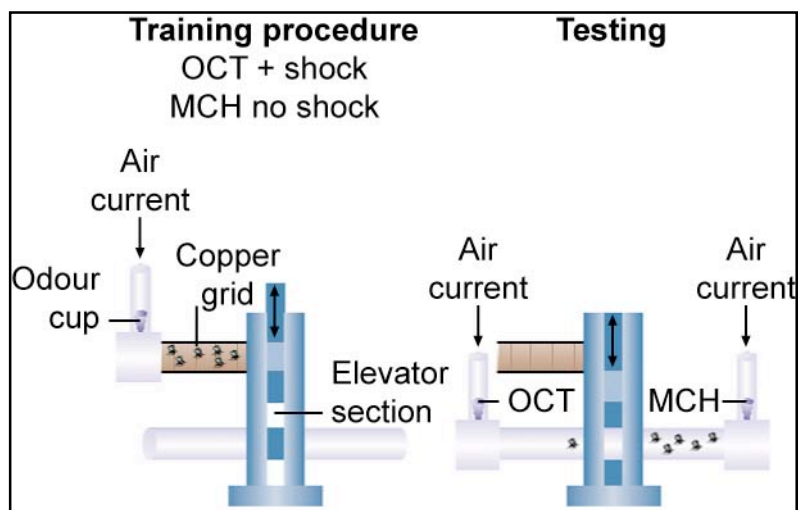


Fig 3. Schematic representation of olfactory conditioning learning. During training, flies experience an odor in conjunction with electric shock punishment. During subsequent testing, the flies preferentially avoid the shock-associated odor. Picture was obtained from (Waddell and Quinn, 2001) and modified for PhD thesis.

In *D. melanogaster*, olfactory classical conditioning is a robust and well-studied type of learning. In this assay, a group of ~100 flies is trained in a chamber, with an inner surface covered with an electrifiable printed-circuit grid. Odours are delivered into the chamber by airflows. The flies are exposed to one odour (e.g. 3-octanol; OCT) while the walls of the chamber are electrified (CS+). They then experience another odour (e.g. 4-methylcyclohexanol; MCH) without shock (CS-). The flies are then tested for learning or memory performance by transporting them to a choice point between converging airflows suffused with the two odours. After training, the animals are forced to run toward one of the two converging odours presented to them in a T-maze, and their selective avoidance of the shock-associated odour is again calculated into a performance index (PI). A single learning index is the average from two groups of flies trained to avoid each of the two odours. Depending on training protocol in such a learning assay memories of flies persists for hours or days (Tully and Quinn, 1985; Tully et al., 1994).

3.3.2 Memory phases

In *D. melanogaster* four phases of memories have been described: short-term memory (STM), which decays less than an hour; middle-term memory (MTM), lasting from one to three hours; and two forms of long-term memory (LTM) persists for 24 hours or more that are distinguished by different training protocols. One is independent of gene transcription (anaesthesia-resistant memory, ARM), whereas the second one, observed after training with interspersed rest interval (spaced training) is gene transcription dependent (Tully et al., 1994).

Many of LTM associated genes encode components of the cAMP signalling pathway, such as the adenylyl cyclase encoded by the *rutabaga* (*rut*) gene (Livingstone et al., 1984); the cAMP phosphodiesterase encoded by the *dunce* (*dnc*) gene (Dudai et al., 1976); the cAMP dependent protein kinase (PKA) subunits encoded by the *DC0* and *PKA-RI* gene (Skoulakis et al., 1993; Goodwin et al., 1997) and the transcription factor CREB encoded by the *dCREB2* (*CrebB-7A*) gene (Yin et al., 1994; Yin et al., 1995). All of the genes except *dCREB2*, which shows a widespread expression pattern, are highly expressed in mushroom bodies, which are the favoured brain region for CS-US association.

Today, there is a large body of evidence that suggests that the mushroom bodies (MBs) are primary sites for olfactory learning (Heisenberg, 2003; Davis, 2005). The first evidence for a role of the *D. melanogaster* mushroom bodies in olfactory memory came from the study of a collection of mutant fly lines with various anatomical brain defects (Heisenberg et al., 1985). Mushroom body-defective flies were found to sense odours and shock but could not associate these stimuli. Nevertheless, to assess the contribution of the mushroom bodies for associative odour memory, the understanding of the functional anatomy of the olfactory systems is important.

3.3.3 The functional anatomy of the olfactory system

Flies primarily sense odours through ~60 olfactory receptor proteins, one of which is expressed in each of the ~1400 olfactory receptor neurons (ORNs) that reside in the sensory bristles on the antennae and maxillary palps on each side of the head (reviewed by (Lessing and Carlson, 1999; Davis, 2004). It has been shown that ORNs expressing the same olfactory receptors project to the same glomerulus among the ~50 glomeruli in

the antennal lobe (Gao et al., 2000; Vosshall et al., 2000; Couto et al., 2005; Fishilevich and Vosshall, 2005).

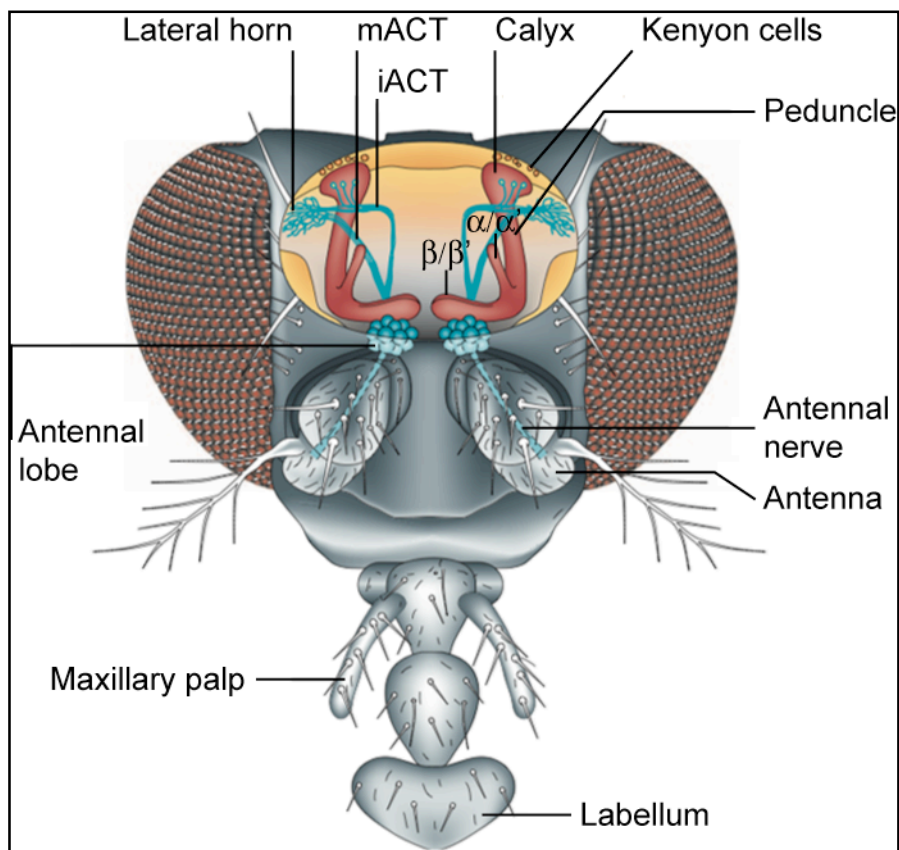


Fig 4. Schematic representation of *D. melanogaster* head. Dorsal view of fly head showing the main elements of the olfactory pathway. Odours are sensed by olfactory receptor neurons in the antennae and maxillary palps. These neurons project axons along the antennal nerve to the antennal lobe glomeruli. From there information is relayed by projection neurons in the inner and medial antennocerebral tract (iACT and mACT) to the mushroom body and to the lateral horn. Picture obtained from (Keene and Waddell, 2007) and modified for PhD thesis.

Glomeruli are morphologically distinguishable areas in the antennal lobe that contain the presynaptic terminals of olfactory receptor neurons (Keene and Waddell, 2007). In the antennal lobe, the cholinergic ORNs form excitatory synapses with at least three classes of neurons: excitatory cholinergic projection neurons (PNs), inhibitory GABAergic local interneurons (iLNs) and excitatory cholinergic local interneurons (eLNs) (Stocker et al., 1997; Jefferis et al., 2001; Marin et al., 2002; Wilson and Laurent, 2005; Shang et al., 2007). Because flies have about ~180 PNs, therefore each glomerulus is sampled on average by 3–5 PNs (Stocker et al., 1997). The PNs extend dendrites into a single antennal lobe glomerulus and transmit olfactory information from the antennal lobe to two locations in the brain: the calyx of mushroom bodies and to the lateral horn

(Jefferis et al., 2001; Marin et al., 2002; Wong et al., 2002). The PNs are organized into at least two different neural tracts — the inner and medial antennocerebral tract (ACT). PNs of the inner ACT form synapses in the mushroom body calyx and lateral horn, whereas PNs in the medial ACT bypass the mushroom body calyx and go straight to the lateral horn (Stocker et al., 1997). The calyx is a compartment of the mushroom bodies where the presynaptic projection neurons synapse with the dendrites of the Kenyon cells (Keene and Waddell, 2007). Beyond the anatomy the organization of PN-MB connectivity is not well understood. This is shown by the fact that the ~2500 mushroom body cells (Kenyon cells) in each hemisphere are named on their axonal projection domain in the mushroom body lobes, rather than by their dendritic fields in the calyx. The axonal projection of mushroom bodies branch into vertically and horizontally oriented neuropil regions known as lobes. The vertical lobes consist of the α and α' lobes. The horizontal lobes consist of the β , β' , and γ lobes (Crittenden et al., 1998). The significance of this morphological arrangement is poorly understood, and as a result, their role in olfactory memory as memory acquisition, storage and retrieval is not clearly differentiate between $\alpha\beta$, $\alpha'\beta'$ and γ lobes.

3.3.4 The role of mushroom bodies in long-term memory

The most olfactory learning experiments with mutant flies have led to the a model in which MB neurons associate the odour CS with the shock US and store the aversive associations within the specific neurons that are activated by a particular odour (Heisenberg, 2003; Davis, 2005). This model is supported by the demonstration that transient blockade of MB synaptic transmission during acquisition, storage, and/or retrieval indicates a requirement for MB output only during memory retrieval (Dubnau et al., 2001; Schwaerzel et al., 2002; McGuire et al., 2003; Davis, 2005). The relevance of MB neuron output for memory formation implies that memory could be represented at MB output synapses or synapses that are upstream of MB output synapses. Although there is evidence for a role of upstream antennal lobe (AL) circuits in memory in other insects (Stopfer and Laurent, 1999; Daly et al., 2004), but only one live imaging study in *D. melanogaster* has been shown that short-term change in AL neural activity occurs after aversive olfactory training (Yu et al., 2004). Another input to the MB comes from the Dorsal Paired Medial (DPM) neurons, which innervate the mushroom body lobes.

DPM neurons express a neuropeptide involved in the regulation of cAMP synthesis, encoded by the *amnesiac* (*amn*) gene (Feany and Quinn, 1995). The intermediate memory phase (MTM) was proposed after the discovery of this gene (Quinn et al., 1979). Mutant *amn* flies forgot the odour within one to three hours. Expressing the *amn* gene in DPM cells restores normal olfactory memory to *amn* mutant flies. Blocking synaptic transmission from the DPM neurons blocks one-hour memory but leaves immediate learning intact (Waddell et al., 2000). Further behavioural analysis could show that output from DPM neurons is critical after training for memory stability and is not required during acquisition or recall (Keene et al., 2004; Yu et al., 2005; Keene et al., 2006). DPM neuron projections to MB $\alpha'\beta'$ lobe neurons appear to be sufficient to stabilize aversive odour memory, suggesting that a DPM neuron-to-MB $\alpha'\beta'$ neuron connection could be critical for memory consolidation (Keene et al., 2006). Keene et al. could show that stable memory requires the sequential involvement of different MB neuron subsets. The $\alpha'\beta'$ lobe neurons are required during and after training to acquire and stabilize olfactory memory, whereas, $\alpha\beta$ lobe neuron output is only required to retrieve the memory (McGuire et al., 2001; Krashes et al., 2007). The analysis of DPM neurons suggests that a more complex and dynamic process underlies olfactory memory. So it seems that there is more consensus about the information input into the MB whereas the output of the MB remains still unclear.

3.3.5 The molecular mechanism of long-term memory

The mushroom bodies are not obviously connected to one particular region of the brain. Instead, they send information to many of the surrounding, poorly defined, neuropil areas as for example the central complex. The central complex consists of four substructures, the ellipsoid body, the fan-shaped body, the nodulii and the protocerebral bridge. The function of the central complex is not clear; it may mediate communication between the two hemispheres and is believed to be a control centre for many different behavioural outputs (Heisenberg and Wolf, 1993). There is evidence that the central complex are also involved in LTM (Wu et al., 2007). But still a clear picture of the neuronal circuits and networks that are involved in LTM or its modification has not yet emerged.

In contrast to STM and MTM much less is known about the mechanisms that are

relevant for LTM. While there is general agreement that these memory processes require DNA transcription and RNA translation, it is still unclear which neurons and neuronal networks are involved in these mechanisms. In *D. melanogaster* the primary signal for the activation of learning-associated transcription is thought to be the cyclic-adenosine monophosphate (cAMP)/ Protein Kinase A (PKA) pathway (Yin and Tully, 1996). In this pathway, cAMP activates PKA in the cytoplasm resulting in a translocation of the catalytic subunit of PKA into the nucleus; where it phosphorylates and activates the transcription factor dCREB2 (Yin et al., 1994; Kandel, 2001). In this study, an additional pathway is described suggesting that nuclear Ca^{2+} signalling might play a role in LTM in *D. melanogaster*.

3.4 Hippocampal neurons

3.4.1 Organization and role of the hippocampus in long term memory

The hippocampus is a part of the forebrain, located in the medial temporal lobe. The hippocampus consists of the dentate gyrus, the Cornu Ammonis fields (CA1-CA3), and the subiculum. The main information input to the hippocampus is via the entorhinal cortex and the main information output from the hippocampus is via the subiculum. Between entorhinal cortex and subiculum, three major pathways of the hippocampus are described. The perforant pathway from entorhinal cortex forms excitatory connections with the granule cells of the dentate gyrus (Bliss and Lomo, 1973). The mossy fiber pathway, formed by the axons of the granule cells of the dentate gyrus, connects the granule cells with the pyramidal cells in area CA3 of the hippocampus (Lu et al., 1997). The Schaffer collateral pathway connects the pyramidal cells of the CA3 region with the pyramidal cells in the CA1 region of the hippocampus (Collingridge et al., 1983).

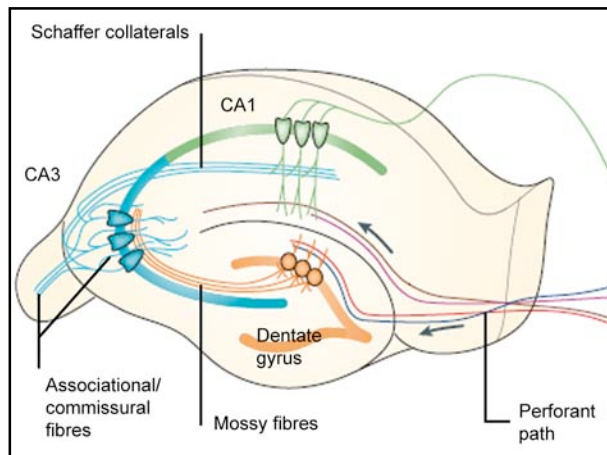


Fig 5. Schematic representation of the hippocampus. The major input is carried by axons of the perforant path, which convey sensory information from neurons in layer II of the entorhinal cortex to the dentate gyrus. Perforant path axons make excitatory synaptic contact with the dendrites of granule cells. Granule cells project, through their axons (the mossy fibres), to the proximal apical dendrites of CA3 pyramidal cells, which, in turn, project to ipsilateral CA1 pyramidal cells through Schaffer collaterals and to contralateral CA3 and CA1 pyramidal cells through commissural connections. Picture obtained from (Neves et al., 2008) and modified for PhD thesis.

Studies have identified an essential role for the hippocampus in: spatial learning (O'Keefe and Dostrovsky, 1971; Bachevalier et al., 1999; Zola et al., 2000), recognition memory (Pascalis and Bachevalier, 1999; Zola et al., 2000) and working memory (Laroche et al., 2000). But it seems that memory processing is not restricted to one area, rather the integrity of connections between several brain areas is necessary for information storage. It is still unclear what are the molecular mechanisms for storage of memory information (Neves et al.,

2008), but it is widely believed that memory formation is dependent on changes in synaptic efficiency that permit strengthening of associations between neurons; indeed, activity-dependent synaptic plasticity at appropriate synapses during memory formation is believed to be both necessary and sufficient for storage of information (Kandel, 2001; Lynch, 2004).

3.4.2 Long-term potentiation (LTP)

In 1894, Ramón y Cajal originally hypothesized that information storage based on changes in strength of synaptic connections between neurons that are active. Donald O. Hebb supported this hypothesis in one of his famous work ("The organization of behaviour", 1949) and proposed that if two neurons are active at the same time, the synaptic efficiency of the appropriate synapse will be strengthened. The first full description of LTP by Bliss et al. reported that trains of high-frequency stimulation to the rabbit perforant path caused a sustained increase in efficiency of synaptic transmission in the granule cells of the dentate gyrus (Bliss and Lomo, 1973).

Some characteristics of LTP (e.g. cooperativity, associativity and input specificity) have support the hypothesis that LTP may be a biological mechanism for at

least some forms of memory (Lynch, 2004). Some observations support this hypothesis: e.g. rhythmic bursts of activity that induce LTP mimic naturally occurring theta rhythm recorded in the hippocampus during exploratory behaviour (Larson et al., 1986; Rose and Dunwiddie, 1986; Diamond et al., 1988; Greenstein et al., 1988). Inhibitors of hippocampal LTP (AP5) also block hippocampal learning and retention of tasks (Morris et al., 1986). LTP was first time described in the granule cells of the dentate gyrus (Bliss and Lomo, 1973). But it is not restricted to the hippocampus rather it is an almost ubiquitous property of excitatory synapses throughout the brain. Indeed, it is difficult to find an excitatory pathway that does not express one or more forms of LTP (Malenka, 2003).

As discussed earlier at least two phases of memory are described: short-term memory, which persists for a few hours, and long-term memory, which persists for several days or much longer. At the cellular level, the storage of long-term memory is associated with gene expression, de novo protein synthesis, and formation of new synaptic connections. It has been shown that protein synthesis is required to maintain long-term memory and it seems that long-term memory is accompanied by enlargements of dendritic spines and associated postsynaptic densities (Yuste and Bonhoeffer, 2001; Malenka and Bear, 2004; Matsuzaki et al., 2004). These structural changes may be necessary to consolidate information-storage process (Kauer and Malenka, 2007). Consistently, protein synthesis inhibitors can block persistent memory but leave short-term memory unaffected, suggesting that stable long-lasting memories based on gene activation that is triggered at the time of the experience. Interestingly, also LTP consists of distinct phases involving different molecular mechanisms. The early phase (E-LTP), which lasts 2–3 h, is independent of protein synthesis, while more persistent long-lasting LTP (L-LTP), which lasts several hours in vitro and weeks in vivo, requires synthesis of new proteins (Lynch, 2004).

3.4.3 Molecular mechanism of LTP

The form of LTP that appears to be important for spatial memory is the NMDA receptor-dependent form that occurs at the Schaffer collateral pathway. Pharmacological and genetic disruption of this type of LTP results in impaired performance in tasks that require spatial memory (Chen and Tonegawa, 1997, Kentros, 1998 #1280). The

activation of the NMDA receptor requires simultaneously postsynaptic glutamate release and postsynaptic membrane depolarization. This relieves the voltage-dependent Mg^{2+} block of the NMDA receptor and allows the Ca^{2+} influx into the postsynaptic dendritic spines (Kauer and Malenka, 2007). These characteristics of the NMDA receptor directly relate to its important physiological roles in synaptic plasticity as a molecular coincidence detector (Lynch, 2004). These were demonstrated in CA1 and dentate gyrus, using the specific competitive NMDA receptor antagonist AP5 and the noncompetitive NMDA-associated channel blocker MK801 (Collingridge et al., 1983; Coan and Collingridge, 1987; Coan et al., 1987). The increase of the Ca^{2+} concentration is an important trigger for LTP. As consequence of the Ca^{2+} influx, a complex intracellular signalling cascade is activated that includes several protein kinases, especially Ca^{2+} /Calmodulin-dependent protein kinase II (CaMKII) (Malenka and Nicoll, 1999).

CaMKII is one of the most abundant proteins in neurons comprising 1–2% of the total protein concentration. CaMKII is particularly highly expressed at the synapse in presynaptic and postsynaptic compartments (Fink and Meyer, 2002). Conversely, the long-lasting CaMKII activity is independent of calcium but it is triggered by calcium-dependent autophosphorylation. This finding led to the concept that CaMKII is used as a “molecular memory molecule” (Malenka et al., 1989; Malinow et al., 1989; Fukunaga et al., 1993; Ouyang et al., 1997). Given these results, it was of interest to determine the targets for CaMKII.

It was shown that CaMKII interact with the AMPA receptor GluR1 subunit (Barria et al., 1997; Mammen et al., 1997) that results in an increased number of AMPA receptors in the postsynaptic plasma membrane (Malenka and Nicoll, 1999; Malenka and Bear, 2004). AMPA receptors are composed of the four different subunits GluR1–GluR4 (Hollmann and Heinemann, 1994; Rosenmund et al., 1998). It is controversially discussed whether CaMKII interact directly with AMPA receptor subunits (Ehlers, 2000) or indirectly via other proteins with AMPA receptor (e.g. Stargazin (Stg) and Stg-like TARPs) (Chen et al., 2000; Schnell et al., 2002). A current model is that, during LTP, phosphorylation of GluR1 by CaMKII enhances its conductance, while phosphorylation of the AMPA receptor associated Stargazin controls the trafficking to the synapse (Boehm and Malinow, 2005).

The role of CaMKIV and the activation of the transcription factor CREB have already discussed (section 1.1.1. “Nuclear calcium signals induce CREB- mediated gene expression”). Of course, many studies of LTP presented here have been only partly elucidated and some studies are neglected, but are intensively reviewed elsewhere.

3.4.4 DNA delivering system based on recombinant adeno-associated virus (rAAV)

3.4.4.1 Inverted terminal repeats (ITR)

Recombinant adeno-associated virus (rAAV) has become an attractive vehicle for delivering transgenes to the central nervous system (CNS) due to its lack of toxicity and absence of inflammatory response. The virus is a member of the *Parvoviridae* family; AAV generally requires a helper virus (e.g. adenovirus or herpesvirus) to establish a productive infection (Casto et al., 1967; Atchison, 1970; Richardson and Westphal, 1984). The shell of rAAV is approximately 25 nm in diameter and encapsidates a single-stranded DNA genome of 4.7 kb that consists of two large open reading frames (ORFs) flanked by inverted terminal repeats (ITR). The ITRs are required for genome replication and packaging (McLaughlin et al., 1988). It is not absolutely clear which sequences within the ITR are required for packaging or what the immediate DNA precursor for packaging is (Zhou and Muzyczka, 1998). The two open reading frames (ORFs) encoding the nonstructural and structural viral proteins (Srivastava et al., 1983).

3.4.4.2 Capsid proteins are encoded by *cap* gene

The right half of the genome contains the ORF for the *cap* gene, which encodes three capsid proteins, VP1, VP2 and VP3 from two mRNAs, which are derived from a primary transcript by alternative splicing and are expressed under the control of the p40 promoter (Green and Roeder, 1980; Trempe and Carter, 1988). Both spliced transcripts (2.3-kb RNAs) differ only with respect to their 3' acceptor sites, which are apparently located only 27 nucleotides apart. The largest protein (VP1 [87 kDa]) is generated from the slightly larger message (2.3 kb_{VP1}), whereas the other two proteins (VP2 [72 kDa] and VP3 [62 kDa]) are translated from the smaller message (2.3kb_{VP2/VP3}), by alternative use of an ACG initiator encoded for VP2 and a downstream AUG initiator that encoded for VP3 (Becerra et al., 1985; Muralidhar et al., 1994). Because the larger message (2.3

kb_{VP1}) is preferred to be spliced out, resulting in a reduced level of VP1 protein synthesis and within the smaller message (2.3kb_{VP2/VP3}), the ACG codon is a much weaker translation initiation signal, therefore the ratio of the three capsid proteins is 1(VP1): 1 (VP2): 18 (VP3) (Rabinowitz and Samulski, 2000).

3.4.4.3 Rep proteins are encoded by *rep* gene

The left half of the genome contains the ORF for the *rep* gene, which encodes four nonstructural Rep proteins, Rep78, Rep68, Rep52 and Rep40 according to their sizes in kDa (Tratschin et al., 1984; Mendelson et al., 1986; Trempe et al., 1987; Weitzman et al., 1994). The two larger Rep proteins, Rep78 and Rep68, are synthesized from unspliced and spliced transcripts initiated at the p5 promoter; the smaller Rep proteins, Rep52 and Rep40, are synthesized from the p19 transcripts (Kyostio et al., 1994). Rep68 and Rep78 can specifically bind the hairpin configuration formed by the AAV inverted terminal repeat sequence (Im and Muzyczka, 1989), but no site-specific DNA binding could be detected for Rep52 and Rep40 (Im and Muzyczka, 1992). Like Rep 68, Rep78 has an ATP-dependent, site-specific, and strand-specific endonuclease activity that specifically cuts the AAV origin at the inverted terminal repeats (Im and Muzyczka, 1990, 1992).

Because the viral *rep* and *cap* genes are deleted in rAAV, reversion to wild type is not a serious concern. Even if it were to occur, the wild-type virus (wtAAV), as mentioned before is non-pathogenic and incapable of autonomous replication (Janson et al., 2001). Deletion of the wtAAV *rep* gene prevents the integration properties in non-dividing cells and therefore the vector DNA exists mainly in episomal form. Hermonat et al. were the first using AAV as a general transduction vector, replacing the AAV *Cup* genes with the neomycin resistance gene under the control of the SV40 early promoter (Hermonat and Muzyczka, 1984). Later, modern AAV vectors have 96% of the viral genome removed from the vector, leaving only the ITRs (McLaughlin et al., 1988; Samulski et al., 1989). The absence of viral sequences means that no *de novo* viral protein synthesis occurs following transduction, minimizing the amount of foreign protein available to trigger immune responses.

3.4.4.4 AAV serotypes

Eight different AAV serotypes have been described (Chiorini et al., 1997; Chiorini et al., 1999; Xiao et al., 1999; Sanlioglu et al., 2000; Gao et al., 2002). A serotype, by definition, is a newly isolated virus that does not efficiently cross-react with neutralizing sera specific for all other existing and characterized serotypes. Of all known AAV serotypes AAV 2 is the best-characterized serotype so far. It is known that AAV2 transduces a wide range of tissue types (e.g. liver, muscle, lung, and central nervous system) but only with moderate efficiency. Therefore researchers have exploited cross-packaging strategies to compare the transduction efficiencies of serotypes of AAV vectors in different tissues. In general, AAV1 and 5 exhibit higher transduction frequencies than AAV2 in all regions injected within the CNS (Burger et al., 2004).

3.4.4.5 Receptor binding and intracellular processing of rAAV

AAV2 capsid proteins first bind to heparan sulfate proteoglycans at the cell surface (Summerford and Samulski, 1998) and subsequently interact with cofactors like the human fibroblast growth factor receptor 1 (Qing et al., 1999), hepatocyte growth factor receptor (Kashiwakura et al., 2005) and $\alpha V_{\beta}5$ integrin (Summerford et al., 1999; Wu et al., 2006) which may stabilize the virus attachment or participate during internalization. Mutagenesis data of AAV2 suggest that the binding ability to heparan sulfate proteoglycans depends on the correct assembly of VP trimers. In particular, a motif of five basic amino acids (R484, R487, R585, R588 and K532) has been identified contributed to the heparin binding (Kern et al., 2003; Opie et al., 2003). Less is known about receptors of other serotypes. Chen et al. could show first time that transduction with AAV1 was completely inhibited by removal of α 2-3 sialic acid with sialidase, while heparin had no effect (Chen et al., 2005).

After binding to cell surface receptors, in the case of AAV2, particles are endocytosed into the cell via clathrin-coated pits. This event requires dynamin, a 100-kDa cytosolic GTPase that selectively regulates clathrin-mediated endocytosis (Duan et al., 1999). Into the cell, AAV escapes from early endosome by acidification. The acidic pH of the endosomal lumen is likely to induce conformational changes e.g. exposure of the phospholipase A2 (PLA2) domain located at the N-terminus of VP1 (Bleker et al., 2005).

Following release from the endosome, AAV rapidly moves to the cell nucleus and accumulates perinuclearly beginning within 30 min after the onset of endocytosis pathways. Interestingly, the majority of the intracellular virus particles remain in a stable perinuclear compartment in spite of gene expression from nuclear AAV genomes can be detected (Bartlett et al., 2000). How the virus genome enters the nucleus and whether virus particles uncoats in the nucleus, in the cytoplasm or in the endosome is still an open question. In the presence of Adenovirus, however, cytoplasmic AAV quickly translocated into the nucleus as intact particles as early as 40 min after coinfection. AAV appears to enter the nucleus through a mechanism independent of the nuclear pore complex, since agents that block the nuclear pore do not affect AAV nuclear entry. The rapid nuclear translocation of intact AAV capsids in the presence of Adenovirus suggested that one or more capsid proteins of Adenovirus might be altering trafficking (Xiao et al., 2002).

3.4.4.6 Promoter based transduction efficiency and specificity

As mention before any differences observed in transduction efficiency between the different serotypes are likely due to diversity in the viral capsid proteins, their receptor tropism, and/or their intracellular trafficking following cell entry. Therefore, a mosaic virus composed of a mixture of capsid subunits from different serotypes enhances the transgene expression. Using a mixture of AAV1 and 2 helper constructs, Hauck et al. generated mosaic viruses that combine the transduction characteristics of AAV1 and AAV2 (Hauck et al., 2003). Variations in transduction efficiency have also been observed *in vivo* studies depending on the viral promoters. Klein et al. compared recombinant adeno-associated virus (rAAV) vectors incorporating either the immediate early cytomegalovirus (CMV) promoter or the neuron-specific enolase (NSE) promoter. Transduction in hippocampus resulting from the NSE promoter-containing construct was more efficient and persistent than that resulting from the CMV promoter containing construct (Klein et al., 1998). In addition, transgene expression from the hybrid CMV-chicken β -actin (CBA) promoter, consisting of a fusion between the chicken β -actin promoter with the CMV promoter enhancer sequences, is even more efficient (Klein et al., 2002). Cell specific transgene expression depends on the promoter properties, it has been shown that gene expression from AAV2 or AAV5 can be restricted to neurons *in vitro* by incorporating the hSYN or CBA promoter or restricted mainly to astrocytes by

using the mCMV promoter (Kugler, 2003, Shevtsova, 2005). Regardless of the promoter used, transduction efficiency can also be increased using posttranscriptional regulatory elements such as the Woodchuck hepatitis virus element posttranscriptional regulator (WPRE). Accordingly, Xu et al. have reported that WPRE increased transgene expression by 13-fold in the striatum and by 35-fold in the hippocampus (Xu et al., 2001).

The ability of rAAV to stably transduce a wide variety of neuronal cell types in the brain at any developmental stage, from *in utero* to adult or senescent animals in all brain regions through stereotaxic delivery, as well as ability of either short-term or long-term CNS gene expression makes it extremely popular for *in vivo* expression.

3.5 Freshwater polyp: nuclear and cytoplasmic Ca²⁺-imaging

3.5.1 The freshwater polyp *H. vulgaris*

In the 1740s, the Swiss scientist Abraham Trembley discovered that the freshwater polyp hydra, which belongs to the cnidaria phylum, could regenerate their heads and feet and if cut into a few pieces all of them would regenerate to form new individuals. This model has some advantages for morphological and molecular studies of regeneration including: the optical transparency of the two tissue layers and the rapid growth rate with a population doubling time of 3.5 days (Bosch, 2007). Hydra is made up of two cell layers (the ectoderm and endoderm) separated by a thin extracellular matrix (ECM) called the mesoglea. Functional studies have established that cell mesoglea interaction is critical to developmental processes in hydra (Deutzmann et al., 2000; Sarras et al., 2002; Shimizu et al., 2002). The mature mesoglea contains macromolecules such as laminins, collagens, heparan sulfate proteoglycans and fibronectin-like molecules (Sarras and Deutzmann, 2001). Regeneration starts with the immediate retraction of the mesoglea which subsequently has to be rebuilt (Shimizu et al., 2002). The key role of the mesoglea in hydra epithelial homeostasis is also underlined by the discovery that the survival of hydra epithelial cells depends on their anchorage to extracellular matrix molecules (Kuznetsov et al., 2002). Key regulators for degrading or remodelling the ECM are metalloproteases (Deutzmann et al., 2000; Fowler et al., 2000; Sarras et al., 2002; Shimizu et al., 2002).

Hydras body plan is organized as a gastric tube with a mouth and ring of tentacles at the head pole and a peduncle and basal disk at the foot pole. The organism has about 20 different cell types that are distributed along the longitudinal axis in a specific pattern (Sarras et al., 2002). Cells either belong to the ectodermal or endodermal epithelial cell lineage, or to the interstitial cell lineage. Epithelial cells are epitheliomuscular cells covering the outside of the animal or lining the gastric cavity (Bosch, 2007). Interstitial cells are mostly localized in the interstitial space between ectodermal epithelial cells and provide precursors for gland cells, neurons, nematocytes and germ cells. The hydra nervous system is organized as a nerve net that extends throughout the animal and is made up of two cell lineages: the sensory mechanoreceptor cells, named nematocytes, and the neurons, with typical synapses (Westfall, 1996).

Cells of hydra are in constant division and turnover. This division occurs by stem cells in the body column that lead to differentiated body column cells that are constantly displaced toward the poles (Campbell, 1967). The axial pattern of the animal is maintained by a gradient of head formation competence, commonly referred to as the head activation gradient. The gradient is maximal near the head decreasing down the body column. As a consequence of this extensive cell turnover, hydra is highly regenerative. Therefore, any isolated fragment of the hydra body, which is larger than a few hundred epithelial cells, can regenerate into complete animal. Even aggregates of dissociated cells will regenerate into viable polyps (Gierer et al., 1972; Technau et al., 2000).

3.5.2 Molecular mechanism involved in head regeneration

Regeneration processes in multi-cellular animals depend on several signalling transduction pathways. Studies of model organisms have identified a number of such pathways responding to external signals and leading to changes in cell behaviour. However, most model organisms are all bilaterians. Investigations of the roles of signal transduction pathways have revealed that a number of the well-known developmental signalling pathways were already existing in hydra (Steele, 2002; Bosch, 2007). At least two signalling pathways involved in the regulation of the head formation in hydra are described. One is mediated by PKC (Muller, 1996; Cardenas et al., 2000) and the other is mediated by STK, the hydra homologue of Src (Cardenas et al., 2000; Fabila et al., 2002;

Cardenas and Salgado, 2003). In addition, there is evidence for the involvement of a third signalling pathways regulating the head formation. Manuel et al. could show that PI3K and ERK1/2 are also involved in the head formation. It seems that ERK1/2 plays a central role in regulating the activities of the PKC, STK and PI3K pathways towards the transcription of head-specific genes (Arvizu et al., 2006; Manuel et al., 2006). In rodents, an indirect target for ERK1/2 pathway is the transcription factor CREB. Galliot et al. identified a hydra related CREB (hyCREB) participated in the CRE binding complex (Galliot et al., 1995). More recently, Kaloulis et al. further explored the role of hyCREB using an antibody against hyCREB, which specifically detects phosphoSer133-hyCREB positive nuclei. They observed a dramatic increase in the number of phospho-hyCREB positive nuclei at the regenerating tips of the head early during regeneration (Kaloulis et al., 2004).

The transparency of the outer and inner cellular layer of hydra and the knowledge about the different signalling pathways makes it extremely interesting for *in vivo* Ca²⁺ imaging.

4 Material and Method

4.1 Material: media, buffer and antibodies

4.1.1 Fruit fly: preparation of larval muscle cells

Haemolymph like (HL3) adjusted to pH 7.2, described (Stewart et al., 1994)

	HL3 (plus CaCl ₂)	HL0 (free CaCl ₂)	HL3 (high K ⁺)
NaCl	70 mM	70 mM	70 mM
KCl	5 mM	5 mM	35 mM
CaCl ₂	1.5 mM		1 mM
MgCl ₂	20 mM	20 mM	10 mM
NaHCO ₃	10 mM	10 mM	10 mM
Trehalose	5 mM	5 mM	5 mM
Sucrose	115 mM	116,5 mM	84 mM
HEPES	5 mM	5 mM	5 mM
ddH ₂ O	to 1000ml	to 1000ml	to 1000ml

4.1.2 Fruit fly: preparation and *in vivo* imaging of adult flies

Ringer solution adjusted to pH 7.3

Hepes	5mM
NaCl	130mM
KCl	5mM
MgCl ₂	2mM
CaCl ₂	2mM
Sucrose	36mM

4.1.3 Fruit fly: immunohistochemistry (IHC)

Fixative solution used for fruit fly and hippocampal neurons

Paraformaldehyde	4%
Sucrose	4%
1xPBS	to 100ml

Washing and dilution buffer (PAT) for whole mount fly brains

BSA	1%
Triton X-100	0.5%
Na-acide	0.05%
NGS (normal goat serum)	3% (added before blocking step)
1xPBS	to 100ml

Washing and dilution buffer (PBST) used for larvae

Tween 20	0.3%
NGS (normal goat serum)	5% (added before blocking step)
1xPBS	to 100ml

Primary antibodies: Immunohistochemistry of larvae and whole mount brains

Mouse monoclonal anti Myc SC-40	(IHC 1:200)	Santa Cruz
Rabbit polyclonal anti GFP	(IHC 1:200)	Molecular Probes

Secondary antibodies: Immunohistochemistry of larvae and whole mount brains

Goat anti mouse Cy3	(IHC 1:200)	Dianova
Goat anti mouse Alexa488	(IHC 1:200)	Molecular Probes
Goat anti rabbit Alexa488	(IHC 1:200)	Molecular Probes

Antibodies are diluted in PBST (larvae) or in PAT (whole mount brains)

4.1.4 Hippocampal neurons: media for dissociated cells

Media used for preparation and culturing of primary hippocampal neurons are previously described (Diploma thesis of JM. Weislogel, 2003)

4.1.5 Hippocampal neurons: media for cultured brain slice

OTC medium were prepared as described (Stoppini et al., 1991)

MEM high Glucose (6,5mg/ml) plus Hepes	50ml
Horse serum	25ml
Hank's solution	25ml
ddH ₂ O	to 100ml

4.1.6 Hippocampal neurons: anaesthesia for in vivo injection

Sleep mix

Fentanyl	20 μ l	Fentanyl-Janssen
Medetomidin	30 μ l	Dormitor©
Midazolam	80 μ l	Dormicum©15/3
Dilution 1:2 with ddH ₂ O, used 3 μ l/g body weight		

Wake up mix

Atipamzol	120 μ l	Antisedan©
Flumazenil	200 μ l	Anexate©
Naloxon	120 μ l	Narcanti©
Undiluted 5 μ l /g body weight		

4.1.7 Hippocampal neurons: media for acute brain sliceSlicing solution (gassed with 95% O₂ and 5% CO₂)

Sucrose	150mM
NaCl	40mM
KCl	4mM
MgCl ₂	7mM
NaH ₂ PO ₄	1.25mM
CaCl ₂	0.5mM
Glucose	10mM
NaHCO ₃	26mM

Artificial cerebrospinal fluid (gassed with 95% O₂ and 5% CO₂)

NaCl	125mM
KCl	3.5mM
MgCl ₂	1.3mM
NaH ₂ PO ₄	1.2mM
CaCl ₂	2.4mM
Glucose	10mM
NaHCO ₃	26mM

Potassium methylsulphate based solution (pH adjusted to 7.35 with KOH)

KCH ₃ SO ₄	145mM
NaCl	8mM
HEPES	10mM
K ₂ -phosphocreatine	10mM
Mg ₂ -ATP	4mM
Na ₃ -GTP	0.3mM

4.1.8 Hippocampal neurons: western blot (WB) and immunohistochemistry (IHC)

12% separation gel

SDS	10%
Tris-HCl, pH 8.8	1.5 M
AMBA (Acrylamide, Bis Acrylamide)	30%
APS (Ammonium Persulfate)	10 %
TEMED	0.1 %
ddH ₂ O	to 100ml

4.5% stacking gel

SDS	0.4%
Tris-HCl, pH 6.8	0.5 M
AMBA (Acrylamide, Bis Acrylamide)	30%
APS (Ammonium Persulfate)	10 %
TEMED	0.1 %
ddH ₂ O	to 100ml

Sample buffer: western blot (WB)

Glycerol	10%
SDS	3%
Tris-HCl, pH 6.8	10mM
β -mercaptoethanol	5%
Bromphenolblue	0.1%

Washing buffer (PBST): western blot

Tween 20	0.01%
1xPBS	to 100ml

Blocking and dilution buffer: western blot

Milk powder	5%
PBST	to 100ml

Dilution and blocking buffer: Immunohistochemistry

BSA	2%
Triton X-100	0.1%
NGS (normal goat serum)	10% (added before blocking step)
1xPBS	to 100ml

Primary antibodies: Immunohistochemistry (IHC) or western blot (WB)

Rabbit polyclonal anti hrGFP	(WB 1:1000)	Stratagene
Rabbit polyclonal anti GFP	(IHC 1:1000 or WB 1:10000)	Molecular Probes
Rabbit polyclonal anti CREB	(WB 1:1000)	NEB
Rabbit polyclonal anti pCREB	(WB 1:1000)	Upstate
Rabbit polyclonal anti ATF3 C-19	(WB 1:800)	Santa Cruz
Rabbit polyclonal anti Gal4 DBD	(WB 1:2000)	Santa Cruz
Rabbit polyclonal anti cFos SC-52	(WB 1:5000)	Santa Cruz
Mouse monoclonal anti CaM	(WB 1:10000)	Upstate
Mouse monoclonal anti Myc SC-40	(IHC 1:1000 or WB 1:1000)	Santa Cruz
Mouse monoclonal anti Flag M2	(IHC 1:1000 or WB 1:1000)	Sigma
Mouse monoclonal anti α tubulin	(WB 1:250000)	Sigma

Secondary antibodies: Immunohistochemistry (IHC) or western blot (WB)

Goat anti mouse Cy3	(IHC 1:800)	Dianova
Goat anti rabbit Cy3	(IHC 1:800)	Dianova
Goat anti mouse Alexa 488	(IHC 1:800)	Molecular Probes
Goat anti rabbit Alexa 488	(IHC 1:800)	Molecular Probes
Goat anti mouse HRP	(IHC 1:5000)	Dianova
Goat anti rabbit HRP	(IHC 1:5000)	Dianova

Antibodies are diluted either in western blot or immunohistochemistry dilution buffer

4.1.9 Freshwater polyps: hydra medium

Media used for culture and imaging experiment of *H. vulgaris* are previously described (Technau, 1992). Either CaCl_2 or KCl used for stimulation experiments were diluted to final concentration of 90mM directly in hydra medium.

4.2 DNA Plasmids and transgenic flies

4.2.1 Following DNA plasmids were obtained

DNA plasmid name	Reference
EYFP-Nuc	Cloentech
pN1 GCaMP	(Nakai et al., 2001)
GCaMP 1.6 and GCaMP 1.6 (E140K)	(Ohkura et al., 2005)
GCaMP 2.0	(Tallini et al., 2006)
Inverse Pericam	(Nagai et al., 2001)
YC 3.60 (yellow cameleon)	(Nagai et al., 2004)
VC 6.1	(Evanko and Haydon, 2005)
TN-XL	(Mank et al., 2006)
D3 cpV	(Palmer et al., 2006)
DRIP (DsRed2-referenced Inverse Pericam)	(Shimozono et al., 2004)
mCherry	(Shaner et al., 2004)
mRFPmars	(Muller-Taubenberger et al., 2006)
hoTG actin EGFP	(Wittlieb et al., 2006)
rAAV myc	(Zhang et al., 2007)

rAAV CaMBP4 flag	(Zhang et al., 2007)
rAAV hrGFP	(Zhang et al., 2007)

4.2.2 Following transgenic flies expressing the Ca²⁺-indicators were obtained

Name/Genotype	Reference
UAS GCaMP	(Wang et al., 2003)
UAS TN-L15	(Griesbeck, 2004)
UAS TN-XL	(Mank et al., 2006)
UAS CaM2.1-8.2	(Diegelmann et al., 2002)
Gal4 MB247; UAS CaM2.1-8.2	Dr. A. Fiala, Würzburg, Germany
Gal4 Or83b; UAS CaM2.1-8.2	Dr. A. Fiala, Würzburg, Germany
Gal4 MB247	Dr. A. Fiala, Würzburg, Germany
Gal4 MHC	Dr. C. Goodman, Berkeley, CA
Gal4 OK6	Dr. C. O’Kane, Cambridge, UK
Gal4 OK107	(Connolly et al., 1996)
Gal4 Or83b	Dr. A. Fiala, Würzburg, Germany
Gal4 Feb170	(Siegmund and Korge, 2001)
Hs-Gal4 (P26)	(Xia et al., 2005)
2U (wild-type)	Dr. T. Tully, Cold Spring Harbor, NY
Ubi Histon 2A-RFP	Dr. J. Großhans Heidelberg, Germany

4.3 Cloning of Ca²⁺-indicators and Ca²⁺/CaM buffer (hippocampal neurons)

The Ca²⁺-indicators were delivered into cultured hippocampal neurons either by Lipofectamin 2000 (Invitrogen GmbH, Karlsruhe, Germany) based transfection (Weislogel et al., 2003) or by recombinant Adeno-associated virus (Zhang et al., 2007). Live imaging using the synthetic Ca²⁺-indicator Fluo-3 was done (Weislogel et al., 2003).

4.3.1 Nuclear Ca²⁺-indicator: pN1 GCaMP NLS

5’NheI and 3’BamHI sides were added by PCR to the entire coding sequence of pN1 GCaMP 1.3 (Nakai et al., 2001). The PCR product was subcloned into pCR blunt vector (Zero Blunt PCR cloning kit; Invitrogen GmbH, Karlsruhe, Germany) to yield

GCaMP blunt and sequenced (GATC Konstanz, Germany). Subsequently, the coding sequence was inserted into 5'NheI and 3'BglIII sides of pEYFP-Nuc (Clontech) to yield pN1 GCaMP NLS. The 3'BglIII side of pEYFP-Nuc (Clontech) was deleted by ligation with the 3'BamHI side of the PCR product. The following primers were used: 5' TTG CTA GCG CTA CCG GAC TCA GAT 3' (forward) and 5' CTG GAT CCC TTC GCT GTC ATC ATT 3' (reverse).

4.3.2 Nuclear localized EYFP: rAAV EYFP-Nuc

The vectors used to construct and package rAAVs have been described previously (Klugmann et al., 2005), and were provided by Matthias Klugmann and Matthew During. The rAAV expression vector was modified in the lab by Dr. Sheng Jia Zhang. 5'NheI side was deleted and a multiple cloning site (MCS) containing a myc-tag was inserted into 5'BamHI and 3'EcoRI sides of rAAV expression vector to yield rAAVmyc (Zhang et al., 2007).

5'BglIII and 3'XbaI sides were added by PCR to pM13 NLS VP16. The PCR product was inserted into rAAVmyc to yield rAAV M13 NLS VP16 myc (see section 4.3.11). 5'BamHI and 3'NheI sides of rAAVmyc were deleted and 5'NheI and 3'BamHI were created by ligation with the PCR product. The coding sequence of pEYFP-Nuc (Clontech) was inserted into 5'NheI and 3'BglIII sides of rAAV M13 NLS VP16 myc to yield rAAV EYFP-Nuc.

4.3.3 Nuclear Ca²⁺-indicator: rAAV GCaMP NLS

The coding sequence of pN1 GCaMP NLS was inserted into 5'NheI and 3'BamHI sides of rAAV EYFP-Nuc to yield rAAV GCaMP NLS.

4.3.4 Nuclear Ca²⁺-indicator: rAAV Inverse Pericam NLS (rAAV IP NLS)

5'NheI and 3'BglIII sides were added by PCR to the entire coding sequence of Inverse Pericam pcDNA 3 (Nagai et al., 2001). The PCR product was inserted into 5'NheI and 3'BglIII sides of rAAV EYFP-Nuc to yield rAAV Inverse Pericam NLS (rAAV IP NLS). The following primers were used: 5' TTT TGC TAG CGC CAC CAT GAA GAG G 3' (forward) and 5' GAT GAC AGC AAA GAG ATC TTC T 3' (reverse).

4.3.5 Nuclear Ca²⁺-indicator: rAAV GCaMP 1.6 NLS

5'NheI and 3'BglII sides were added by PCR to the entire coding sequence of pN1 GCaMP 1.6 (Ohkura et al., 2005). The PCR product was inserted into 5'NheI and 3'BglII sides of rAAV EYFP-Nuc to yield rAAV GCaMP 1.6 NLS. The following primers were used: 5' TTA GTG AAC CGT CAG ATC CGC TAG 3' (forward) and 5' AGG CAA GAT CTC TTC GCT GTC ATC 3' (reverse).

4.3.6 Nuclear Ca²⁺-indicator: rAAV GCaMP 2.0 NLS

5'AgeI and 3'BglII sides were added by PCR to the entire coding sequence of pN1 GCaMP 2.0 (Tallini et al., 2006). The PCR product was inserted into 5'AgeI and 3'BglII sides of rAAV EYFP-Nuc to yield rAAV GCaMP 2.0 NLS. The following primers were used: 5' TTA ACC GGT GGA TCC CGC CAC CAT GCG GGG 3' (forward) and 5' AGC CAG ATC TCT TCG CTG TCA TCA 3' (reverse).

4.3.7 Nuclear localized EYFP: rAAV EYFP Cherry Nuc

5'BspEI and 3'XhoI sides were added by PCR to the entire coding sequence of pBS34 mCherry (Shaner et al., 2004). Additionally, five amino acids linker sequences (GGSGG) were added to the 3' and 5' end of the PCR product by PCR. The PCR product was inserted into 5'BspEI and 3'XhoI sides of rAAV EYFP-Nuc to yield rAAV EYFP Cherry Nuc. The following primers were used: 5' TAT CCG GAA GAT CTG GTG GCA GCG GTG GCA TGG TGA GCA AGG GCG AG 3' (forward) and 5' GCA AGC TTC TCG AGT GCC ACC GCT GCC ACC CTT GTA CAG CTC GTC CAT GC' (reverse).

4.3.8 Nuclear localized EYFP: rAAV EYFP-Nuc Cherry

5'BglII and 3'HindIII sides were added by PCR to the entire coding sequence of pBS34 mCherry (Shaner et al., 2004) and additionally, two five amino acids linker sequences (GGSGG) were added to the 3' and 5' end. The PCR product was inserted in frame into 5'BamHI and 3'HindIII sides of rAAV EYFP-Nuc to yield rAAV EYFP-Nuc Cherry. The 5'BamHI side of rAAV EYFP-Nuc was deleted by ligation with 5'BglII site of the PCR product. Primers see section 4.3.7.

4.3.9 Nuclear Ca²⁺-indicator: rAAV GCaMP2 NLS Cherry

Coding sequence of rAAV GCaMP2 NLS were digested and in frame inserted into 5' AgeI and 3' BglII sites of rAAV EYFP-Nuc Cherry to yield rAAV GCaMP2 NLS Cherry.

4.3.10 Nuclear Ca²⁺/CaM buffer: pM13 NLS VP16 and p2xM13 NLS VP16

The Ca²⁺-indicator pN1 GCaMP 1.3 (Nakai et al., 2001) were used as template to amplify the chicken smooth muscle M13 peptide and parts of the cpEGFP. Either one or two copies of the PCR product were inserted into the pVP16 AD cloning vector (BD Biosciences, Clontech) to yield pM13 NLS VP16 and p2xM13 NLS VP16 (Zhang et al., 2006).

4.3.11 Nuclear Ca²⁺/CaM buffer: rAAV (2x) M13 NLS VP16 myc

5' BglII and 3' XbaI sites were added by PCR to the entire coding sequence of either pM13 NLS VP16 or p2xM13 NLS VP16. Both PCR products were cloned into rAAVmyc to yield either rAAV M13 NLS VP16 myc or rAAV 2xM13 NLS VP16 myc. The following primers were used: 5' TTT GGA GGA GAT CTA AGC TAG CGC 3' (forward) and 5' CAT TAT CTA GAA GCT TCT GCA GAC 3' (reverse)

4.3.12 Nuclear Ca²⁺/CaM buffer: rAAV (2x) M13 NLS myc

5' BamHI and 3' XbaI sites were added by PCR to the entire coding sequence of either pM13 NLS VP16 or p2xM13 NLS VP16. Both PCR products were cloned into rAAVmyc to yield either rAAV M13 NLS myc or rAAV 2xM13 NLS myc. The following primers were used: 5' TCC TCG GAT CCA GAA GTA GTG AAG 3' (forward) and 5' TTC CTA GCT CTA GAG TCC AGA TCG 3' (reverse)

4.4 Cloning of Ca²⁺-indicators and Ca²⁺/CaM buffer (transgenic flies)

To generate a transgenic fly expressing the nuclear localised Ca²⁺-indicator, the Gal4/UAS (Brand and Perrimon, 1993) system was used to direct the expression of the indicator to specific cells of interest. The embryo injection to generate the transgenic flies was done by Best Gene Company (Chino Hills, California) and at least five independent transformants expressing the gene of interest heterozygous were sent back to the lab.

4.4.1 Nuclear Ca²⁺-indicator: UAS GCaMP NLS

The coding sequence of GCaMP NLS blunt (see section 4.3.1) was inserted into 5'BglII and 3'NotI sites of UAS injection vector to yield UAS GCaMP NLS. The 5'BglII side of UAS injection vector was deleted by ligation with the 5'BamHI site of GCaMP NLS blunt.

4.4.2 Nuclear Ca²⁺-indicator: UAS GCaMP2 NLS Cherry

Coding sequence of rAAV GCaMP2 NLS Cherry were inserted into 5'BamHI and 3'EcoRI sides of pCR blunt vector (Invitrogen- Zero Blunt PCR cloning kit) to yield GCaMP2 NLS Cherry blunt. Coding sequence of GCaMP2 NLS Cherry blunt was inserted into 5'BglII and 3'NotI sites of UAS injection vector to yield UAS GCaMP2 NLS Cherry. The 5'BglII side of UAS injection vector was deleted by ligation with the 5'BamHI site of GCaMP2 NLS Cherry blunt.

4.4.3 Nuclear Ca²⁺/CaM buffer: UAS 2xM13 NLS myc

Coding sequence of rAAV 2xM13 NLS myc were inserted into 5'BamHI and 3'EcoRI sides of pCR blunt vector (Invitrogen- Zero Blunt PCR cloning kit) to yield 2xM13 NLS myc blunt. Coding sequence of 2xM13 NLS myc blunt was inserted into 5'BglII and 3'NotI sites of UAS injection vector to yield UAS 2xM13 NLS myc. The 5'BglII side of UAS injection vector was deleted by ligation with the 5'BamHI site of 2xM13 NLS myc blunt.

4.4.4 Nuclear Ca²⁺/CaM buffer positive control: UAS CaMBP4 myc

5'NheI, 5'BamHI and 3'BglII sides were added by PCR to the entire coding sequence of rAAV CaMBP4 flag (Zhang et al., 2007). CaMBP4 consists of four copies of the rabbit skeletal muscle M13 peptide (Wang et al., 1995). The PCR product was inserted into 5'NheI and 3'BamHI sides of rAAV 2xM13 NLS myc to yield rAAV CaMBP4 myc. The entire coding sequence of rAAV CaMBP4 myc was inserted into 5'BamHI and 3'EcoRI sides of pCR blunt vector (Invitrogen- Zero Blunt PCR cloning kit) to yield CaMBP4 myc blunt. Subsequently, the coding sequence of CaMBP4 myc blunt was inserted into 5'BglII and 3'NotI sites of UAS injection vector to yield UAS CaMBP4 myc. The 5'BglII side of UAS injection vector was deleted by ligation with the

5'BamH1 site of CaMBP4 myc blunt. The following primers were used: 5' AAT TGC TAG CGG ATC CCC CAT GGG ACC C 3' (forward) and 5' CGA TAG ATC TGT AGT CAC TGC C 3' (reverse).

4.4.5 Nuclear Ca²⁺/CaM buffer negative control: UAS mM13 NLS myc

A negative control were designed by Dr. Carla Margulies and synthesised by the GeneArt Company. The original 2xM13 NLS myc was modified by three amino acid substitutions in both copies of M13 (first M13: W11E, V18K and L24R; second M13 W62E, V69K and L75R) and by deletion of the first Xho1 site within the coding sequence UAS 2xM13 NLS myc. The synthesised sequence of pGA4 mut 2xM13 was inserted into 5'NheI and 3'XhoI sites of rAAV 2xM13 NLS myc to yield rAAV mut 2xM13 NLS myc and now named mM13 NLS myc. Coding sequence of rAAV mM13 NLS myc were inserted into 5'BamHI and 3'EcoRI sides of pCR blunt vector (Invitrogen- Zero Blunt PCR cloning kit) to yield mM13 NLS myc blunt. Coding sequence of mM13 NLS myc blunt was inserted into 5'BglII and 3'NotI sites of UAS injection vector to yield UAS mM13 NLS myc. The 5'BglII side of UAS injection vector was deleted by ligation with the 5'BamH1 site of mM13 NLS myc blunt.

4.5 Cloning of Ca²⁺-indicators (transgenic hydra)

To generate a transgenic hydra expressing the nuclear and cytoplasmic Ca²⁺-indicator GCaMP, embryo injection at two to eight cell stage were done as described (Wittlieb et al., 2006).

4.5.1 Nuclear/ cytoplasmic Ca²⁺-indicator: hyGCaMP and hyGCaMP NLS

5'NheI, 3'BglII and 3'EcoRI sides were added by PCR to the entire promoter sequence of hoTG actin EGFP (Wittlieb et al., 2006). The PCR product was inserted into 5'XbaI and 3'EcoRI to yield ΔXbaI hoTG actin. The 5'XbaI side of hoTG actin EGFP vector was deleted by ligation with the 5'NheI site of the PCR product. A MCS containing additional restriction sites was inserted into 5'BglII and 3'EcoRI sides to yield ΔXbaI hoTG actin MCS. The following primers were used for the MCS: 5' GAT CTA GCT TCG CTA GCT GCA GTC GAC GGT GGA TCC ACC TAA G 3' (forward) and

5' GAT CTA GCT TCG CTA GCT GCA GTC GAC GGT GGA TCC ACC TAA G 3'
(reverse).

Due to AT-rich genome of *H. vulgaris* the entire coding sequence of pN1 GCaMP NLS (see section 4.3.1) was optimised by the Operon Company according to NCBI taxonomy browser to yield pPCR-Script GCaMP NLS. 5'NheI and 3'BamHI sides were added to the ends of the synthesised gene and additionally, a BglIII side upstream of the nuclear localisation signal was created. The optimised sequence of pPCR-Script GCaMP and pPCR-Script GCaMP NLS were inserted into 5'NheI and 3'BamHI sides of Δ XbaI hoTG actin MCS to yield Δ XbaI hoTG actin GCaMP and Δ XbaI hoTG actin GCaMP NLS (named here hyGCaMP and hyGCaMP NLS).

4.5.2 Nuclear Ca²⁺-indicator: hyGCaMP NLS mars

5'BglIII and 3'EcoRI sides were added by PCR to the entire coding sequence of mRFPmars (Muller-Taubenberger et al., 2006) and additionally, a five amino acids linker sequence (GGSGG) was also added to the 5' end. The PCR product was inserted in frame into 5'BamHI and 3'EcoRI sides of hyGCaMP NLS to yield hyGCaMP NLS mars. The 5'BamHI side of hyGCaMP NLS was deleted by ligation with the 5'BglIII site of the PCR product. The following primers were used: 5' TAT AGA TCT GGT GGC AGC GGT GGC ATG GCA TCA TCA GAA GAT G 3' (forward) and GGT AGA CAT TCA ACA GGT GCA TAA GAA TTC GCC 3'(reverse).

4.5.3 Cytoplasmic Ca²⁺-indicator: hyGCaMP mars

The PCR product of mRFPmars (see section 4.5.2) was inserted in frame into 5'BamHI and 3'EcoRI sides of pPCR-Script GCaMP to yield pPCR-Script GCaMP mars. Subsequently, the entire coding sequence of pPCR-Script GCaMP mars was inserted into 5'NheI and 3'EcoRI sides of hyGCaMP to yield hyGCaMP mars.

4.6 Fruit fly: culture, *in vivo* imaging and behaviour assay

4.6.1 Fruit fly: culture and genetics

Flies were cultured on standard medium at 25°C, 60% relative humidity. Standard medium was made according to standard medium used at Bloomington *Drosophila*

stock centre (homepage http://flystocks.bio.indiana.edu/Fly_Work/media-recipes/media-recipes.htm). Standard medium: 8g/l agar, 18g/l yeast, 10g/l soy flour, 80g/l yellow cornmeal, 22g/l light corn syrup, 80g/l malt extract and 6,25ml/l propionic acid.

For immunostaining in larvae, flies carrying UAS transgenes (listed above) were crossed with muscle specific driver line (Gal4 MHC). For live imaging in larvae, flies carrying UAS transgenes containing GCaMP (Wang et al., 2003) or GCaMP NLS were crossed with motoneurons specific (Gal4 OK6) driver lines. 3rd instar larvae were used for staining as well as for imaging.

For *in vivo* imaging in adult flies, flies carrying UAS transgenes containing GCaMP (Wang et al., 2003) or GCaMP NLS were crossed with mushroom body specific driver line Gal4 MB247 (Dr. A. Fiala, Würzburg, Germany). New hatched flies (female) were collected and cultured for additional 5-6 days on standard medium at room temperature and transferred over night to 25°C before used next day for imaging.

For the odour avoidance assay, all transgenic flies were outcrossed into 2U wild-type (Dr. T. Tully, Cold Spring Harbor, NY) background for at least six generations by standard *Drosophila* genetics. Flies carrying UAS transgenes containing 2xM13 NLS myc or 2U (wild-type) were crossed with heat shock driver line P26 (Xia et al., 2005). Flies were kept on standard medium at 18°C and 70% relative humidity to prevent leaky expression. Two to three days after hatching, flies were collected for heat shock and training. Heat shock induction was carried out according to an established protocol with same hs-GAL4 driver line (Xia et al., 2005).

4.6.2 Fruit fly: immunostaining and live imaging of 3rd instar larvae

To test the expression level of the transgenic lines generated in this study immunostaining of larvae were done. Preparation were done as described (Stewart et al., 1994; Sigrist et al., 2000). Briefly, third instar larvae were dissected by making a longitudinal mid-dorsal incision and pinning the cuticle flat in haemolymph-like saline HL0 (HL3, Ca²⁺ free) solution. The internal organs were carefully removed to expose the body-wall muscles and the nervous system. Larvae preparations were incubated in fixative solution for 10min at RT. Larvae preparations were washed in *Drosophila* larvae washing buffer (PBST) at RT. After incubation with 5% normal goat serum (NGS) for

1h, primary antibody (diluted in *Drosophila* antibody dilution buffer) was added and kept overnight at 4°C. Next day, larvae preparations were washed again in PBST and secondary antibody (diluted in *Drosophila* antibody dilution buffer) was added and incubated for 1h at RT. Finally, larvae preparations were counterstained and mounted in VECTASHIELD® containing DAPI (1.5µg/ml). Larvae preparations were imaged using a Leica SP2 confocal microscope with an HCX PL APO CS 40x 1.25 oil UV objective (Leica Microsystems GmbH, Wetzlar, Germany). Confocal z-stacks were processed using ImageJ and Adobe Photoshop software.

To test the brightness and kinetics of UAS GCAMP NLS Ca²⁺-imaging were done. The preparation of the larval brain are in the beginning similar to steps as described (Stewart et al., 1994; Sigrist et al., 2000). Briefly, third instar larvae were dissected by making a longitudinal mid-dorsal incision and pinning the cuticle flat in haemolymph-like saline HL0 (HL3, Ca²⁺ free) solution. The internal organs were carefully removed to expose the body-wall muscles and the nervous system. The nervous system were transferred to the perfusion chamber (LIS, Reinach, Switzerland) and completely submerged with continuously flowing (1.0 ml/min) HL0 solution. A small metal ring on top of the larval brain was used to reduce movement artefacts. Larval brains were imaged using a Leica SP2 confocal microscope with an HCX PL APO CS 40x 1.25 oil UV objective (Leica Microsystems GmbH, Wetzlar, Germany). Time series as well as confocal z-stacks were processed using ImageJ, Windows Excel and Adobe Photoshop software. $\Delta F/F$ was calculated as $\Delta F/F = (F - F_0)/F_0$. F= fluorescence and F₀= baseline fluorescence corresponding to the average fluorescence over a 60 sec window before stimulation.

4.6.3 Fruit fly: behaviour assay

Olfactory associative learning was measured by training 2–3 days old flies with a Pavlovian conditioning procedure (Tully and Quinn, 1985). Groups of about 60 flies are placed in the training chamber with air drawn through the chamber at 750 ml/min. The flies are exposed to this novel environment for 90 seconds. Flies received one training session, during which they were exposed for 60sec sequentially to one odour (conditioned stimulus, CS+, 3-octanol (OCT) or 4-methyl-cyclohexanol (MCH)) paired

with 60V electric shock (US) and then a second odour (unconditioned stimulus, CS-, OCT or MCH) without US. The 60V electric shock is delivered in 1.5 sec pulses with 4.5 sec pauses.

Conditioned odour avoidance was tested immediately after training. During testing, flies were exposed simultaneously to the CS+ and CS- in a T-maze for 2 min. Then, flies were trapped in either T-maze arm, anaesthetized, and counted. From this distribution, a performance index (PI) was calculated as the number of flies avoiding the shocked odour minus that avoiding the non-shocked odour divided by the total number of flies and finally multiplied by 100. A equal distribution (no learning) yielded a PI of 0 and 100% distribution away from the CS+ yielded a PI of 100 (Xia et al., 2005). The pure odours were diluted 1.5:1000 (OCT) and 1:1000 (MCH) in mineral oil. To eliminate naive odour bias, experiments are performed in a counterbalanced design and averaged, with one group of flies used in the calculation of the PI being trained to the first odour and a second group to the second odour.

24h memory was evaluated after spaced or massed training, which induces strong, long-lasting memory for conditioned avoidance (Tully et al., 1994). Spaced training consists of ten cycles of one-session training, where a 15 minutes rest interval is introduced between each session. Massed training consists of ten cycles of one-session training, where one session immediately follows the previous one. Then flies were tested for memory retention of conditioned avoidance at the choice point of the T-maze after one day. Performance index was calculated as described before.

4.6.4 Fruit fly: *in vivo* imaging

Functional imaging procedures were similar to those already described (Yu et al., 2004; Yu et al., 2005). Flies were immobilized in culture bottle on ice without CO₂ anesthesia and mounted in blue pipette tips and their exposed heads secured to the tip opening with silicon cement. The head was covered with polyethylene foil, where which was sealed against the cuticle with silicone. A small area of foil and cuticle was removed from the top of the head capsule and this allowed optical access to the mushroom bodies. The brain was immediately bathed with Ringer solution. Tracheal air sacks and glands covering the brain were removed from head capsule (Riemensperger et al., 2005).

Finally, flies were mounted beneath a 20x objective (NA = 0.9) on an upright microscope (BX51WI, Olympus, Hamburg, Germany) equipped with a CCD camera (Photometrics Coolsnap HQ, Roper Scientific, Ottobrunn, Germany) connected through a software interface (Metafluor, Universal Imaging Systems and Molecular Devices, Downington PA, USA) to a computer monitor. Excitation light was generated by a monochromator coupled to a light source with a 75W Xenon arc lamp (Optoscan and Optosource, Cairn, Faversham, UK). UAS GCaMP and UAS GCaMP NLS were excited at 480nm with a bandwidth of 20nm through a BA470-490 filter (Olympus) and emission was passed through a BA510-550 filter before collection at the CCD chip. Due to strong photoisomerization of GCaMP, experiments were performed at a constant imaging rate (2Hz). A constant air stream was guided through a Pasteur pipette with the tip placed at a distance of 5mm from the fly's antennae. The pure odours were delivered a rate of 1ml/s. Odour (OTC 10^{-1}) was spread on a small piece of filter paper inside of a syringe barrel and the syringe barrel was placed in line with the pressurized air (Riemensperger et al., 2005). Electric shock pulses were applied to the fly's abdomen. A total of 10 pulses of electric shock at 90V were delivered with each shock lasting between 50ms and 300ms with 500ms rest interval. Time series were processed using Metafluor. Subsequently, analysis was done using Windows Excel and Adobe Photoshop software. $\Delta F/F$ was calculated as $\Delta F/F = (F - F_0)/F_0$. F= fluorescence and F_0 = baseline fluorescence corresponding to the average fluorescence over a 60 sec window before stimulation.

4.6.5 Fruit fly: whole mount immunostaining of adult brains

Fly brains were prepared similar as described (Krashes et al., 2007). Briefly, fly brains were dissected in ice-cold Schneider's Drosophila Medium (Gibco Invitrogen, Gaithersburg, MD, USA) and incubated in fixative solution overnight at 4°C. Brains were washed in Drosophila washing buffer (PAT) at RT. After incubation with 3% normal goat serum (NGS) for 1h, primary antibody (diluted in Drosophila antibody dilution buffer) was added and kept overnight at 4°C. Next day, brains were washed again in PAT and secondary antibody (diluted in Drosophila antibody dilution buffer) was added and kept overnight at 4°C. Next day, brains were washed again in PAT overnight. Finally, brains were counterstained and mounted in VECTASHIELD® containing DAPI

(1.5 μ g/ml). Brains were imaged using either Leica SP2 confocal microscope with HCX PL APO CS 40x 1.25 oil UV objective (Leica Microsystems GmbH, Wetzlar, Germany) or Zeiss LSM 5 Exciter with Zeiss 40x EC Plan-NEOFLUAR objective (Zeiss Application Center, Heidelberg). Confocal z-stacks were processed using ImageJ and Adobe Photoshop software.

4.7 Hippocampal neurons: culture and *in vitro*, *in vivo* imaging

4.7.1 Hippocampal neurons: culture and stimulation of primary

The procedure used to isolate and culture hippocampal neurons has been described previously (Bading and Greenberg, 1991; Bading et al., 1993, Weislogel, et al. 2003). Briefly, hippocampal neurons from newborn C57Bl6J mice (Charles River, Sulzfeld, Germany) were cultured in Neurobasal media (Invitrogen, Gaithersburg, MD, USA) containing 1% rat serum, B27 (Invitrogen, Gaithersburg, MD, USA), and penicillin and streptomycin (Sigma). Hippocampal neurons from newborn Sprague-Dawley rats were prepared in the same way with the exception that the growth media was with B-27 serum-free supplement (Invitrogen GmbH, Karlsruhe, Germany). Neurons were infected with rAAVs after 4 days *in vitro* (DIV) and stimulations were done at 10-12 DIV when transgene protein expression has peaked to remain at stable level as described (Zhang et al., 2007). Action potential bursting was induced by treatment with the GABA_A receptor antagonist Bicuculline (50 μ M) as described previously (Hardingham et al., 2001; Arnold et al., 2005).

4.7.2 Hippocampal neurons: immunostaining of dissociated cells

Primary hippocampal neurons were incubated in fixative solution for 15 min at RT. Cells were washed in 1xPBS at RT. After incubation with blocking buffer for 1h, primary antibody (diluted in antibody dilution buffer) was added and kept overnight at 4°C. Next day, cells were washed again in 1xPBS and secondary antibody (diluted in antibody dilution buffer) was added and incubated for 1h at RT. Finally, cells were counterstained with nuclear marker Hoechst 33258 (Invitrogen), Moviol (Calbiochem) mounted. Cells were imaged using a Leica SP2 confocal microscope with an HCX PL APO CS 40x 1.25 oil UV objective (Leica Microsystems GmbH, Wetzlar, Germany). Confocal z-stacks

were processed using ImageJ and Adobe Photoshop software.

4.7.3 Hippocampal neurons: western blot analysis of dissociated cells

For sodium dodecyl sulfate poly acrylamide gel-electrophoresis (SDS-PAGE) neurons were lysed by adding 200 μ l pre-heated 1xLaemmli and transferred into Eppendorf tubes. Additionally, samples were boiled for 5 min to denature all protein. Sample were loaded on 12% SDS poly acrylamide gels and were run at 35mA/gel for 90min. Proteins were transferred directly onto a nitrocellulose membrane with a pore size of 0.45 μ m (Schleicher & Schuell) in a wet transfer chamber for 1.5 hours at a constant potential of 20V. As control, membrane was counterstained with Ponceau red (Serva) for 5min. After incubation with Western plot blocking solution for 1h primary antibody (diluted in Western plot blocking solution) was added and kept overnight at 4°C. Next day, membrane was washed with PBST. The secondary antibody (diluted in Western plot blocking solution) was applied for 30 min and then washed off with PBST. Finally, membrane was subjected to an enhanced chemiluminescence solution (ECL, Amersham) and afterward exposed to Kodak Hyperfilm for the desired time. Films were developed in a Chemiluminescence Film developer M35M-Omat Processor (Kodak).

4.7.4 Hippocampal neurons: preparation and infection of cultured brain slice

The brain slice culture technique represents a simple but effective procedure to maintain *in vitro* nervous tissue. 5-6 days old newborn Sprague Dawley rats (Charles River, Sulzfeld, Germany) were used for the slice cultures. The procedure used to isolate and culture hippocampal brain slices has been described previously (Stoppini et al., 1991). Briefly, brain slices were cultured on 0.4 μ m pore size membranes supplied by Millipore (Billerica, Massachusetts, USA) in a humidified atmosphere of 5 % CO₂ at 37 °C. A half OTC medium change was performed every third day. Brain slices were infected either with nuclear Ca²⁺-indicator (rAAV GCaMP 1.6 NLS, rAAV GCaMP 2.0 NLS, rAAV GCaMP2 Cherry) or nuclear localized EYFP (rAAV EYFP-Nuc) at 4 or 5 DIV. A total volume of 2,5 μ l containing about 1x10¹¹ genomic virus particles were added directly on top of the slice preparation. Ca²⁺ live imaging was done 10 days after virus application when transgene protein expression has peaked to remain at stable level. Slices were stimulated either with 50 μ M Bicuculline or 50mM KCl, (see section 1.5.1).

Additionally, slices were fixed over night in fixative solution and counterstained with the nuclear marker Hoechst 33258 (Invitrogen).

4.7.5 Hippocampal neurons: *in vivo* injection and slice preparation of juvenile rats

Nuclear Ca^{2+} -indicators (rAAV IP NLS, rAAV GCaMP 1.6 NLS, rAAV GCaMP 2.0 NLS) were delivered by stereotaxic injection (Kopf Instruments, Tujunga, CA) into the hippocampus of Sprague Dawley rats (Charles River Breeding Laboratories) at P23 weighing ~44g as described previously (Cetin et al., 2006). Animals were anesthetized intraperitoneal with sleep-mix. A total volume of $3\mu\text{l}$ containing about 2×10^9 genomic virus particles were injected unilaterally at flow rate of 200 nl/min using a microprocessor-controlled mini-pump (World Precision Instruments, Sarasota, FA). The following coordinates relative to Bregma were: anteroposterior, -4.3 mm; mediolateral, -4.1 mm; dorsoventral (2xlineshot), -3.6 and -3.9 mm from the skull surface. After operation, animals were antagonised by wake up mix treatment, applied subcutaneously. Animals had free access to food and water and were housed under diurnal lighting conditions. At P35-39, rats were anaesthetized by inhalation and killed by decapitation. The brain was rapidly removed and submerged in ice-cold slicing solution. $300\mu\text{m}$ thick acute slices were cut using a vibratome (CU65 Cooling Unit & HM650V Vibratome, Microm, Walldorf, Germany) in slicing solution maintained at 0°C .

Hippocampii were dissected out of each slice and transferred to a holding chamber containing artificial cerebrospinal fluid. Slices were maintained at 32°C for the first 30 min and then returned to room temperature until used for recording over the subsequent 4h. The experiments were carried out according to ethical guidelines for the care and use of laboratory animals for experiments, and were approved by the local animal care committee (Karlsruhe, Germany).

4.7.6 Hippocampal neurons: *in vivo* injection and slice preparation of adult rats

Nuclear Ca^{2+} -indicator (rAAV GCaMP2 NLS Cherry) and control (rAAV EYFP-Nuc) were delivered by stereotaxic injection (Kopf Instruments, Tujunga, CA) into dorsal hippocampus of male Sprague Dawley rats (Charles River Breeding Laboratories) weighing 200-250g as described previously (Cetin et al., 2006). Animals were

anesthetized intraperitoneal with sleep-mix. A total volume of $3\mu\text{l}$ containing about either 1×10^9 or 1×10^{13} genomic virus particles were injected unilaterally at flow rate of 200 nl/min using a microprocessor-controlled mini-pump (World Precision Instruments, Sarasota, FA). The following coordinates relative to Bregma were: anteroposterior, -3.8 mm; mediolateral, -2.8 mm; dorsoventral, -2.8 to -3.8 mm from the skull surface. After operation, animals were antagonised by wake up mix treatment, applied subcutaneously. Animals had free access to food and water and were housed under diurnal lighting conditions. Three weeks after rAAV delivery when transgene protein expression has peaked to remain at stable level, rat brains were perfused using standard procedures (Klugmann et al., 2005). Briefly, rats were killed by transcardiac perfusion under deep anesthesia with injection of Narkoren ($500\mu\text{l}$ pro 250g). After perfusion with 100ml PBS, brains were fixed by perfusion of 200ml, 10 % buffered neutral formalin, pH 7.4 (Sigma), removed, and postfixed overnight before cryoprotection in 30% sucrose/PBS. Brain slices ($40\mu\text{m}$) were cut at $-15\text{ }^\circ\text{C}$ using a cryostat (Jung Frigocut 2800N Leica) and collected in 1xPBS containing 0.04% thimerosal. Slices were incubated in 1xPBS containing 0.1% Triton X-100 (Merck) for 1h at RT, washed with PBST and finally, counterstained with Hoechst for 5 min. Slices were Moviol (Calbiochem) mounted on slides (Super Frost Plus; Menzel GmbH & Co KG). The experiments were carried out according to ethical guidelines for the care and use of laboratory animals for experiments, and were approved by the local animal care committee (Karlsruhe, Germany).

4.7.7 Hippocampal neurons: patch-clamp recording and Ca^{2+} -imaging of young rats

Patch-clamp recording and Ca^{2+} -imaging of P35 rats was carried out by Dr. Peter Bengtson (IZN). Briefly, single slices were transferred to a recording chamber (PM-1, Warner Instruments, Hamden, CT, USA) and completely submerged with warmed ($32\text{ }^\circ\text{C}$), continuously flowing (2.5 ml/min) ACSF. Patch electrodes (3-4 $\text{M}\Omega$) were made from borosilicate glass (1.5 mm, WPI, Sarasota, FL, USA) and filled with a potassium methylsulphate based solution. Recordings were made with a Multiclamp 700A or 700B amplifier, digitized through a Digidata 1322A A/D converter, acquired and analysed

using pClamp 9 software (Axon Instruments and Molecular Devices, Union City, CA, USA).

Evoked excitatory post-synaptic currents (eEPSCs) were recorded in response to 100 μ s long constant current pulse stimuli (40 to 200 μ A) from constant current bipolar stimulators (A365 stimulus isolators, World Precision Instruments, Sarasota, Florida, USA) connected to the two barrels of theta-glass capillaries (Hilgenberg, Malsfeld, Germany) pulled to a tip of about 4 μ m and filled with ACSF. Stimulators were placed in the stratum radiatum and stratum oriens at a distance of approximately 50 μ m from the apical dendrite toward the CA3 region. High frequency stimulation (HFS) protocols consisted of 100Hz stimulations of specified durations. Such bursts of HFS were repeated at the intervals indicated.

Neurons were viewed with differential interference contrast optics through a 20x (N.A. 0.9) objective on an upright microscope (BX51WI, Olympus, Hamburg, Germany) equipped with a CCD camera (Photometrics Coolsnap HQ, Roper Scientific, Ottobrunn, Germany) connected through a software interface (Metafluor, Universal Imaging Systems and Molecular Devices, Downingtown PA, USA) to a computer monitor. Excitation light was generated by a monochromator coupled to a light source with a 75W Xenon arc lamp (Optoscan and Optosource, Cairn, Faversham, UK). Nuclear Ca^{2+} -indicators were excited at 480nm with a bandwidth of 20nm through a BA470-490 filter (Olympus) and emission was passed through a BA510-550 filter before collection at the CCD chip. Due to strong photoisomerization of nuclear Ca^{2+} -indicators, experiments were performed at a constant imaging rate (2Hz) and only after baseline intensities had stabilized after the onset of imaging. Time series were processed using Metafluor. Subsequently, analysis was done using Windows Excel and Adobe Photoshop software. $\Delta F/F$ was calculated as $\Delta F/F = (F - F_0)/F_0$. F= fluorescence and F_0 = baseline fluorescence corresponding to the average fluorescence over a 60 sec window before the first burst

4.8 Freshwater polyp: culture, microinjection and *in vivo* imaging

The freshwater polyps *H. vulgaris* (AEP strain) were mass-cultured according to standard procedures at 18°C (Wittlieb et al., 2006). Polyps were fed according to the additional experiments with *Artemia salina*. To induce gametogenesis for microinjection

experiments animals were fed daily for 2 weeks and then fed only twice per week. For imaging experiments at least 24h unfed polyps were used.

4.8.1 Freshwater polyp: embryo microinjection

One weeks after gametogenesis induction, testis were detectable and after two weeks oogenesis started. Embryos were removed from females and microinjected with the either hyGCaMP or hyGCaMP NLS expression constructs at the two- to eight-cell stage as described (Wittlieb et al., 2006). Microinjection was done using a fluorescence stereomicroscope (SMZ 1500, Nikon) and micromanipulator (Eppendorf). The construct was injected by using pneumatic pump (PV 820, World Precision). The constructs (0.1 μ l; 0.6 μ g/ μ l) were injected into the embryos. Each embryo was injected only once. During the injection procedure, embryos were kept in hydra medium at RT. Microinjected embryos were transferred to 35mm culture dishes and incubated for 3 weeks at 18°C in hydra medium. After hatching, either hyGCaMP or hyGCaMP NLS expressing cells became visible as small patches in either ectoderm or endoderm or both layers. Polyps expressing homogeneously hyGCaMP or hyGCaMP in ectoderm or endoderm cells were generated by randomly budding.

4.8.2 Freshwater poly: *in vivo* imaging

Polyps expressing homogeneously hyGCaMP or hyGCaMP in ectoderm or endoderm cells were used for Ca²⁺ live imaging. At least 24h before imaging experiments started polyps feeding were stopped to reduce artificial background signals. Young polyps were placed on glass coverslip (\varnothing 18 mm, Carl Roth, Karlsruhe, Germany) covered with hydra medium. Locomotion was reduced by a small metal net on top of the animal. Finally, coverslip was transferred to the perfusion chamber (LIS, Reinach, Switzerland) and placed upon the microscopic stage. Transgenic polyps were imaged using either an confocal spinning disc (ERS-FRET, Perkin Elmer) on inverted microscope (TE2000, Nokia) with a 20x water immersion objective at the Nikon Imaging Center Heidelberg or an inverted non-confocal fluorescence microscope (Axio Observer, Zeiss) with 5x and 10x EC Plan-NEOFLUAR objective at the Zeiss Application Center Heidelberg. Pictures were taken by using either the CCD camera (Orca-ER, Hamamatsu), or the CCD camera (AxioCaM MRm, Zeiss). Confocal time series were processed using

UltraViews software, Perkin Elmer. Non-confocal time series were processed using AxioVision software, Zeiss. Subsequently, analysis was done using ImageJ, Windows Excel and Adobe Photoshop software. $\Delta F/F$ was calculated as $\Delta F/F = (F-F_0)/F_0$. F = fluorescence and F_0 = baseline fluorescence corresponding to the average fluorescence over a 30 sec window.

5 Results

5.1 Visualisation of nuclear Ca^{2+} signals in hippocampal neurons

The main focus of the present study was to visualise changes in nuclear Ca^{2+} concentration *in vivo*. The measurements of nuclear Ca^{2+} concentrations as previously described (Hardingham et al., 2001) were done using the chemically synthesized Ca^{2+} -indicator Fluo-3. However, chemically synthesized Ca^{2+} -indicators have significant limitations. For example, although these indicators are loaded into cells as acetoxymethyl esters, such loading does not enable targeting to specific cells and/or compartments *in vivo*.

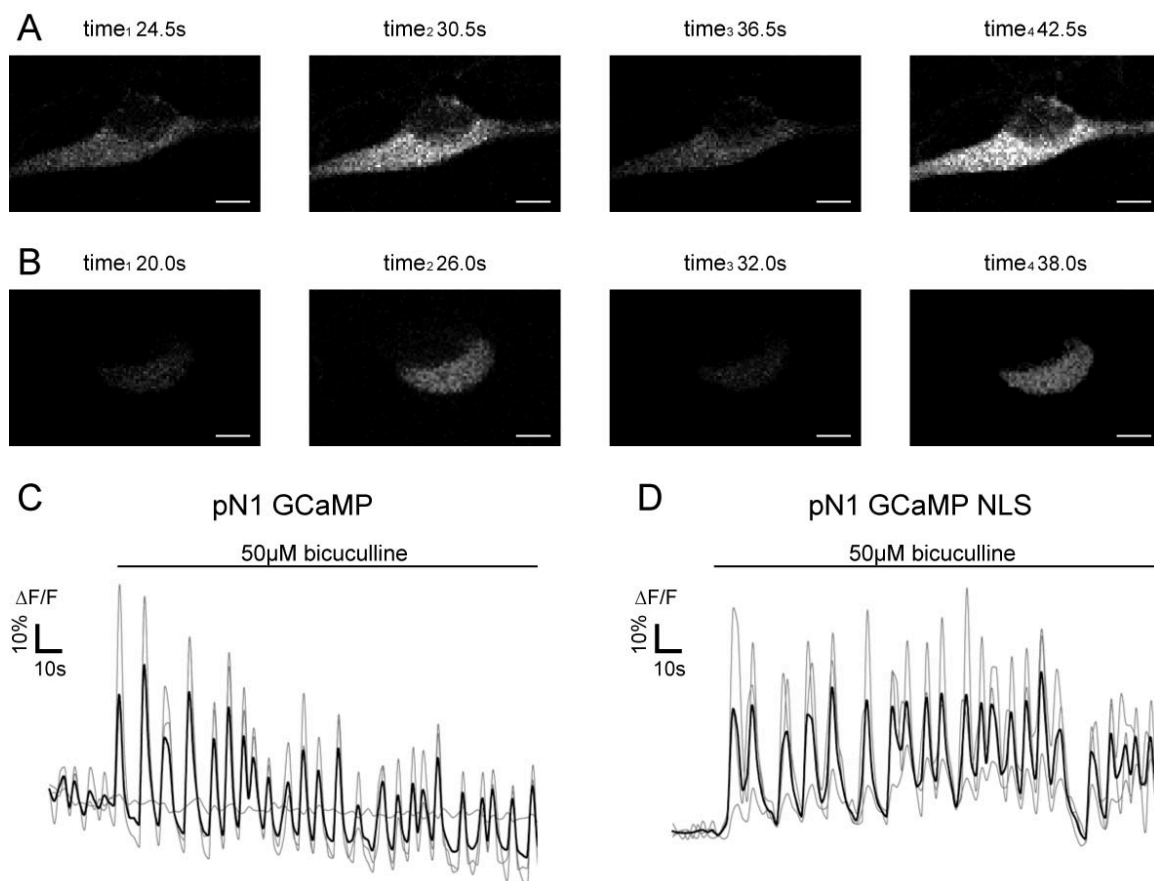


Fig. 7 Ca^{2+} -imaging using recombinant Ca^{2+} -indicators in dissociated cells. Hippocampal neurons were transfected with either pN1 GCaMP (A) or pN1 GCaMP NLS (B). Bursts of action potentials were triggered with the GABA_A receptor antagonist bicuculline ($50\mu\text{M}$). Representative pictures of a time series show changes in fluorescence of neurons expressing the Ca^{2+} -indicators. Scale bars are $5\mu\text{m}$ (A) and $4\mu\text{m}$ (B). Analyses of time series are shown for pN1 GCaMP (C) and for pN1GCaMP NLS (D). Images were taken every 2 sec. The bold black line indicates the average of $n=3$ cells.

To monitor Ca^{2+} signals in distinct cellular compartments, particularly in the cell nucleus, a nuclear localization signal was fused to the amino terminus of pN1 GCaMP (Nakai et al., 2001). Confocal microscopy analysis of neurons expressing either pN1 GCaMP or pN1 GCaMP NLS were done to demonstrate the localisation of the indicators (Fig. 7A and 7B). No differences in changes of due to the amino terminal modification in pN1 GCaMP NLS were observed in comparison with pN1 GCaMP in neurons. Oscillatory Ca^{2+} changes with a frequency of 0.1Hz induced by application of $50\mu\text{M}$ bicuculline, a GABA_A receptor blocker, was previously visualised using Fluo-3 (Hardingham et al., 2001) (Hardingham et al., 2001) in neural networks composed mostly of glutamatergic excitatory neurons (~90%) as well as some GABAergic inhibitory interneurons (~10%). Comparing the results obtained with Fluo-3 to those obtained with the recombinant Ca^{2+} -indicators it could be shown that both pN1 GCaMP and pN1 GCaMP NLS were suitable for monitoring calcium oscillations of 0.1 Hz. The average of amplitudes, $\Delta\text{F}/\text{F}$, after bicuculline stimulation measured in neurons expressing pN1 GCaMP was in % = 27.1 ± 32.0 . The average peak time from begin of stimulation to peak of the first maximum was in sec = 2.0 ± 0.0 (n= 3 cells, Fig. 7C). In neurons expressing pN1 GCaMP NLS $\Delta\text{F}/\text{F}$ was in % = 46.7 ± 30.3 . The peak time was in sec = 4.5 ± 1.0 (n = 3 cells, Fig. 7D). Due to the temperature sensitivity of pN1 GCaMP, neurons were cultured after transfection at 28°C . No fluorescence signal could be detected in hippocampal neurons transfected either with pN1 GCaMP or pN1 GCaMP NLS incubated at 37°C after transfection (data not shown).

5.2 Blocking nuclear Ca^{2+} /CaM signalling pathway in hippocampal neurons

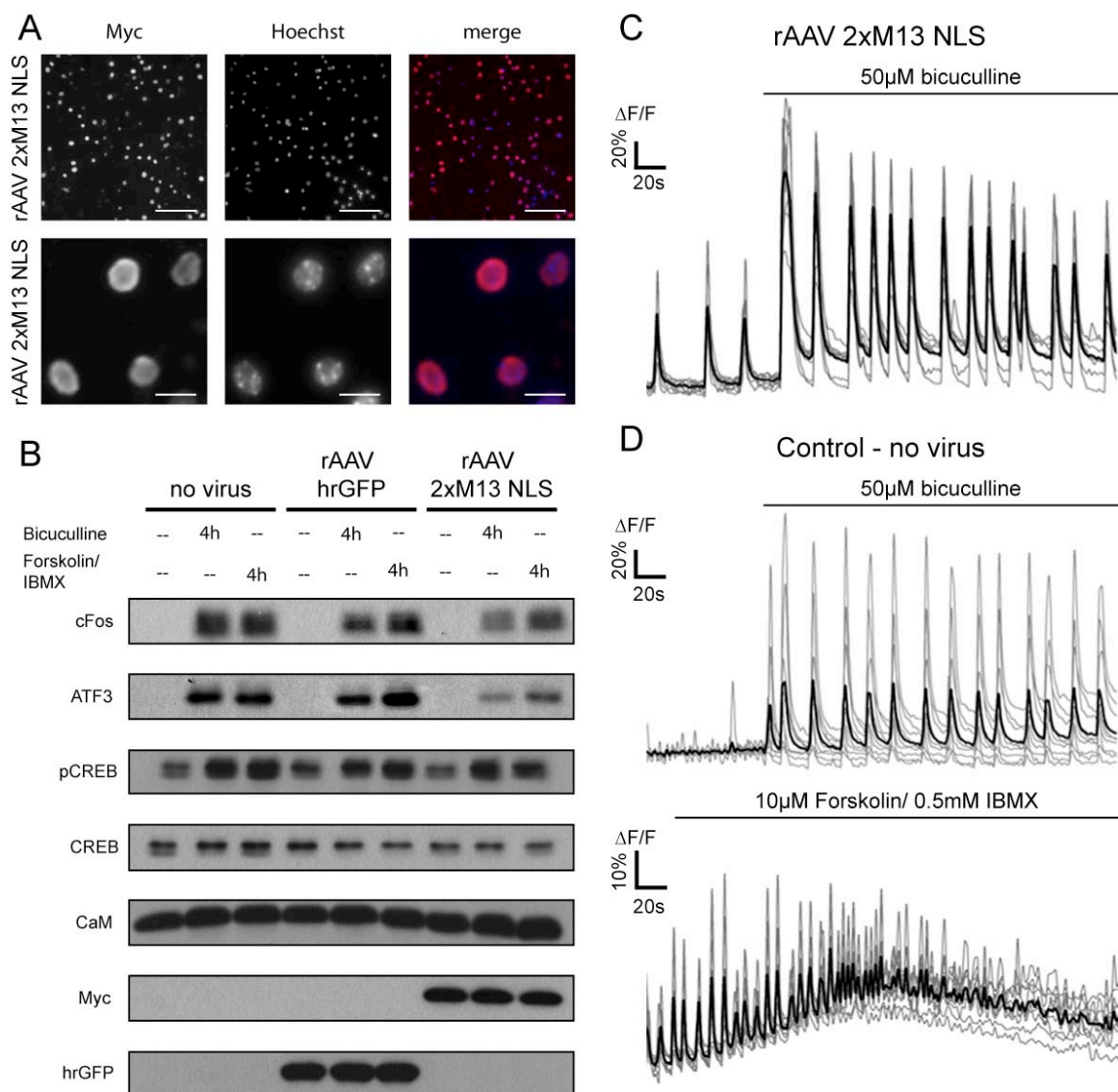


Fig. 8 Characterisation of the Ca^{2+} /CaM inhibitor: rAAV 2xM13 NLS myc. Immunostaining (A), western blot analysis (B) and Ca^{2+} -imaging (C) of hippocampal neurons infected with rAAV expressing 2xM13 NLS myc. The inhibitor is Myc tagged and was detected with Myc antibody. Nuclei of cells were counterstained with Hoechst. Representative overview and detail images are shown. Scale bars are 100 μm (upper panel) and 20 μm (lower panel) (A). Blockade of activity-dependent induction of cFos and ATF3 expression in neurons expressing the inhibitor. Uninfected neurons or neurons infected with rAAVs expressing either 2xM13 NLS myc or hrGFP as control were treated for 4 hrs with bicuculline (50 μM) to induce AP bursting, for 4 hrs with 10 μM Forskolin/ 0.5mM IBMX to increase cAMP concentration, or were left unstimulated. Calmodulin was used as loading control. CREB and pCREB were used as control to show that CREB activation via other pathways was unaffected (B). Time course analyses of changes in fluorescence after stimulation are shown (C, D). No differences were observed between neurons infected with rAAVs expressing 2xM13 NLS myc (C) or uninfected neurons (D). Images were taken every 1.6 sec. The bold black line indicates the average of $n=12$ cells. Western blot data were kindly provided by Dr. B. Buchthal and U. Weiss.

Besides the imaging project a nuclear Ca^{2+} /CaM inhibitor was developed to interfere with nuclear Ca^{2+} signalling. The Ca^{2+} /CaM inhibitor is a nuclear protein that consists of two repeats of the smooth muscle M13 peptide derived from the chicken myosin light chain kinase. The two peptides were separated by a spacer of 26 amino acids, fused to nuclear localization signal (NLS) and for biochemical analysis tagged with Myc epitope. Therefore, the inhibitor was named “2xM13 NLS myc”. Using rAAV-mediated gene transfer, expression of 2xM13 NLS myc was obtained in 80%–95% of the viable hippocampal neurons (Fig. 8A). Expression of the inhibitor in neurons blocks synaptic activity-evoked CREB-mediated gene transcription compared to control. As control noninfected neurons or neurons infected with rAAV hrGFP were chosen. Induction of cFos and ATF3 expression were reduced in neurons infected with rAAV 2xM13 NLS myc to $67.1\% \pm 14.7\%$ (cFos) and $74.6 \pm 7.8\%$ (ATF3) after 4hrs bicuculline ($50\mu\text{M}$) stimulation (Buchthal et al. unpublished data). Induction of cFos and ATF3 expression were also reduced after 4hrs $10\mu\text{M}$ Forskolin/ 0.5mM IBMX stimulation. In contrast to AP bursting after bicuculline stimulation, Forskolin/ IBMX stimulation leads to long lasting elevated nuclear Ca^{2+} level (Fig. 8D), which is sufficient to induce cFos and ATF3 expression. No differences were observed comparing CREB expression in neurons either uninfected or infected. The transcription factor CREB was used as control for virus infection of rAAV hrGFP and rAAV 2xM13 NLS myc. Phosphorylation of CREB at Ser 133 was detected by pCREB antibody. No differences were observed comparing pCREB expression in neurons either uninfected or infected. Therefore, phosphorylation of CREB was not affected in presence of the inhibitor (Fig. 8B). Ca^{2+} live imaging experiments were done to confirm that the inhibitor specifically interacts with the binding partner calmodulin and not binds to other nuclear proteins or buffers nuclear calcium itself. Oscillatory Ca^{2+} changes with a frequency of 0.1Hz induced by application of $50\mu\text{M}$ bicuculline was visualised with Fluo-3. No difference in frequency of the oscillatory Ca^{2+} changes was observed in neurons either infected with the inhibitor (Fig. 8C) or uninfected (Fig. 8D). However, higher amplitudes ($\Delta\text{F}/\text{F}$ in % = 131.9 ± 20.1 n=12cells) were observed in neurons infected with the inhibitor in average compared to amplitudes of uninfected neurons ($\Delta\text{F}/\text{F}$ in % = 46.6 ± 5.1 n=12cells). From these results it cannot be excluded that either the inhibitor or the virus infection itself was

responsible for the increase of amplitudes. Therefore, a control inhibitor was developed that was more similar to rAAV 2xM13 NLS myc. In each peptide of the control inhibitor three charged amino acids responsible for the Ca^{2+} /CaM binding properties of M13 were replaced by uncharged amino acids.

5.3 Visualisation of Ca^{2+} signals in 3rd larvae of *D. melanogaster*

Due to the temperature sensitivity of the nuclear Ca^{2+} -indicator pN1 GCAMP NLS *in vivo* imaging of cellular activity in rodents at physiological temperature was limited to postsynaptic signalling in smooth muscle (Ji et al., 2004). However, any Ca^{2+} signals could not be detected in cultured hippocampal neurons transfected either with pN1 GCAMP or pN1 GCAMP NLS at 37°C.

In contrast, using genetically encoded Ca^{2+} -indicators in the *D. melanogaster* central nervous system provides an excellent system to explore the role of nuclear Ca^{2+} in an intact behaving animal. In 2004, Wang et al. visualised Ca^{2+} signals in the mushroom bodies of *D. melanogaster* crossing UAS GCaMP (Wang et al., 2004) with the MB specific Gal4 driver line, OK107 (Connolly et al., 1996). Since the aim of the study was to monitor nuclear Ca^{2+} signals *in vivo* either direct by using the nuclear Ca^{2+} -indicator or indirect by using the nuclear Ca^{2+} /CaM inhibitor, transgenic flies were engineered based on GCaMP NLS and 2xM13 NLS myc. To direct the expression of the transgenes to cells of interest, the GAL4/UAS-system were used (Brand and Perrimon, 1993).

Because the larval neuromuscular junction has been a simple and useful system to study plasticity, UAS GCaMP NLS was expressed under control of muscle specific Gal4 promoter in larval muscle cells to verify the expression pattern. Confocal microscopy analysis of 3rd instar larvae (Gal4 MHC/ UAS GCAMP NLS) after dissection (Fig. 9A) and GFP staining was done to demonstrate the nuclear localisation of the indicator (Fig. 9B). Due to syncytial character of larval muscle cells no signal in 3rd instar larvae (Gal4 MHC/ UAS GCAMP) was detected expressing GCaMP under control of the muscle specific Gal4 promoter after GFP staining (data not shown). In addition, UAS GCaMP NLS was expressed under control of motoneuron specific Gal4 promoter in neuronal cells of 3rd instar larvae (Gal4 OK6/ UAS GCAMP NLS). The larval brain was removed from

the body-wall muscles and isolated imaged in haemolymph-like saline solution. Single nuclei could be clearly identified by confocal microscopy z-stack analysis (Fig. 9C).

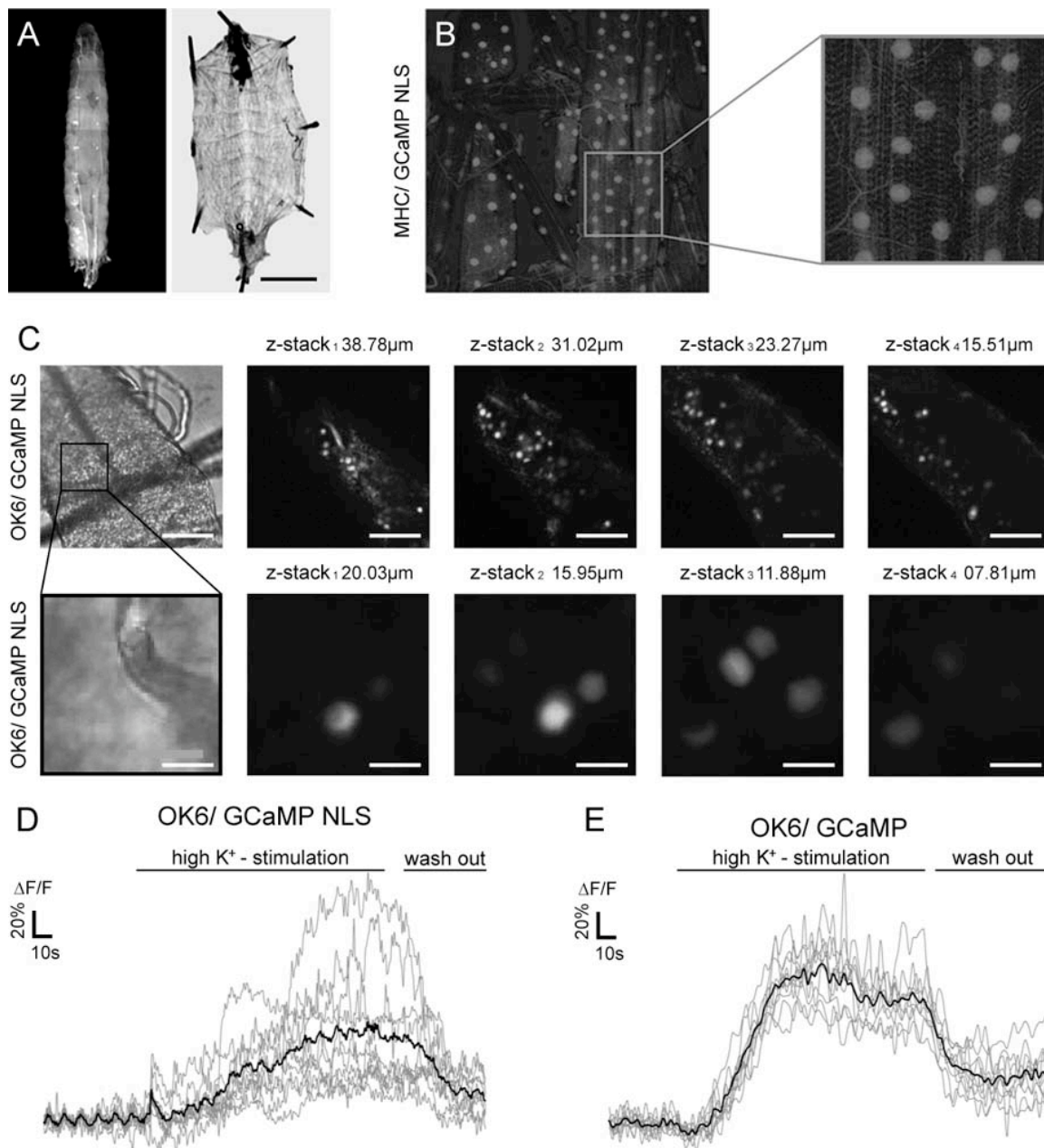


Fig. 9 Characterisation of 3rd instar larvae expressing GCaMP NLS. DIC images of 3rd instar larva before and after dissection. Scale bar is 1mm (A). Immunostaining of 3rd instar larvae expressing GCaMP NLS in muscle cells. GCaMP NLS was detected with GFP antibody (B). 3rd instar larva expressing GCaMP NLS in motoneuron. Representative overview and detailed images of larval ventral cord at 4 different optical sections are shown. Scale bars are 40 μ m and 9 μ m (C). Larvae expressing either GCaMP NLS (D) or as control GCaMP (E) in motoneuron were used for Ca²⁺-imaging. Time course analyses of changes in fluorescence after high K⁺-stimulation (50mM) and subsequent wash out are shown. Images were taken every 1.6 sec. The bold black line indicates the average of n=15 cells.

Next, it was tested whether changes of Ca^{2+} signals expressing UAS GCaMP NLS could be detected in response to high K^{+} -induced membrane depolarization. Therefore, isolated brains of 3rd instar larvae expressing either UAS GCaMP (Gal4 OK6/ UAS GCaMP) or UAS GCaMP NLS (Gal4 OK6/ UAS GCaMP NLS) were used for live Ca^{2+} -imaging. Both UAS GCaMP and UAS GCaMP NLS were suitable for detecting calcium transients in the larval brain in response to high K^{+} -induced membrane depolarization (Fig 9D and 9E). Surprisingly, in motoneurons expressing either UAS GCaMP NLS or UAS GCaMP a sustained Ca^{2+} level after high K^{+} -stimulation was observed, which was never observed in cultured neurons. The average peak time from begin of stimulation to peak of the plateau was in larvae expressing UAS GCaMP NLS in $\text{sec} = 83.3 \pm 22.6$ and in larvae expressing UAS GCaMP in $\text{sec} = 46.2 \pm 4.8$. The average of the sustained Ca^{2+} level was in larvae expressing UAS GCaMP NLS $\Delta\text{F}/\text{F}$ in $\% = 66.9 \pm 45.3$ $n = 15$) and in larvae expressing UAS GCaMP $\Delta\text{F}/\text{F}$ in $\% = 112.7 \pm 19.9$ $n = 15$. The difference observed comparing UAS GCaMP NLS and UAS GCaMP might depend on either expression levels due to different integration sites of the P-element carrying the transgene or due to difficulties to monitor single nuclei over time in a $0.25\mu\text{m}$ optical section. Nevertheless, these results show that UAS GCaMP NLS expressed in 3rd instar larvae is suitable to detect changes in Ca^{2+} level and is exclusively localised to the nucleus. Therefore, the transgenic fly (UAS GCaMP NLS) allows visualising of nuclear Ca^{2+} signals in complex behavioural experiment as, for example, the olfactory avoidance assay (Tully and Quinn, 1985)

5.4 Blocking nuclear Ca^{2+} /CaM signalling pathway in adult flies

Dr. C. Margulies established the classical olfactory avoidance assay (Tully and Quinn, 1985) in the lab, which allowed addressing the question about role on nuclear Ca^{2+} in long-term memory (LTM) in adult flies. All preliminary results obtained from the olfactory avoidance assay (Fig. 10D - 10F) were measured by Dr. C. Margulies.

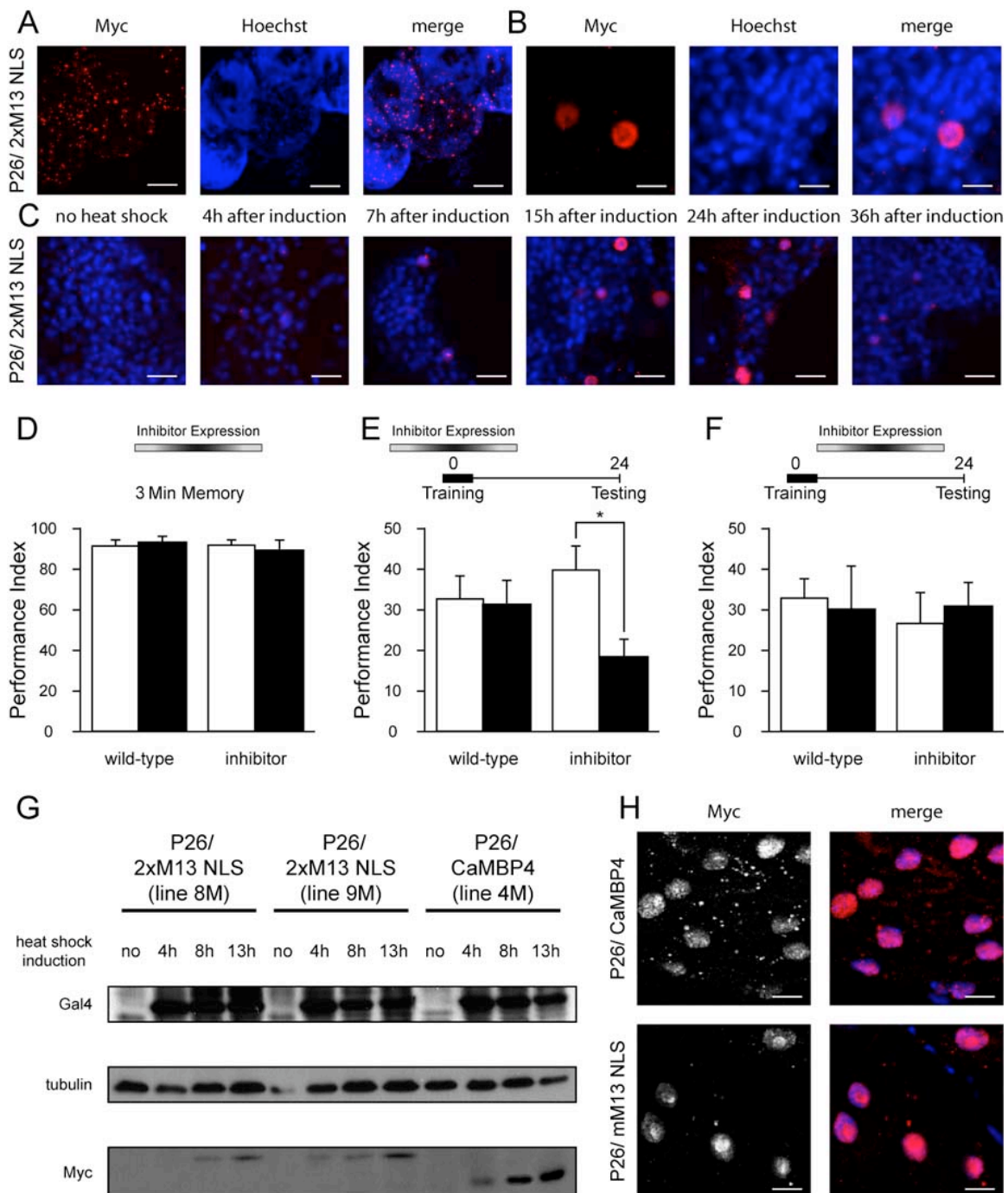


Fig. 10 Blocking of nuclear Ca^{2+} signalling during the acquisition phase of LTM. Immunostaining of a whole mounted fly brain expressing the nuclear Ca^{2+} /CaM inhibitor (2xM13 NLS line 8M). The inhibitor is Myc tagged and was detected with Myc antibody. Nuclei of cells were counterstained with Hoechst. Representative overview (A) and detail images (B) of a brain 15hrs after heat shock induction are shown. Scale bars are $75\mu\text{m}$ (A) and $4\mu\text{m}$ (B). Representative images of a time course of the inhibitor expression level is shown. Scale bars are $9.5\mu\text{m}$ (C). Flies heat-shocked (black bars) or not heat shocked (white bars) were trained in order to test for STM (D) or LTM phenotypes (E, F). Flies expressing the nuclear Ca^{2+} /CaM inhibitor have normal STM. 7 to 10 hours after heat shock, wild-type and transgenic flies were trained with a single training session (lasting 3 minutes) and tested immediately after training (D). Flies expressing the nuclear Ca^{2+} /CaM inhibitor during training have impaired LTM. 7 to 10 hours after heat shock, wild-type and transgenic flies were trained with 5 spaced training sessions and tested 24 hours after training (E). Flies expressing the nuclear Ca^{2+} /CaM inhibitor between training and testing have normal LTM. 4 to 7 hours after heat shock, wild-type and transgenic flies were trained with 5 spaced training sessions and tested 24 hours after training (F). The data represent means (\pm SEM) of at least eight independent PI values. Protein expression of the transgenic flies 2xM13 NLS line 8M, line 9M and line 4M of the transgenic fly CaMBP4 were tested by western blot analysis. The inhibitors are Myc tagged and were detected with Myc antibody. Tubulin was used as loading control and Gal4 as control for the heat shock induction (G). Immunostaining of 3rd instar larva expressing either CaMBP4 or mM13 NLS (positive and negative control for 2xM13 NLS) in muscle cells. Both inhibitors are Myc tagged and were detected with Myc antibody. Nuclei of cells were counterstained with Hoechst. Representative picture of larval muscle cells 15h after heat shock induction are shown. Scale bars are $15\mu\text{m}$ (H). All behavioural data (D-F) were kindly provided by Dr. C. Mareulies.

First, to block nuclear Ca^{2+} /CaM signalling it was determined whether the nuclear Ca^{2+} /CaM inhibitor (UAS 2xM13 NLS myc) was localised in adult flies also exclusively to the nucleus. Flies expressing UAS 2xM13 NLS myc under the control of the Gal4 heat shock promoter P26 (P26/ UAS 2xM13 NLS myc) were dissected 15 hours after a 30-minute heat shock induction of 37°C . Confocal microscopy analysis of whole mount fly brains stained with Myc antibody was done to demonstrate the nuclear localisation of the inhibitor. Nuclei of cells were counterstained with Hoechst (Fig. 10A and 10B). A nuclear staining was neither observed in heat shocked wild type flies (2U) nor in non-heat shocked transgenic flies (P26/ UAS 2xM13 NLS myc) (Bongers et al., 2007). In flies expressing the inhibitor after heat shock, only a few cells within the brain were stained. The staining pattern was observed throughout the entire brain and no obvious clusters could be seen (Fig. 10A). The same results was observed with another UAS 2xM13 NLS myc transgenic fly line based on second independent embryonic injection event and also in flies expressing another transgene UAS GCaMP NLS (Bongers et al., 2007).

A time course of inhibitor expression was done to assess the time window of maximal protein expression (Fig. 10C). The Ca^{2+} /CaM inhibitor was detectable in nuclei of adult flies between 7-24 hours after induction. The results were confirmed by western blot analysis for two lines based on two independent embryonic injection events (6M and 8M). UAS 2xM13 NLS myc were detected 7h after heat shock with Myc antibody in the transgenic line 8M but not in the transgenic line 6M. Antibody against Gal4 was used as control for the heat shock induction and tubulin antibody as loading control (Fig. 10G).

Based on the established assays to generate and measure STM and LTM in *D. melanogaster* (Tully and Quinn, 1985; Tully et al., 1994), the question was addressed whether the transient expression of the nuclear Ca^{2+} /CaM inhibitor (P26/ UAS 2xM13 NLS myc) interferes with memory formation in flies. To exclude genetically caused memory defects due to the injection site of transgene in UAS 2xM13 NLS myc flies short-term memory was tested. Independently of the heat shock, no differences in STM were observed in flies expressing the inhibitor (performance index = non-heat shock 92.5 ± 1.8 and heat shock 90.1 ± 4.2) compared to wild-type flies (performance index = non-heat shock 91.9 ± 3.0 and heat shock 93.5 ± 2.2) (Fig. 10D).

LTM was inhibited in heat shocked transgenic flies (performance index = heat shock 18.2 ± 4.0) compared to heat shocked/ non-heat shocked wild-type (performance index = non-heat shock 32.3 ± 5.3 and heat shock 31.4 ± 5.5), when the nuclear Ca^{2+} /CaM inhibitor was transiently expressed during the time period of acquisition, whereas LTM was not inhibited in non-heat shocked transgenic flies (performance index = non-heat shock 40.8 ± 5.5) (Fig. 10E). Independently of the heat shock, no inhibition of LTM was observed in flies expressing the inhibitor (performance index = non-heat shock 26.9 ± 7.2 and heat shock 31.0 ± 5.4) compared to wild-type flies (performance index = non-heat shock 33.0 ± 4.3 and heat shock 30.4 ± 10.1) at a time period between acquisition and retrieval (Fig. 10F). These data provide evidence for the role of nuclear Ca^{2+} /CaM signalling during the acquisition phase of LTM in flies. To verify these experiments and to confirm the specificity of the M13 interaction, positive and negative control fly lines were generated based on the previously described rAAV mM13 NLS myc and based on a Myc tagged version of the previously published Ca^{2+} /CaM inhibitor rAAV CaMBP4 flag (Wang et al., 1996; Limback-Stokin et al., 2004; Zhang et al., 2007). Protein expression was confirmed by western blot analysis for the transgenic fly lines UAS 2xM13 NLS myc 8M, 9M and the transgenic fly line UAS CaMBP4 myc 4M before heat shock and 4hrs, 8hrs and 13hrs after 30-minute heat shock induction of 37°C (Fig. 10G). Further, UAS mM13 NLS myc and UAS CaMBP4 myc were expressed under control of Gal4 heat shock promoter (P26/ UAS mM13 NLS myc and P26/ UAS CaMBP4 myc) in larval muscle cells to prove the expression pattern. Confocal microscopy analysis of 3rd instar larvae stained with Myc antibody was done to

demonstrate the nuclear localisation of the control transgenes. Nuclei of cells were counterstained with Hoechst (Fig. 10H).

5.5 Visualisation of Ca^{2+} signals in mushroom bodies of adult flies

The results obtained by the olfactory avoidance assay indicate that nuclear Ca^{2+} signals are required during the acquisition phase of LTM, indirectly shown by overexpression of the nuclear Ca^{2+} /CaM inhibitor (UAS 2xM13 NLS myc) in adult flies. Next step was to visualise nuclear Ca^{2+} signals directly using the transgenic flies (UAS GCaMP NLS).

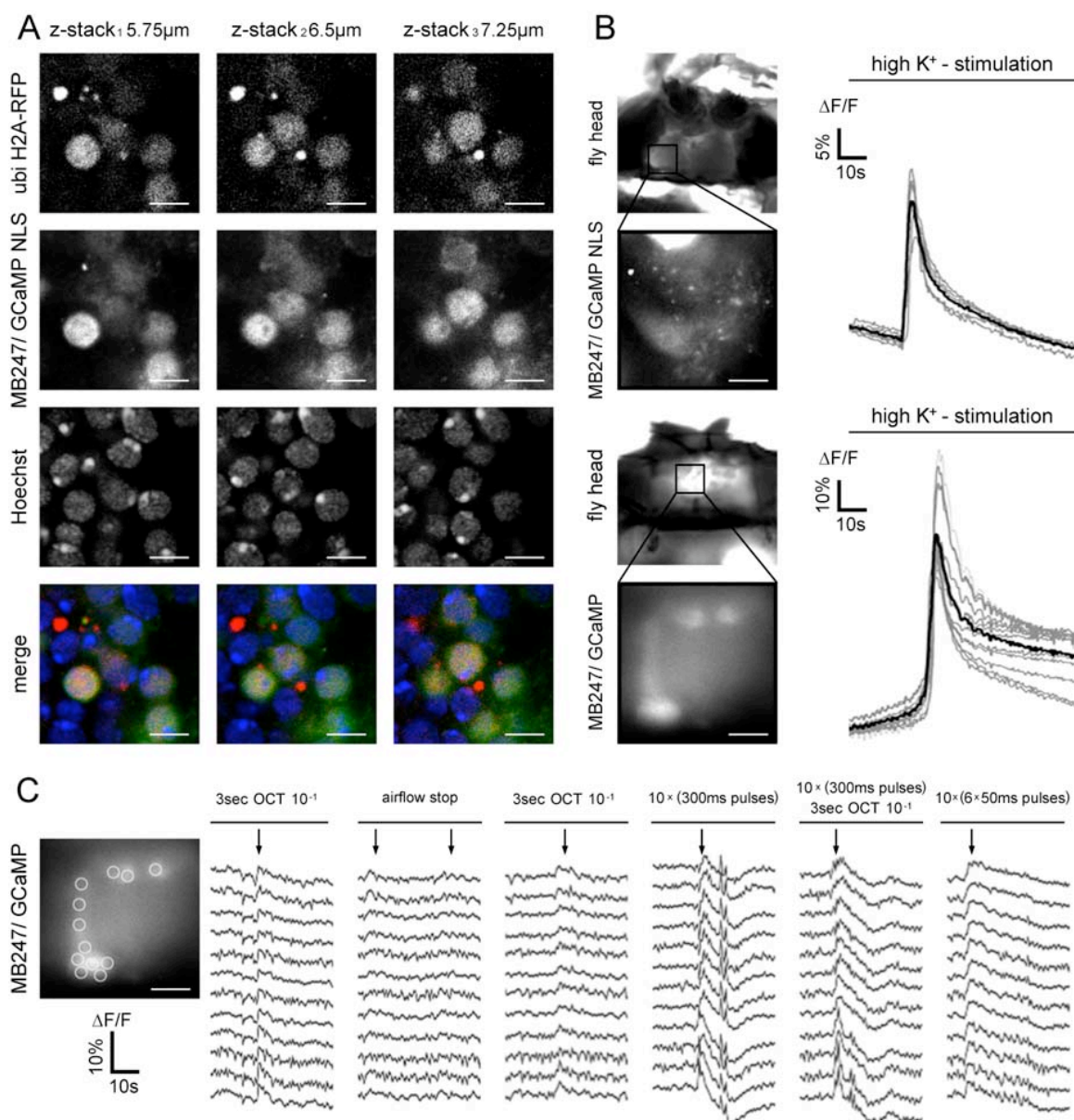


Fig. 11 Ca²⁺-imaging using recombinant Ca²⁺-indicator in adult flies. Immunostaining of a whole mount fly brain expressing the nuclear Ca²⁺-indicator (ubi H2A-RFP; UAS GCaMP NLS) in mushroom body Kenyon cells. Histon 2A-RFP was detectable without antibody staining. GCaMP NLS was detected with GFP antibody. Nuclei of cells were counterstained with Hoechst. Representative images of three different optical sections are shown. Scale bars are 4µm (A). Adult flies expressing either GCaMP NLS or GCaMP in mushroom body Kenyon cells were used for Ca²⁺-imaging. Time course analyses of changes in fluorescence after high K⁺ stimulation are shown. Scale bar is 25µm. Images were taken every 500msec. The bold black line indicates the average of n=12 areas (B). Adult flies expressing GCaMP in mushroom body Kenyon cells were stimulated either with OTC 10⁻¹ or with electrical shock pulses (90V) or both. Time course analyses of changes in fluorescence after presentation of odour and electrical shock pulses are shown. Images were taken every 500msec. Each curve corresponds to one circle indicated at the panel beside (C).

In cell culture but also in 3rd instar larvae the nuclear localisation was confirmed by the counterstaining with Hoechst. It could be observed using confocal microscopy z-stack analysis that in whole mount brain preparation of adult flies Hoechst accumulates for unknown reason in the nucleus, probably in nucleoli, Therefore, the nuclear Ca²⁺-indicator fly (UAS GCaMP NLS) was crossed with a transgenic fly expressing a red fluorescent protein fused to the Histon 2A subunit under the control of an ubiquitin promoter to yield (ubi H2A-RFP; UAS GCaMP NLS). The crossing of the flies was done with the assistance of Dr. Christian Wenzel, ZMBH University of Heidelberg.

To confirm the nuclear localisation, confocal microscopy z-stack analysis of whole mount fly brains stained with GFP antibody of flies expressing UAS GCaMP NLS under the control of Gal4 MB247 (ubi H2A-RFP/+; MB247/ UAS GCaMP NLS myc) was done (Fig. 11A). As expected, optical sections of nuclei expressing ubi H2A-RFP and the UAS GCaMP NLS show congruent pattern of fluorescence signals, but different from the pattern of fluorescence signals obtained with Hoechst counterstaining. These results show that UAS GCaMP NLS was exclusively expressed in the nucleus.

To confirm the functionality of UAS GCAMP NLS in adult flies as previously done in 3rd instar larvae, Ca²⁺ live imaging were done as described (Yu et al., 2004; Yu et al., 2005). To establish the Ca²⁺ live imaging *in vivo*, first flies expressing the cytoplasmic Ca²⁺-indicators UAS GCAMP (Gal4 Or83b/ UAS GCAMP) or UAS CaM2.1-8.2 under control of Gal4 Or83b (Gal4 Or83b; UAS CaM2.1-8.2) in the of receptor neurons of the antennal lobes was used (data not shown). Then, it was tested whether UAS GCaMP NLS were able to detect changes of Ca²⁺ signals in response to high K⁺-induced membrane depolarization in Kenyon cells of the mushroom body. Therefore, flies expressing either UAS GCaMP NLS (Gal4 MB247/ UAS GCaMP NLS)

or UAS GCaMP (Gal4 MB247/ UAS GCaMP) were used for live Ca^{2+} -imaging. Either calcium indicator was suitable to detect Ca^{2+} transients in the mushroom bodies in response to high K^+ -induced membrane depolarization (Fig 11B). Compared to the results obtained from 3rd instar larvae experiments a sharp peak after high K^+ -stimulation was observed. The average peak time from begin of stimulation to peak the maximum response was very different from fly to fly depending on the preparation. Therefore, no calculation was done. The average of amplitudes in flies expressing UAS GCaMP NLS was $\Delta F/F$ in % = 22.0 ± 4.2 and in flies expressing UAS GCaMP $\Delta F/F$ in % = 60.8 ± 14.3 . The differences observed might depend on the same reason listed above (see section 5.3).

In addition to the global Ca^{2+} signals in response to high K^+ -induced membrane depolarization, Ca^{2+} signals evoked either by electrical shock pulses or by odour application were recorded in flies expressing UAS GCaMP under the control of Gal4 MB247 (Gal4 MB247/ UAS GCaMP). Changes in fluorescence were observed after 3 sec application of 3-octanol (OCT) at a concentration 10^{-1} in the lobes (axons) of mushroom bodies. OCT at a concentration of 10^{-1} is sufficient for STM and LTM. The average of amplitudes after first time OCT application was measured in one fly $\Delta F/F$ in % = 3.0 ± 1.7 and the corresponding average peak time was in sec = 1.6 ± 0.2 . The average of amplitudes after second time OCT application was $\Delta F/F$ in % = 2.6 ± 0.6 and the corresponding average peak time was in sec = 1.6 ± 0.2 . No or only slightly changes in fluorescence were observed after airflow stop, which occurred always by switching to the odour application and back (Fig 11C).

Either electrical shock pulse protocols applied to the fly abdomen were able to induce changes in fluorescence recorded from the mushroom body lobes. The average of amplitudes after 3sec protocol I (10x 300ms 90V shock pulses) was $\Delta F/F$ in % = 4.4 ± 1.4 and the corresponding average peak time was in sec = 2.2 ± 0.8 . After application of protocol I a transient increase in Ca^{2+} concentration was observed followed by a decrease in Ca^{2+} concentration below the basal level before stimulation. This was probably caused by the effect of photoisomerisation that is inherent to the Ca^{2+} -indicator. The average of amplitudes after 3sec protocol II (10x (6x50ms) 90V shock pulses) was $\Delta F/F$ in % = 3.9 ± 0.5 and the corresponding average peak time was in sec = 2.2 ± 0.8 . Application of

protocol II induced a sustained increase in Ca^{2+} concentration lasting for in sec = 24.8 ± 3.2 . Pairing electrical stimulation (protocol I) and OCT application, induced changes in fluorescence that were slightly higher as electrical stimulation (protocol I) alone. The average of amplitudes was $\Delta F/F$ in % = 5.3 ± 1.7 and the corresponding average peak time was in sec = 2.4 ± 0.6 (Fig 11C). Since the aim of the project was to visualise nuclear Ca^{2+} signals, the experiments must be repeated with flies expressing UAS GCaMP NLS under the control of Gal4 MB247 (Gal4 MB247/ UAS GCaMP NLS). In parallel, a new transgenic fly was generated expressing the nuclear Ca^{2+} -indicator GCaMP2 NLS fused to a red fluorescent protein, named mCherry (Shaner et al., 2004) (more details at section 5.7.). This transgenic fly will allow distinguishing changes in fluorescence evoked by artefacts from changes in fluorescence evoked by increase in Ca^{2+} concentration by recording two wavelengths simultaneously.

5.6 Visualisation of nuclear Ca^{2+} signals in organotypic slices

In 2005, Ohkura et al. published a modified version of pN1 GCaMP, named GCaMP 1.6. Although GCaMP 1.6 was hardly fluorescent at 37°C when expressed in cells.

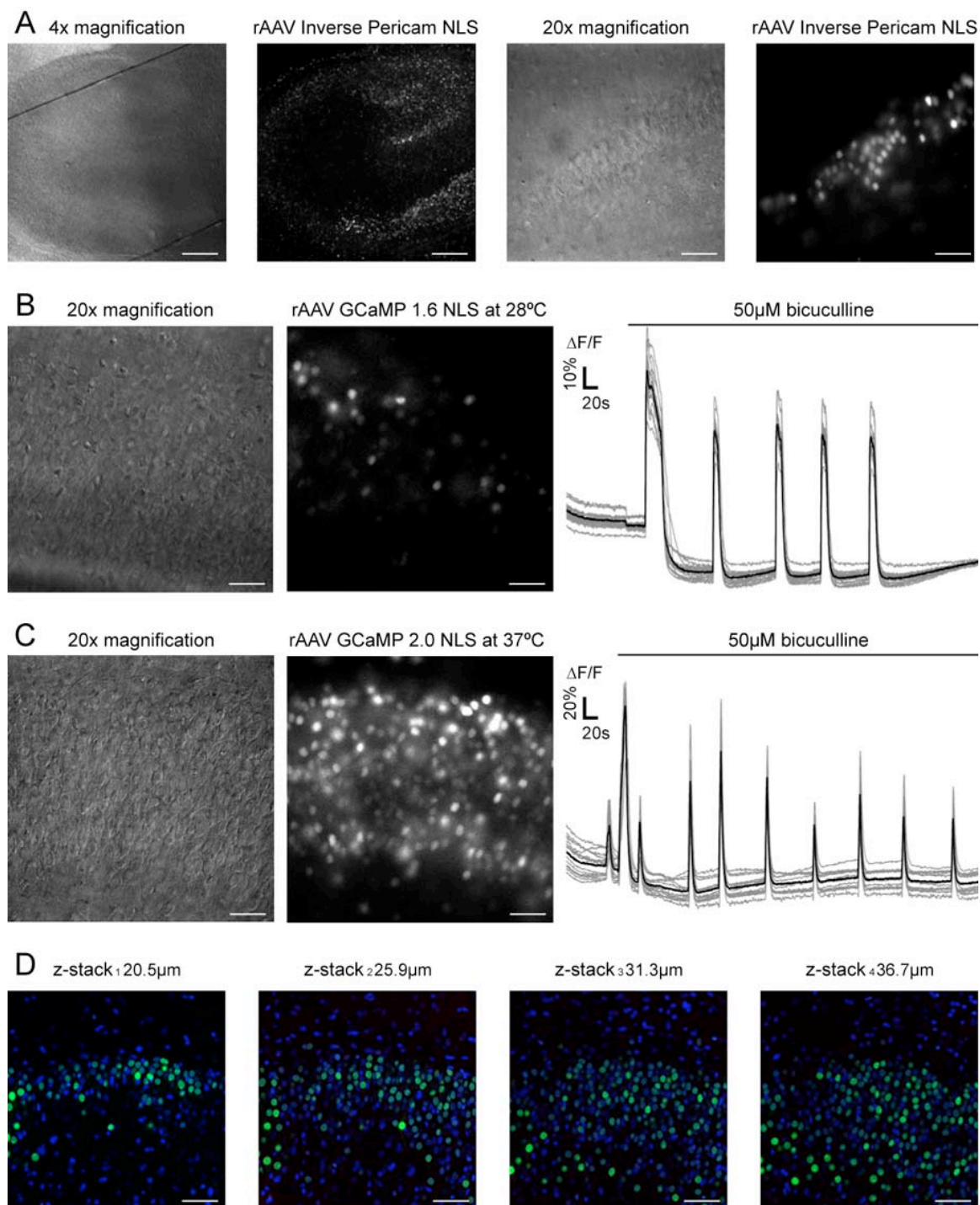


Fig. 12 Nuclear Ca²⁺-imaging using recombinant Ca²⁺-indicators in organotypic brain slice. Live imaging (A), Ca²⁺-imaging (B, C), and immunostaining (D) of cultured hippocampal brain slices infected with rAAV expressing Inverse Pericam NLS (A), GCaMP 1.6 NLS (B), or GCaMP 2.0 NLS (C, D). Overview and detail fluorescence images plus corresponding DIC images are shown. Scale bars are 250 μ m and 50 μ m (A). Ca²⁺-imaging were done at 28°C (B) and at 37°C (C). Time course analyses of changes in fluorescence after 50 μ M bicuculline stimulation are shown. Corresponding DIC and fluorescence images are beside the charts. Images were taken every 500msec. The bold black line indicates the average of n=15 cells (B, C). Brain slice infected with rAAV expressing GCaMP 2.0 NLS were fixed and nuclei of cells were counterstained with Hoechst. Representative overlay images of four different optical sections are shown. Scale bars are 75 μ m (D). Imaging data were kindly provided by D. Ditzel.

An obvious improvement of GCaMP 1.6 over pN1 GCaMP was its brightness and the property to reach a sufficient fluorescence level following temperature change from 37°C to 28°C (Ohkura et al., 2005). The Ca²⁺-imaging experiments were done together with D. Ditzel (Ditzel et al., 2008).

GCaMP 1.6 allowed expressing the nuclear Ca²⁺-indicator by rAAV-mediated gene transfer in hippocampal cells or in organotypic slices. Expression of rAAV Inverse Pericam NLS was used as control infection in organotypic slices (Fig. 12A). A bright green fluorescent signal was observed restricted to the nucleus of neurons infected with rAAV Inverse Pericam (2×10^{11} virus particle/ml). Green fluorescence signal in organotypic slices infected with rAAV GCaMP 1.6 NLS (2×10^{11} virus particle/ml) was hardly to detect at 37°C (data not shown), but the signal increase after 1h incubation at 28°C (Fig. 12B). Oscillatory Ca²⁺ changes with a frequency of 0.0125 Hz induced by application of 50 μ M bicuculline were measured. The average of amplitudes was $\Delta F/F$ in % = 71.9 ± 6.2 and the corresponding average peak time was in sec = 5.3 ± 0.6 (Fig 12B)

In 2007, Tallini et al. published the Ca²⁺-indicator GCaMP 2.0 that was fluorescent at 37°C (Tallini et al., 2006). Therefore, GCaMP 2.0 allowed visualising Ca²⁺ signals at physiological temperature. A bright green fluorescent signal was observed in neurons infected with rAAV GCaMP 2.0 NLS (2×10^{11} virus particle/ml) at 37°C (Fig. 12C). Oscillatory Ca²⁺ changes with a frequency of 0.02 Hz induced by application of 50 μ M bicuculline were measured. The average of amplitudes was $\Delta F/F$ in % = 110.0 ± 17.4 and the corresponding average peak time was in sec = 4.3 ± 0.3 (Fig 12C). To confirm nuclear localisation of neurons expressing rAAV GCaMP 2.0 NLS organotypic slices were fixed and nuclei were counterstained with Hoechst. Several optical sections demonstrated the nuclear localisation of the Ca²⁺-indicator GCaMP 2.0 NLS (Fig 12D). The nuclear Ca²⁺-indicator GCaMP 2.0 NLS allowed for the first time to image nuclear Ca²⁺ signals at physiological temperature necessary for *in vivo* imaging. In contrast to

Ca²⁺-imaging in culture or in brain slice where changes in fluorescence evoked by movement artefacts might be negligibly, fluorescence changes caused purely by movement artefacts will be a serious issue when Ca²⁺ imaging is done in a free moving animal.

5.7 Visualisation of nuclear Ca^{2+} signals using rAAV GCaMP2 NLS Cherry

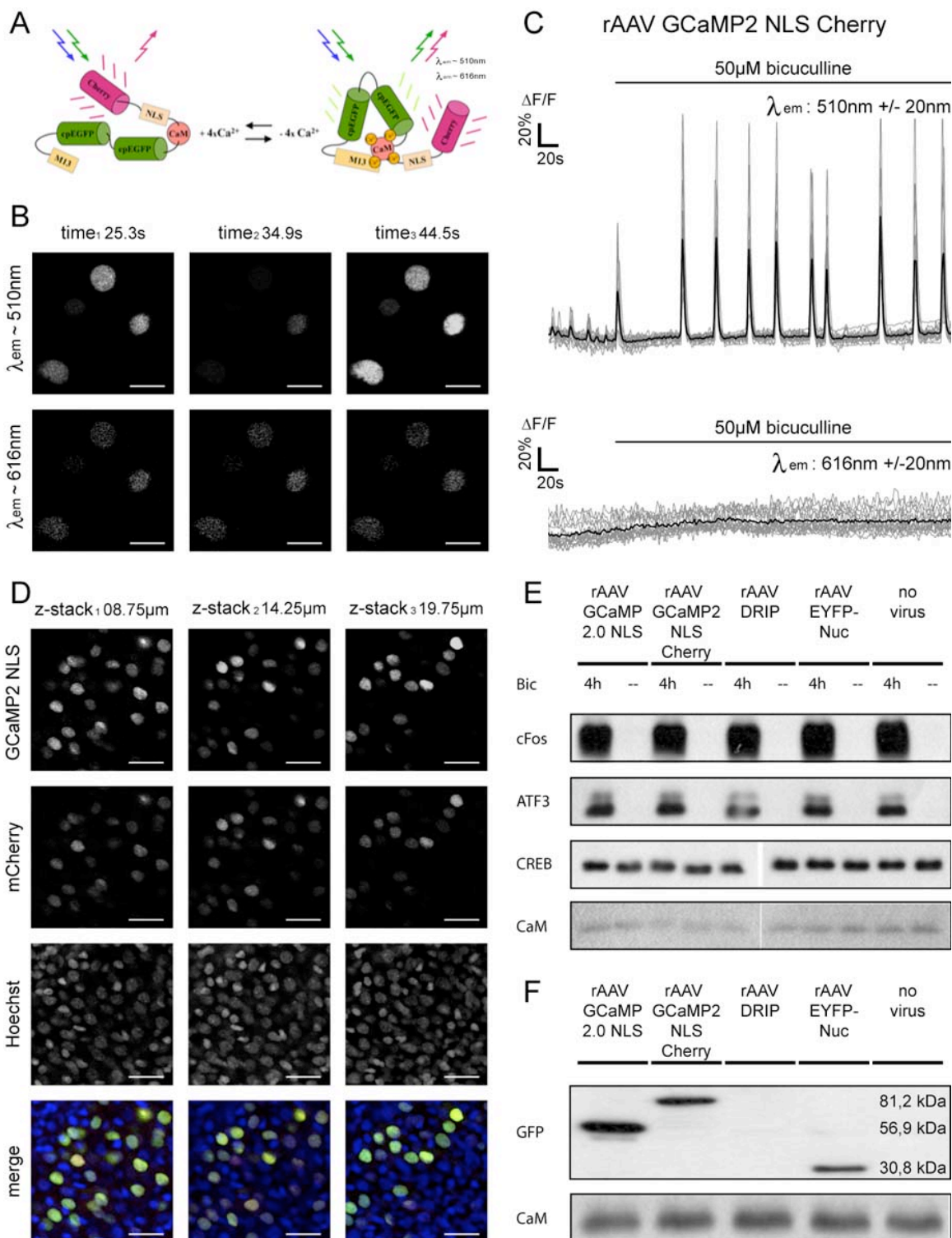


Fig. 13 Characterisation of the Ca²⁺-indicator rAAV GCaMP2 NLS Cherry. Schematic representation of rAAV GCaMP2 NLS Cherry (A). Ca²⁺-imaging of hippocampal neurons infected with rAAV expressing GCaMP2 NLS Cherry. Cells were excited with wavelengths of 488nm and 587nm. Emission light was detected at wavelengths of 510nm +/-20nm (GCaMP 2.0) and 616 nm +/-20nm (mCherry). Representative images of a time series are shown. Scale bars are 15µm (B). Both charts show the time course analyses of changes in fluorescence after 50µM bicuculline detected at the indicated wavelength. Images were taken every 1.6 sec. The bold black line indicates the average of n=12 cells (C). Cultured hippocampal brain slices infected with rAAV expressing GCaMP2 NLS Cherry were fixed and nuclei of cells were just counterstained with Hoechst 33258. Representative images of three different optical sections are shown. Scale bars are 50µm (D). Western blot analyses (E, F) of hippocampal neurons uninfected or infected with rAAV expressing either GCaMP 2.0 NLS, GCaMP2 NLS Cherry, DRIP, or EYFP-Nuc. Uninfected neurons or neurons infected with rAAVs were treated for 4 hrs with bicuculline (50 µM) to induce AP bursting or were left unstimulated. Activity-dependent blockade of the induction of cFos and ATF3 expression is not apparent. CREB was used as control to show that viral infection by itself not induces an increase of cell death. (E). Calmodulin was used as loading control (E, F). Z-stack images and western blot analyses were kindly provided by D. Ditzel.

To use the nuclear Ca²⁺-indicator GCaMP 2.0 NLS *in vivo*, a red fluorescent protein (mCherry) was added to the C-terminus of the indicator. An additional linker was fused to the N-terminus of mCherry to separate the NLS and the red fluorescent protein (Fig 13A). The cloning and imaging experiments were done together with D. Ditzel (Ditzel et al., 2008).

Only a small portion of the GFP emission spectrum overlaps with the excitation spectrum of mCherry (Shaner et al., 2004). Therefore, fluorescence resonance energy transfer (FRET) between the GFP and mCherry within rAAV GCaMP2 NLS Cherry could theoretically occur. Tramier et al. published in 2006 that GFP and mCherry were suitable for FRET based lifetime imaging in living cells (Tramier et al., 2006). However, using rAAV-mediated gene transfer, nuclear expression of GCaMP2 NLS Cherry was obtained in 80%–95% of the viable hippocampal neurons. Nuclear localisation of the indicator was detectable either with $\lambda = 510\text{nm} \pm 20\text{nm}$ (emission spectrum of GFP) or $\lambda = 616\text{nm} \pm 20\text{nm}$ (emission spectrum of mCherry). No signal was observed using the excitation wavelength of GFP ($\lambda = 488\text{nm}$) and emission spectrum of mCherry or vice versa (data not shown). To test whether fluorescence resonance energy transfer (FRET) between the GFP and mCherry within rAAV GCaMP2 NLS Cherry occurred, GFP fluorescence signals were detected within the emission spectrum of GFP and simultaneously, mCherry was bleached to destroy the possible photon acceptor of the GFP emitted photons. No increase of GFP emitted fluorescence signal was observed

Oscillatory Ca²⁺ changes with a frequency of 0.025Hz induced by application of 50µM bicuculline were detected within the emission spectrum of GFP, but no or only slightly change in fluorescence were detected within the emission spectrum of mCherry

(Fig 13B). The average of amplitudes was $\Delta F/F$ in % = 86.1 ± 36.2 and the corresponding average peak time was in sec = 3.1 ± 0.5 (Fig 13C). To confirm nuclear localisation of neurons expressing rAAV GCaMP2 NLS Cherry organotypic slices were fixed and nuclei were counterstained with Hoechst. Several optical sections demonstrated the nuclear localisation of the Ca^{2+} -indicator GCaMP2 NLS Cherry (Fig 13D).

Western blot analysis was done to determine whether either GCaMP 2.0 NLS or GCaMP2 NLS Cherry block synaptic activity-evoked CREB-mediated gene transcription due to buffering nuclear Ca^{2+} signals itself or disturbing Ca^{2+} /CaM binding through the M13 peptide within the Ca^{2+} -indicators. Using rAAV-mediated gene transfer, the expression of GCaMP 2.0 NLS, GCaMP2 NLS Cherry and EYFP NUC was obtained in 80%–95% of the viable hippocampal neurons. For unknown reason, no expression was observed for DRIP infected neurons (Fig. 13F). No blocking effect of synaptic activity-evoked CREB-mediated gene transcription was observed compared to control (i.e. noninfected neurons or neurons infected with rAAV EYFP Nuc). Induction of cFos and ATF3 expression was not reduced in neurons infected with either rAAV GCaMP 2.0 NLS or rAAV GCaMP2 NLS Cherry after 4hrs bicuculline ($50\mu M$) stimulation. Also, no differences were observed comparing CREB expression in neurons either uninfected or infected. Calmodulin was used as loading control (Fig. 13E).

Using rAAV GCaMP2 NLS Cherry as Ca^{2+} -indicator for *in vivo* imaging allowed to distinguish between changes in fluorescence evoked by movement artefacts and changes in fluorescence evoked by increase in nuclear Ca^{2+} concentration. Nevertheless, given the complexity of intact animal brains and failures of several indicators which worked excellent in culture but not *in vivo*, next step was to test whether these indicators were suitable to detect nuclear Ca^{2+} signals in acute brain slices of juvenile and adult rats.

5.8 Visualisation of nuclear Ca^{2+} signals in brain slices

Dr. P. Bengtson established an electrophysiology setup in the lab, which allowed to recording Ca^{2+} signals with a high-speed CCD camera evoked by electrical stimulation in acute slices of juvenile rats. All electrophysiology results were recorded by Dr. P. Bengtson.

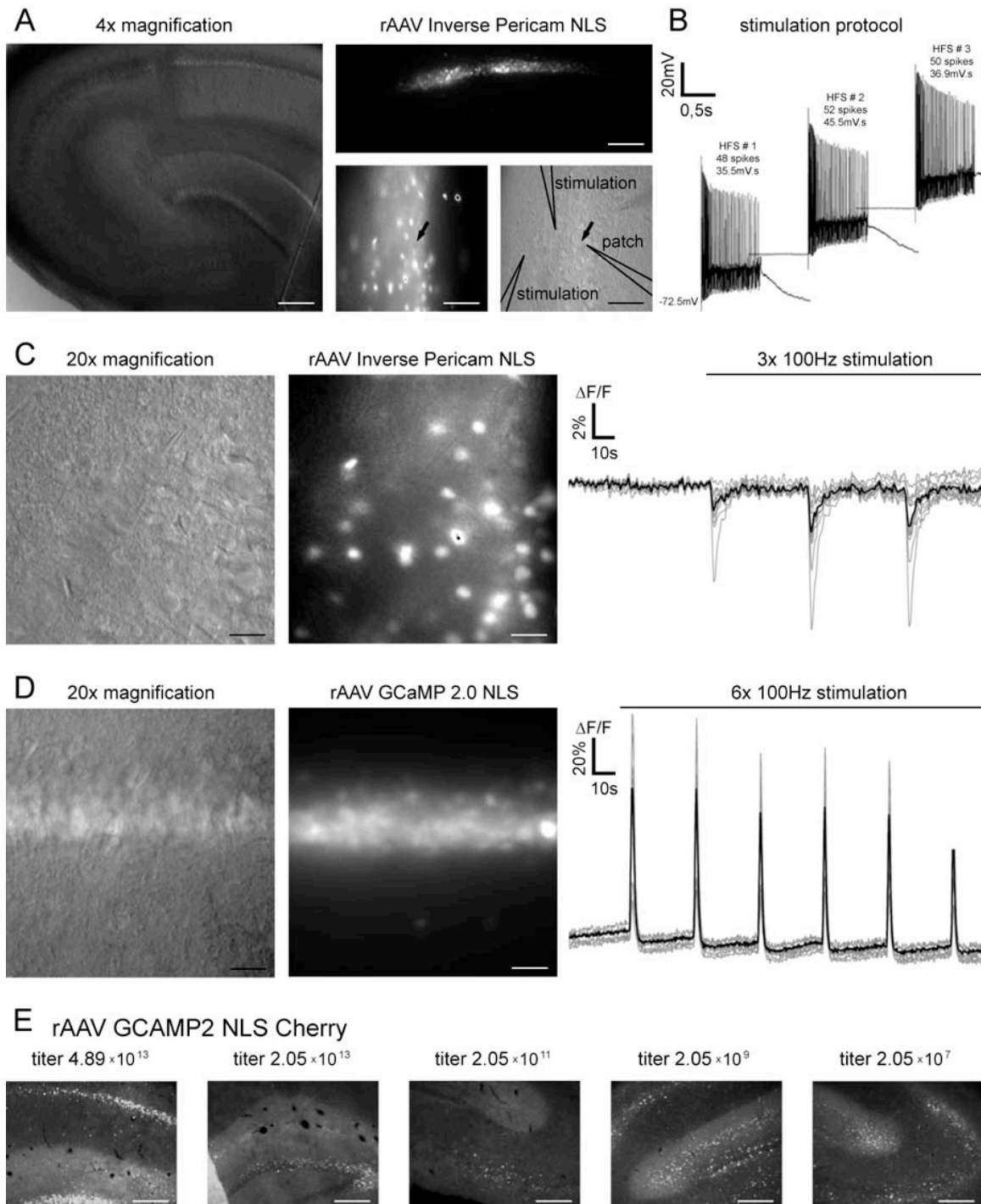


Fig. 14 Nuclear Ca^{2+} -imaging using recombinant Ca^{2+} -indicators in brain slices. Ca^{2+} -imaging of acute hippocampal brain slices of juvenile rats infected with rAAV expressing Inverse Pericam NLS (**A**, **B**) and GCaMP 2.0 NLS (**C**). DIC and fluorescence image of acute brain slice are shown. Scale bars are $250\mu\text{m}$ and $75\mu\text{m}$ (**A**). Schematic representation of stimulation protocol (**B**). Time course analyses of changes in fluorescence after $3 \times 100\text{ Hz}$ (**B**) and $6 \times 100\text{ Hz}$ (**C**) stimulation are shown. Corresponding DIC and fluorescence images are beside the charts. Scale bars are $50\mu\text{m}$. Images were taken every 500msec. The bold black line indicates the average of $n=10$ cells (**B**, **C**). *In vivo* titration of the Ca^{2+} -indicator rAAV GCaMP2 NLS Cherry in adult rats. Images of the fixed hippocampal brain slices infected with rAAV expressing GCaMP2 NLS Cherry are shown. The basal GFP fluorescence of the Ca^{2+} -indicator is shown at five different virus concentrations. Scale bars are $250\mu\text{m}$ (**D**).

The nuclear Ca^{2+} -indicator rAAV Inverse Pericam NLS was used to establish the coordinates of injection site and the virus concentration due to the bright fluorescence at resting conditions. A total volume of $3\mu\text{l}$ containing 2×10^9 virus particles/ml was injected unilaterally into the hippocampus of P23 rats. The rAAV-mediated gene expression requires at least 15 days to peak in the rodent brain and then persists at stable levels without inflammation (Xu et al., 2001). Two to three weeks after surgery, the transduction efficiency was assessed by live imaging experiments of acute brain slices. According to the results obtained in culture robust transgene expression was observed in CA1 pyramidal neurons of rats two weeks after viral infection (2×10^9 virus particle/ml) (Fig 14A). Whole-cell patch clamp recordings were made from CA1 hippocampal pyramidal neurons in brain slices and simultaneously Ca^{2+} signals were recorded evoked by high frequency stimulation (HFS) protocols (Fig 14B).

A bright green fluorescent signal was observed restricted to the nucleus of CA1 hippocampal pyramidal neurons infected with rAAV Inverse Pericam NLS before stimulation. Small Ca^{2+} changes evoked by $3 \times 100\text{Hz}$ electrical stimulations were recorded. The average of amplitudes was $\Delta\text{F}/\text{F}$ in % = 2.3 ± 2.0 and the corresponding average peak time was in sec = 0.9 ± 0.4 (Fig 14C). Most of the CA1 hippocampal pyramidal neurons expressing GCaMP 2.0 NLS show a moderate green fluorescence signal at resting conditions. However, strong changes in nuclear Ca^{2+} concentration evoked by $6 \times 100\text{Hz}$ electrical stimulations were recorded. The average of amplitudes was $\Delta\text{F}/\text{F}$ in % = 77.3 ± 2.3 and the corresponding average peak time was in sec = 1.0 ± 0.3 (Fig 14D).

In addition to the Ca^{2+} -imaging in acute brain slices of juvenile rats, Ca^{2+} -imaging was done in adult rats. Aso et al. described that high dose of virus concentration causes neuronal cell loss according to the injection site in adult rats (Aso et al., 2007). To avoid that the injected virus concentration itself causes cell loss and to determine optimal virus concentration to yield high transfection efficiency, *in vivo* titration of rAAV GCaMP2 NLS Cherry was done in adult rats. Five different virus concentrations were tested ranging from 4.89×10^{13} to 2.05×10^7 virus particles/ml. All virus concentration tested were diluted from a virus batch stored at -80°C except of the highest concentration which were used from a virus batch stored at 4°C . Three weeks after rAAV delivery, when transgene

protein expression has peaked to remain at stable level, rat brains were perfused using standard procedures (Klugmann et al., 2005). Surprisingly, no inflammatory caused cell loss was observed as expected at least for the highest virus concentration of 4.89×10^{13} virus particles/ml. The best results were obtained either at a concentration of 4.89×10^{13} genomic virus particles/ml or at a concentration of 2.05×10^9 genomic virus particles/ml, suggesting that the injection site is more critical as the injected virus concentration. However, it could be shown that GCaMP 2.0 NLS and GCaMP2 NLS Cherry were suitable to visualise nuclear Ca^{2+} signals in acute brain slices.

5.9 Visualisation of Ca^{2+} signals in freshwater polyps using hyGCaMP

The major challenge of Ca^{2+} imaging *in vivo* either in flies or in rodents based on difficulties to emit or detect photons through the intransparent skulls that protect the brains. The freshwater polyp *H. vulgaris* is completely transparent and live imaging through the outer layers to track individual label cells of the endoderm layer has been described at (Wittlieb et al., 2006). Therefore, several transgenic hydra lines were generated expressing the Ca^{2+} -indicator hyGCaMP or hyGCaMP NLS.

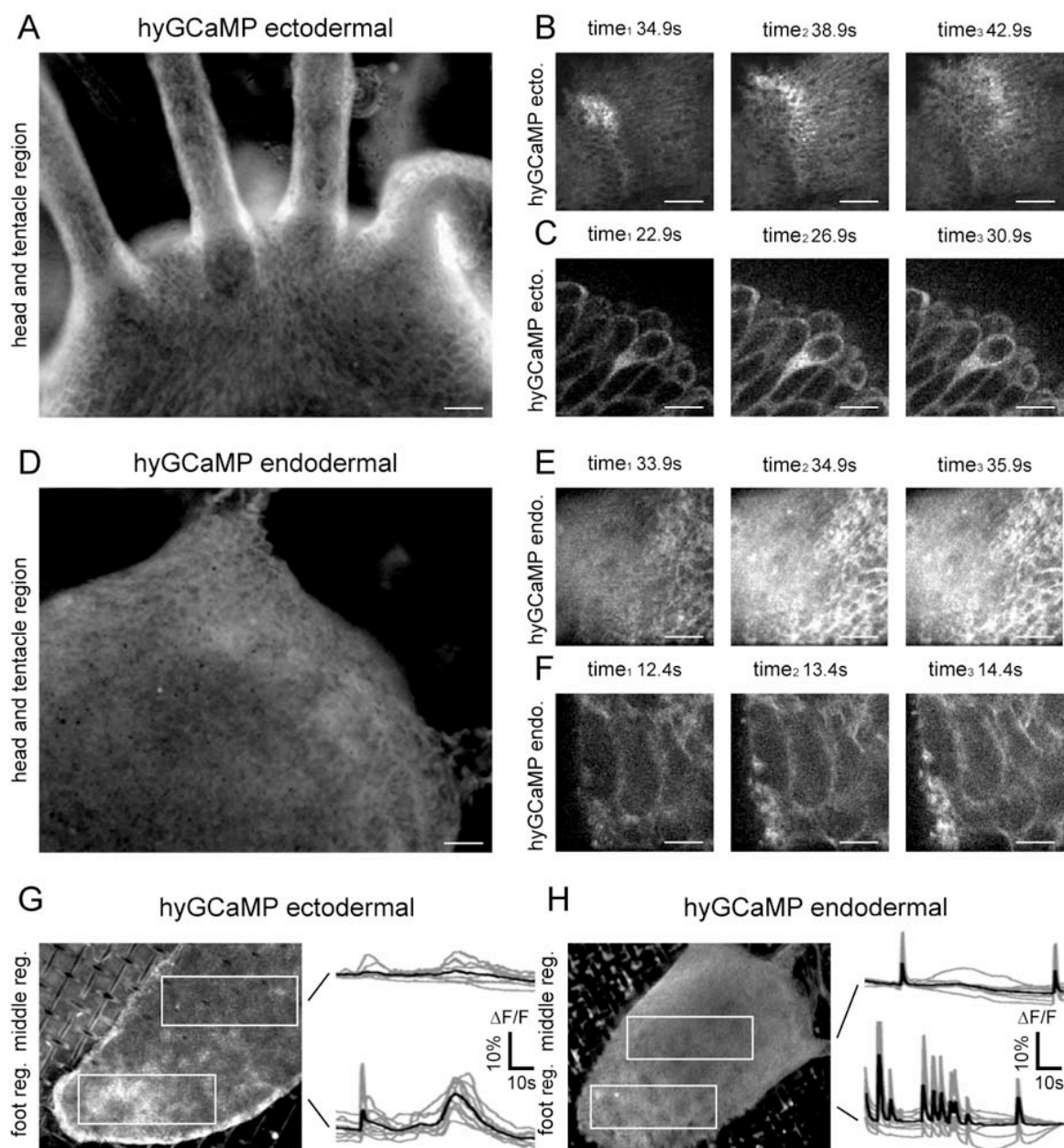


Fig. 15 Visualisation of Ca²⁺ signals in the ectoderm or the endoderm of *H. vulgaris* using hyGCaMP. Ca²⁺-imaging of *H. vulgaris* expressing the Ca²⁺-indicator hyGCaMP either in ectodermal (A-C, G) or endodermal (D-F, H) cells. Overview of indicator expression pattern at head/ tentacle region (ectodermal) is shown. Scale bar is 135µm (A). The time series shows changes in fluorescence recorded from the foot region. Images were taken every 1sec. Scale bar is 75µm (B). Detailed pictures show changes in fluorescence within single cells. Images were taken every 200msec. Scale bar is 20µm (C). Overview of indicator expression pattern at the head/ tentacle region (endodermal) is shown. Scale bar is 135µm (D). The time series shows changes in fluorescence recorded from the foot region. Images were taken every 1sec. Scale bar is 75µm (E). Detailed pictures show changes in fluorescence within single cells. Images were taken every 500msec. Scale bar is 20µm (F). Comparison of Ca²⁺ signals in the ectoderm: foot region vs. middle region. Either chart shows the time course analyses of changes in fluorescence at the indicated regions. Images were taken every 560msec. The bold black line indicates the average of n=12 area within these regions (G). Comparison of Ca²⁺ signals in the endoderm: foot region vs. middle region. Either chart shows the time course analyses of changes in fluorescence at the indicated regions. Images were taken every 560msec. The bold black line indicates the average of n=12 area within these regions (H). Ca²⁺-imaging data were kindly provided by J. Schlüter.

The generation of transgenic hydra lines by DNA injection into early hydra embryos was done by J. Schlüter (Schlüter et al. 2008). After hatching patchy expression of hyGCaMP was observed either in ectodermal or endodermal cells. By further propagation, lines could be established homogeneously expressing hyGCaMP in all ectodermal (Fig. 15A - 15C) or endodermal cells (Fig. 15D - 15F). The Ca²⁺-imaging experiments comparing Ca²⁺ events of ectodermal cells with Ca²⁺ events of endodermal cells were done together with J. Schlüter.

Spontaneous Ca²⁺ signals were visualised through the transparent layers either in ectodermal cells or endodermal cells expressing hyGCaMP. Clearly differences of spontaneous Ca²⁺ events were observed in lines expressing hyGCaMP in all ectodermal cells compared to those lines expressing hyGCaMP in all endodermal cells. Spontaneous changes in Ca²⁺ concentrations in lines expressing hyGCaMP in all ectodermal cells were observed mostly randomly distributed concerning only a few cells. Thus, this kind of Ca²⁺ event was named “lightnings”. “Lightnings” were observed in the head, in the middle and in the foot region (data not shown). In contrast to the constantly occurring small changes in fluorescence, a second kind of spontaneous Ca²⁺ event was observed that occurred infrequently and more often in the foot than in other body regions. This kind of Ca²⁺ event was named “Ca²⁺-wave” (Fig 15B) because the increase in Ca²⁺ concentration started from only a few cells and spread out into the neighbouring cells in a coordinated pattern. The Ca²⁺ signals observed in ectodermal cells diffused rather slowly, typically in the range of seconds, observed either throughout the neighbouring cells (Fig 15B) or within a single cell (Fig 15C).

The spontaneous Ca²⁺ signals visualised in endodermal cells expressing hyGCaMP

differed dramatically from the Ca^{2+} signals visualised in ectodermal cells. In ectodermal cells no Ca^{2+} signals were observed that were similar to the Ca^{2+} events described for endodermal cells (“lightnings”, “ Ca^{2+} -wave”). Further, it was not possible to visualise the diffusion of Ca^{2+} signals either throughout the neighbouring cells (Fig 15E) or within a single cell (Fig 15F), at least with the same microscope setting as used to visualise Ca^{2+} signals expressing hyGCaMP in ectodermal cells. Instead, an increase in Ca^{2+} signals was observed typically in the range of millisecond. These Ca^{2+} signals were not only restricted to a few cells the entire foot region showed fast oscillatory changes in fluorescence (Fig 15E). Thus, this kind of Ca^{2+} event was named “ Ca^{2+} bursts”. “ Ca^{2+} bursts” were also observed in the head or the middle region. Sometimes, sustained Ca^{2+} levels were observed instead of fast oscillatory Ca^{2+} changes.

Next, Ca^{2+} signals of foot and middle region were compared within one animal using an objective of 5x magnification to exclude differences within the transgenic line (e.g. age or feeding behaviour). Differences in the average changes in fluorescence visualised in ectodermal cells expressing hyGCaMP were observed comparing the foot region with the middle region. The average of amplitudes was $\Delta F/F$ in % = 13.7 ± 4.0 in the foot region compared to $\Delta F/F$ in % 1.2 ± 0.3 in the mid region (Fig 15G). Comparing changes in fluorescence visualised in endodermal cells expressing hyGCaMP, the average of amplitudes was $\Delta F/F$ in % = 22.3 ± 17.6 in the foot region compared to $\Delta F/F$ in % 5.6 ± 4.2 in the mid region (Fig 15H).

5.10 Visualisation of nuclear Ca^{2+} signals in freshwater polyps using hyGCaMP NLS

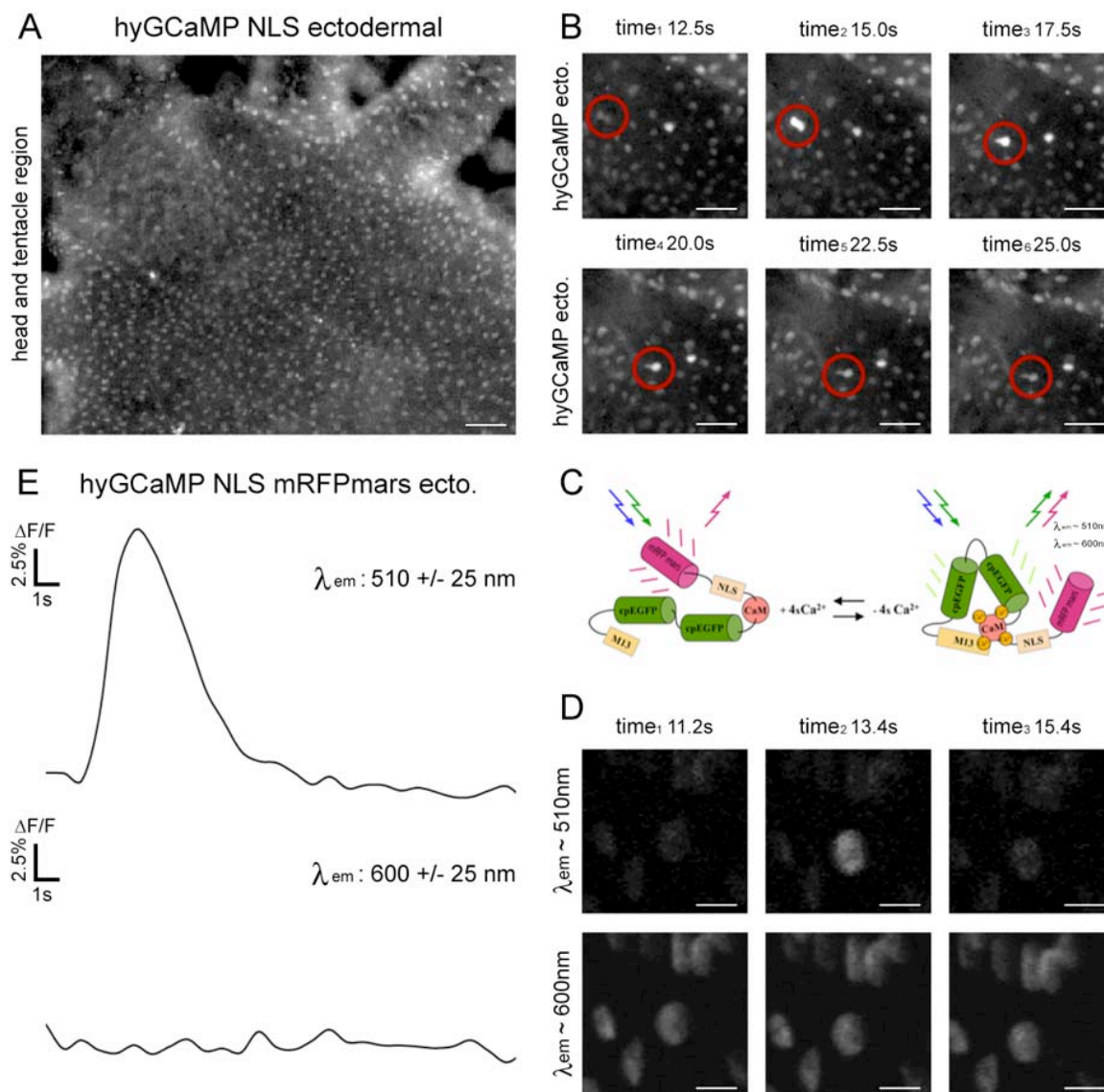


Fig. 16 Visualisation of nuclear Ca^{2+} signals in the ectoderm *H. vulgaris* using hyGCaMP NLS. Ca^{2+} -imaging of *H. vulgaris* expressing the Ca^{2+} -indicator hyGCaMP NLS (**A**, **B**) or hyGCaMP NLS mRFPmars (**D**) in all ectodermal cells. Overview of indicator expression pattern at the head/ tentacle region (ectodermal) is shown. Scale bar is $135\mu\text{m}$ (**A**). Time series shows changes in fluorescence of a single nucleus recorded from the head region indicated by the red circle. Images were taken every 560msec. Scale bar is $75\mu\text{m}$ (**B**). Schematic representation of hyGCaMP NLS mRFPmars (**C**). Transgenic polyp was sequentially excited with wavelengths of 488nm and 568nm and emission light was sequentially detected at wavelengths of 510nm \pm 25nm (hyGCaMP) and 600 nm \pm 25nm (mRFPmars). Either chart shows the time course analyses of changes in fluorescence within one cell at the indicated wavelength. Images were taken every 500msec (**E**). Images of the time series analysed in **D** are shown. Scale bars are $10\mu\text{m}$ (**D**).

The generation and screening of transgenic hydra lines expressing hyGCaMP NLS were done by J. Schlüter. By further propagation, it was possible to establish lines homogeneously expressing hyGCaMP NLS in ectodermal cells. The Ca^{2+} -imaging experiments were done together with J. Schlüter (Schlüter et al. 2008).

In transgenic hydra expressing hyGCaMP NLS fluorescence signals were restricted to the nuclei of all ectodermal cells (Fig. 16A). Single nuclei could be followed over a certain time period. Changes in fluorescence were visualised within the indicated time window (Fig. 16B). The changes in nuclear Ca^{2+} signals observed in transgenic hydra expressing hyGCaMP NLS were in the range of seconds and were comparable to the results obtained with hyGCaMP expressed in ectodermal cells. The amplitude was $\Delta F/F$ in % = 53,0 analysed from the head region of hydra expressing hyGCaMP NLS. As expected, no nuclear Ca^{2+} event was observed similar to the Ca^{2+} event “lightnings” that was visualised with hyGCaMP expressed in ectodermal cells. No nuclear Ca^{2+} event similar to the Ca^{2+} event “ Ca^{2+} -wave” was recorded. The nuclear Ca^{2+} signals observed were randomly distributed and extremely rare. Most of the time, only one nucleus of hundreds showed spontaneous changes in fluorescence (Fig. 16B).

As described before in more details (see section 5.7) changes in fluorescence evoked by movement of a living animal are a serious issue, especially when imaging is done in small regions such as the cell nucleus (Fig. 16B). Therefore, to exclude changes in fluorescence due to artefacts, a fluorescent protein optimised for hydra (mRFPmars) was added to the C-terminus of the indicator (Muller-Taubenberger et al., 2006). An additional linker was fused to the N-terminus of mRFPmars to separate the NLS and the red fluorescent protein (Fig 16C). Theoretically, there is a small overlapping of the excitation spectrum of GFP and emission spectrum of mRFPmars. However, no FRET was measured so far between the two fluorophores. Nuclear expression of hyGCaMP NLS mRFPmars was observed in all ectodermal cells. Nuclear localisation of the indicator was detectable either with $\lambda = 510\text{nm} \pm 25\text{nm}$ (emission spectrum of GFP) or $\lambda = 600\text{nm} \pm 25\text{nm}$ (emission spectrum of mRFPmars). Increases in Ca^{2+} concentration were detected within the emission spectrum of GFP, but no or only slightly change in fluorescence were detected within the emission spectrum of mRFPmars (Fig 16D). The amplitude of the single nuclei recorded was $\Delta F/F$ in % = 20.8 (Fig 16E).

6 Discussion

In the nervous system, calcium (Ca^{2+}) acts as an intracellular second messenger responsible for controlling several cellular mechanisms such as proliferation, development, learning and memory. Especially, changes in the nuclear Ca^{2+} concentration following synaptic activity are the molecular basis for such cellular mechanisms (Hardingham et al., 1997; Chawla and Bading, 2001; Hardingham et al., 2001; Limback-Stokin et al., 2004; Papadia et al., 2005; Zhang et al., 2007). Given the central role of nuclear Ca^{2+} in the control of adaptive responses, one would like to visualise nuclear Ca^{2+} in physiological context of behavioural experiment. But visualisation of Ca^{2+} signals by fluorescent indicators have some disadvantages when used in a biological context: 1) Photobleaching limits the total number of photons that a single fluorescent molecule can emit. 2) Excited fluorophors often create reactive chemical species in their vicinity; these species can cause damage to surrounding molecules and thus be toxic to the cell. 3) Fluorescent indicators bind to or interact with molecules that they detect, so indicators can act as buffers and compete with natural targets. Expression of indicators, especially at very high levels, can therefore change the biological processes being studied. 4) Physical and optical properties of fluorescent indicators are extremely different and therefore difficult to compare.

6.1 Nuclear Ca^{2+} -indicator pN1 GCaMP NLS

Measurements of nuclear Ca^{2+} signals require the introduction of Ca^{2+} -indicators into the cell. The most widely used Ca^{2+} -indicators are chemically synthesized fluorescent indicators (Grynkiewicz et al., 1985; Takahashi et al., 1999). These indicators are easily loaded but are difficult to target precisely in specific intracellular locations. The development of recombinant Ca^{2+} -indicator proteins allows genetic targeting to specific cell compartments. In a previous study, the recombinant Ca^{2+} -indicators pN1 GCaMP (Nakai et al., 2001) and Inverse Pericam (Nagai et al., 2001) were compared in hippocampal neurons (Weislogel et al. 2003). To visualise specifically nuclear Ca^{2+} signals a nuclear localization signal (NLS) was attached to the amino terminus of pN1 GCaMP. It seems that the attached NLS is exposed and does not project toward the

interior of the indicator because pN1 GCaMP NLS localised exclusively to the nucleus. Further, it is unlikely that the NLS disturbs the interaction between the M13 and calmodulin because disturbance/defect in the interaction of both domains is responsible for detection of changes in fluorescence and would lead to reduced Ca^{2+} sensitivity. Indeed, the nuclear Ca^{2+} -indicators pN1 GCaMP NLS was suitable to visualise slow oscillatory Ca^{2+} changes induced by application of $50\mu\text{M}$ bicuculline (GABA_A receptor blocker) in hippocampal neurons (Fig. 7B and 7D). Similar Ca^{2+} responses to HiK and bicuculline were seen with pN1 GCaMP NLS and pN1 GCaMP suggesting an unaltered function of the indicator (Fig. 7A and 7C). Therefore, it seems that the amino terminal end tolerant genetically manipulation.

6.2 Nuclear Ca^{2+} /CaM inhibitor: rAAV 2xM13 NLS myc

Blocking of CREB mediated gene transcription by interfering with downstream signals of nuclear Ca^{2+} /CaM pathway using the Ca^{2+} /CaM inhibitor CaMB4 (Wang et al., 1995) was previously shown *in vivo* by (Limback-Stokin, 2004). CaMBP4 consists of four copies of the skeletal muscle M13 peptide derived from the rabbit myosin light chain kinase (KRRWKKNFIAVSAANRFKK) (Blumenthal and Krebs, 1987; Wang et al., 1996), whereas the nuclear Ca^{2+} /CaM inhibitor used in this study consists of only two copies of the smooth muscle M13 peptide derived from the chicken myosin light chain kinase (GPVDSSRRKWNKTGHAVRAIGRLSS) (Rhoads and Friedberg, 1997; Romoser et al., 1997; Nakai et al., 2001). For an unknown reason rAAV 2xM13 NLS myc shows a staining pattern localised to the nuclear border suggesting a concentration of the construct at or near the nuclear envelope (Fig. 8A). A similar pattern was previously observed in COS-7 cells transfected with CaMBP4 (Wang et al., 1995).

Using rAAV-mediated gene transfer, expression of 2xM13 NLS myc in neurons blocks synaptic activity-evoked CREB mediated gene transcription compared to control (i.e. noninfected neurons or neurons infected with rAAV hrGFP). Induction of cFos and ATF3 expression were strongly reduced in neurons infected with rAAV 2xM13 NLS myc after 4hr bicuculline ($50\mu\text{M}$) stimulation (Fig. 8B), which specifically activates the nuclear Ca^{2+} /CaM pathway (Pokorska et al., 2003). Surprisingly, induction of cFos and ATF3 expression were also reduced after 4hr $10\mu\text{M}$ Forskolin/ 0.5mM IBMX stimulation

(Buchthal et al. unpublished data). It is known that Forskolin/ IBMX stimulation leads to an increase of the second messenger cAMP, which activates PKA causing its translocation to the nucleus and activation of CREB mediated gene transcription (e.g. cFos and ATF3) (Mayr and Montminy, 2001). It is not clear whether Forskolin activates the observed long lasting elevated nuclear Ca^{2+} level via cAMP–PKA activation (Fig. 8D). Nevertheless, 2xM13 NLS myc blocks Forskolin/ IBMX induced cFos and ATF3 expression activated by nuclear Ca^{2+} signalling. The Ca^{2+} live imaging experiments confirm the specificity of the nuclear Ca^{2+} /CaM-inhibitor, but for unknown reasons 2xM13 NLS myc infected neurons showed higher amplitude bicuculline-induced Ca^{2+} signals compare to the uninfected neurons. From these results one can't exclude that either the inhibitor or virus infection itself was responsible for the increase of amplitudes. It is likely that the increase of amplitudes caused by blocking nuclear Ca^{2+} signalling during the development of the neuronal network. Therefore, an inert control more similar to rAAV 2xM13 NLS myc was developed, where in each peptide of M13 three charged amino acids responsible for the Ca^{2+} /CaM binding properties of M13 are replaced by uncharged amino acids. The mutated inhibitor was named mM13 NLS myc. But the functional tests of this control are still under investigation.

6.3 Visualisation of nuclear Ca^{2+} signals in 3rd instar larvae

In 3rd instar larvae GCaMP NLS is exclusively expressed in the cell nucleus, but hard to detect without GFP antibody staining. To increase protein expression level the P-element containing UAS GCaMP NLS were genetically immobilised and randomly integrated into a new chromosomal site. Fly lines UAS GCaMP NLS 3.1 and UAS GCaMP NLS 7.3 were used for live imaging, but still the fluorescent signal is smaller compare to UAS GCaMP. Therefore, the difference observed in the larval brain expressing either UAS GCaMP NLS (Fig 9D) or UAS GCaMP (Fig 9E) depends more likely on the expression levels due to integration sites of the P-elements as on different Ca^{2+} concentration within the nucleus compare to the cytoplasm. In general, it is difficult to monitor changes in fluorescent within single nuclei over time in small optical section due to x/y- or z-movements. However, these results show that UAS GCaMP NLS

expressed in 3rd instar larvae are suitable to detect changes in Ca²⁺ concentration and is exclusively localised to the nucleus.

6.4 Blocking nuclear Ca²⁺/CaM signalling pathway in adult flies

Both learning and early memory are disrupted in *dunce* and *rutabaga* mutants, suggesting that these genes primarily are involved in STM (Tully et al., 1994). In 1994, Tully et al. show that in flies fed cycloheximide (CXM: protein-synthesis inhibitor) learning and memory retention during the first 7 hr was unaffected, whereas in CXM-fed flies LTM was blocked (Tully et al., 1994). Interestingly, it seems that only 50% level of inhibition of protein synthesis in whole-brain tissue is sufficient to disrupt LTM (Tully et al., 1994).

Flies expressing the nuclear Ca²⁺/CaM inhibitor 2xM13 NLS myc during the time period of acquisition showed an impaired LTM after space training (Fig. 10E), whereas STM was unaffected (Fig. 10D). Expression of nuclear Ca²⁺/CaM inhibitor under the control of Hs-Gal4 was restricted to a few cells within the brain (Fig. 10A) suggesting that blockade of those cells could be sufficient to impair LTM. LTM is not affected in flies expressing the inhibitor at a time period between acquisition and retrieval (Fig. 10F).

These data provide for the first time an evidence for the role of nuclear Ca²⁺/CaM signalling during the acquisition phase of LTM in flies, but has to be confirmed by further control experiments. Therefore, LTM studies will be repeated using either a second fly line expressing 2xM13 NLS myc and in addition a new fly line expressing a Myc tagged version of rAAV CaMBP4 flag (Wang et al., 1996; Limback-Stokin et al., 2004; Zhang et al., 2007) were generated (Fig. 10H).

6.5 Visualisation of Ca²⁺ signals in mushroom bodies of adult flies

The results obtained by the olfactory avoidance assay indicate that nuclear Ca²⁺ signals seem to be required during the acquisition phase of LTM. This was inferred from the result that overexpression of the nuclear Ca²⁺/CaM inhibitor (UAS 2xM13 NLS myc) in adult flies interferes with LTM. It is not clear which brain region are involved in LTM. The mushroom bodies are the most favoured regions within the fly brain for transcription-dependent memory because several genes involved in LTM are mushroom

body specific (Dudai et al., 1976; Livingstone et al., 1984; Skoulakis et al., 1993; Goodwin et al., 1997; Dubnau et al., 2003; Didelot et al., 2006). Further, the mushroom bodies can be removed from the adult fly brain by pulsefeeding hydroxyurea to larvae (de Belle, 1994 #766) or by mutations (Heisenberg et al., 1985). Such studies indicate that the mushroom bodies are required for olfactory learning and memory (Heisenberg et al., 1985; de Belle and Heisenberg, 1994). Previous studies have reported that mushroom body synaptic output is dispensable during memory acquisition and storage but required for the retrieval of aversive odour memory (Dubnau et al., 2001; McGuire et al., 2001; Schwaerzel et al., 2002; Davis, 2005), but most mushroom body Gal4 drivers lines only label a fraction of Kenyon cells, and little effort has been expended to quantify the extent of expression in each line (Keene and Waddell, 2007). Krashes et al. could show that neurotransmission from the $\alpha'\beta'$ subset of mushroom body neurons is required to acquire and stabilize aversive odour memory, but is dispensable during memory retrieval. In contrast, neurotransmission from mushroom body $\alpha\beta$ neurons are only required for memory retrieval (Krashes et al., 2007).

To confirm the preliminary data of the odour avoidance assay, *in vivo* imaging was performed in the lab to visualise changes in Ca^{2+} signals during a LTM inducing training protocol. *In vivo* imaging in *D. melanogaster* in context of olfactory learning provides a suitable technique first time described in 2002 by Fiala et al. (Fiala et al., 2002) and further developed by Yu et al. (Yu et al., 2004). The difference observed in the larval brain expressing either UAS GCaMP NLS (Fig 9D) or UAS GCaMP (Fig 9E) after high potassium stimulation was also observed in adult flies. These findings suggest that differences in Ca^{2+} level of the nucleus and the cytoplasm are most likely due to differences in the expression levels of the indicators (Fig. 11B) and cannot be attributed to preparation or the imaging system which was identical.

Small changes in fluorescence were recorded either after electrical shock pulse or odour application or both stimuli paired in flies expressing UAS GCaMP under control of a mushroom body specific driver line (Fig. 11C). The results obtained for the electrical stimulation are similar to the previously published data (Yu et al., 2005), but in that study Ca^{2+} signals were recorded from DPM neurons. It is not clear if Ca^{2+} signalling in that subset of neurons is comparable to the Ca^{2+} signalling within Kenyon cells.

Riemensperger et al. measured Ca^{2+} signals evoked by electrical shock pulses in adult fly brains, but in that studies a different preparation technique and another Ca^{2+} indicator was used (Riemensperger et al., 2005). In addition, Ca^{2+} signals were recorded from dopaminergic projection neurons and not from mushroom bodies, which makes it more difficult to compare. To compare Ca^{2+} signals, calibration of the fluorescent signals would be necessary, but is extremely difficult *in vivo*.

Whereas the results obtained after electrical stimulation are in the range of previously published studies, differ the odour evoked Ca^{2+} signals completely from a previous study. Wang et al. reported large fluorescence transients in a subset of Kenyon cells after odour application (Wang et al., 2004). It is still unclear if these differences were due to the Gal4 driver line, the odours used, the use of two-photon microscopy or (most likely) differences in preparation and odour application. Improving fly preparation, odour application and imaging techniques will undoubtedly improve odour-evoked and stimulation-evoked fluorescence responses in our experiments. Further, the generation of a new transgenic fly expressing the nuclear Ca^{2+} -indicator GCaMP2 NLS fused to a red fluorescent protein, named mCherry (Shaner et al., 2004) might solve the problem described between UAS GCaMP and UAS GCaMP NLS due to higher basal fluorescence of GCAMP2. In addition, flies expressing UAS GCAMP2 NLS Cherry will allow us to distinguish changes in fluorescence evoked by artefacts from changes in fluorescence evoked by increases in Ca^{2+} concentration.

6.6 Visualisation of nuclear Ca^{2+} signals in brain slices

Several Ca^{2+} indicators including Inverse Pericam (Nagai et al., 2001), GCaMP 1.6 (Ohkura et al., 2005) and GCaMP 2.0 (Tallini et al., 2006) were cloned into a modified rAAV vector containing three tandem repeats of the nuclear localization signal from simian virus large T-antigen at the carboxy-terminus of the multiple cloning site (Fischer-Fantuzzi and Vesco, 1988). The nuclear Ca^{2+} indicators were express by rAAV-mediated gene transfer in hippocampal slices cultures. The expression of all used indicators were restricted to the nucleus. Among the tested indicators rAAV Inverse Pericam NLS shows by far the brightest fluorescence signal at 37°C (Fig 12A), whereas rAAV GCaMP 1.6 NLS was barely visible at that temperature. All indicators showed a large decrease in

fluorescence at the start of excitation but recovered fluorescence after several seconds in the dark, indicating that the fluorescence decrease results from photoisomerization, but not from bleaching. All indicators were able to detect oscillatory Ca^{2+} changes induced by bicuculline application over long recording periods (1hr) with no or only slight bleaching effects (Fig. 12B and 12C). The indicators rAAV Inverse Pericam NLS and rAAV GCaMP 2.0 NLS show a much brighter basal fluorescence than rAAV GCaMP 1.6 NLS making infected cells much easier to locate. All three indicators showed a similar dynamic range (fluorescence difference between minimum and maximum Ca^{2+} concentrations) consistent with previous reports (Koltikoff 2007; Polugrotto 2004). Responses to bicuculline application were observed in hippocampal slices cultures infected with rAAV Inverse Pericam NLS, but only small changes in fluorescence amplitudes were measured. These translate to large signals when represented as $\Delta F/F$ but are often difficult to detect from the raw fluorescence signal making interpretations from on-line live analysis difficult during experiments. Comparing all tested Ca^{2+} indicators including FRET based indicators like YC 3.60 (Nagai et al., 2001), VC 6.1 (Evanko and Haydon, 2005), TN-XL (Mank et al., 2006) and D3 cpV (Palmer et al., 2006), rAAV GCaMP 2.0 NLS seems to be most suitable for *in vivo* imaging of nuclear Ca^{2+} signals due to improved brightness and thermo stability. Two recently studies reported the use of GCaMP 2.0 *in vivo* either expressed in cardiomyocyte or cerebellar granule cells of transgenic mice (Tallini et al., 2006; Diez-Garcia et al., 2007).

6.7 Visualisation of nuclear Ca^{2+} signals using rAAV GCaMP2 NLS Cherry

Changes in fluorescence due to movement artefacts are negligible in culture or in brain slices, but will be a serious issue for *in vivo* imaging. Distinguishing between fluorescence signals recorded due to movement and changes in Ca^{2+} concentration are important. Especially, for small changes in fluorescence visualized by single chromophore Ca^{2+} -indicator as Inverse Pericam or GCaMP such small changes are difficult to differentiate. Shimozono *et al.* modified the Ca^{2+} -indicator Inverse Pericam by attaching red fluorescent protein dsRed2 via a short linker to the C terminus (Shimozono et al., 2004). Based on that construct, a far-red fluorescent protein mCherry (Shaner et al., 2004) was attached to rAAV GCaMP 2.0 NLS.

The maturation of the protein is not affected due to attachment of mCherry. The indicator is fully functional at 37°C and is exclusively localised to the cell nucleus detected either within the emission spectrum of GFP or within the emission spectrum of mCherry (Fig. 13B). Therefore, it is unlikely that the attached mCherry protein projects towards the interior of the indicator and make it inaccessible by masking the NLS for binding to proteins involved in nuclear import. Further, it is unlikely that mCherry disturbs the interaction between the M13 and calmodulin because disturbance/defect in the interaction of both domains is responsible for detection of changes in fluorescence and would lead to reduced Ca²⁺ sensitivity. Indeed, the Ca²⁺-indicator rAAV GCaMP2 NLS Cherry was suitable to detect Ca²⁺ transient over long time periods and no significant bleaching effect was observed. A part of the GFP emission spectrum overlapped with the excitation spectrum of mCherry as described (Shaner et al., 2004). Tramier et al. reported that GFP and mCherry were suitable for FRET based lifetime imaging in living cells (Tramier et al., 2006). But in hippocampal neurons expressing GCaMP2 NLS Cherry no or only slight changes in fluorescence were detected within the emission spectrum of mCherry, whereas large changes in fluorescence at the same time were detected within the emission spectrum of GFP after application of bicuculline (Fig 13C). The changes in fluorescence were comparable to previously reported Ca²⁺ signals visualised by rAAV GCaMP 2.0. Therefore, decrease of the GFP signal evoked by FRET was not observed in cell culture. To determine whether the modification has influence on infection efficiency, dissociated neurons (Fig 13B) and organotypic slice cultures (Fig 13D) of rat hippocampus were infected with rAAV GCaMP2 NLS Cherry. In spite of large coding sequence of GCaMP2 NLS Cherry and the limited packing capacity of rAAV, no or negligible differences in transfection efficiency was observed compares to the other indicator.

Since the tested Ca²⁺-indicators based on interaction between the Ca²⁺ binding protein calmodulin (CaM) and M13, it might be possible that endogenous Ca²⁺ or endogenous calmodulin be inhibited or buffered by overexpression of the nuclear Ca²⁺-indicators and so not longer available for nuclear Ca²⁺ signalling. Effects on signalling pathways and subsequent gene expression were tested with Western Blot analysis. Induction of cFos and ATF3 expression was not reduced in neurons infected either with

rAAV GCaMP 2.0 NLS, rAAV GCaMP2 NLS Cherry or rAAV EYFP NUC or left uninfected after 4hr bicuculline stimulation. Indicating that the infection with nuclear Ca^{2+} -indicators did not affect nuclear Ca^{2+} signalling pathways (Fig 13E).

6.8 Visualisation of nuclear Ca^{2+} signals in brain slices

The role of nuclear Ca^{2+} as the link between synaptic stimulation and gene transcription has only been intensively investigated in cell culture (Hardingham et al., 2001).. This raises the question whether nuclear Ca^{2+} plays a role in cell systems with a more complex, more physiological organisation such as acute brain slices? Do nuclear Ca^{2+} events occur in brain slices or *in vivo* and if so, is it possible to trigger them by synaptic stimulation. Two publications have described nuclear Ca^{2+} signals in acute brain slices with regard to late phase LTP (Johanning and Holthoff, 2006; Raymond and Redman, 2006). The role of these nuclear Ca^{2+} signals in transcription-dependent plasticity is controversial and unclear. Furthermore, the complexity of the mammalian brain makes it difficult to extrapolate results from *in vitro* experiments to the intact brain. Ideally one would like to image nuclear Ca^{2+} signals within the intact hippocampus induced by neural activity during the performance of behavioural tasks. To date, no one has published results using Ca^{2+} -indicator delivered by rAAV or localised to a subcellular compartment *in vivo*. Such results have been achieved in this thesis, by visualising nuclear Ca^{2+} signals evoked by electrical stimulation in acute brain slices of the hippocampus using either rAAV Inverse Pericam NLS or rAAV GCaMP 1.6 NLS or rAAV GCaMP 2.0 NLS.

The difference observed in dynamic ranges and Ca^{2+} responses between *in vitro* and *in vivo* assays has been discussed in details in the introduction. Briefly, either the Ca^{2+} /CaM binding peptide M13 of indicators binds to endogenous calmodulin or the calmodulin domain of the indicator participate in nonproductive interactions with endogenous calmodulin targets. Consistent with this idea, Hasan et al. have reported that 50% of the intracellular indicator is immobile and unresponsive to Ca^{2+} *in vivo* (Hasan et al., 2004).

According to that a bright green fluorescent signal restricted to the nucleus of CA1 hippocampal pyramidal neurons infected with rAAV Inverse Pericam NLS were

observed in acute brain slices of juvenile rats, but only small Ca^{2+} changes evoked by 3x100Hz electrical stimulations were recorded (Fig 14C). However, strong changes in nuclear Ca^{2+} concentration were measured in CA1 hippocampal pyramidal neurons expressing rAAV GCAMP 2.0 NLS (Fig 14D). The results obtained with rAAV GCAMP 2.0 NLS in acute slice are comparable to results obtained in organotypic slices (Fig 12C). That could mean that the reported buffering effect is not a general problem of Ca^{2+} -indicators rather it depends more on the spatial orientation of the functional domains. Consistent with that, Kotlikoff et al. reported that decreased fluorescence signal seems to be depending on the orientation between the donor and acceptor fluorophores in FRET based indicators, which may allow an enhanced vulnerability to interact with endogenous proteins. But to confirm that idea more experiments has to be done (Kotlikoff 2007).

Another point of discussion belongs to virus concentration used for *in vivo* injection. Aso et al. (unpublished data) described that high dose of virus concentration caused neuronal cell loss according to the injection site in adult rats. Analysis of adult rat brain slices (Fig. 14E) showed that neurons at CA1-CA3 regions could successfully be infected with either lower concentrations of rAAV GCaMP2 NLS Cherry ($2,05 \times 10^9$) or high concentrations of rAAV GCaMP2 NLS Cherry (4.89×10^{13}). Because of titration method by qPCR one cannot differentiate between infectious and uninfected viruses, which could explain the discrepancy observed. Further it is known that length and DNA sequence of the gene of interest influences packaging of the virus, which could result in higher dose of uninfected viruses. Toxicity will result from too much protein delivered by rAAV into cells. Nevertheless, either rAAV GCaMP 2.0 NLS or rAAV GCaMP2 NLS Cherry are suitable to visualise nuclear Ca^{2+} signals in acute brain slices and will be useful tools for *in vivo* imaging in freely moving animals.

6.9 Visualisation of Ca^{2+} signals in freshwater polyps using hyGCaMP

In vivo imaging studies are extremely useful, but always difficult to handle due to complex organization of the organism. So far only parts of animal could be imaged, but not the entire animal. Another question was whether nuclear calcium signals are restricted to higher organism or do they also exist in simpler organized animals. One of the simplest nervous systems described in the animal kingdom has the freshwater polyp

hydra. Due to the optical transparency of the outer and inner layer, hydra is ideal for live imaging experiments of an intact animal.

First, the entire coding sequence of pN1 GCaMP and pN1 GCaMP NLS were transiently expressed under the control of hydra specific actin promoter. But no fluorescence signals were observed. Like many other lower eukaryotes, in cnidarians the codon usage is very biased in favour of codons with an A or T at the third position, whereas vertebrate species more frequently display G or C (Galliot and Schummer, 1993). To express GCaMP or GCaMP NLS in *H. vulgaris* the entire coding sequence of pN1 GCaMP NLS was codon optimised according to NCBI taxonomy browser. The Ca²⁺-indicator hyGCaMP show a green fluorescence signal either in ectodermal or endodermal cells (Fig. 15A and 15D). Spontaneous changes in Ca²⁺ concentrations in ectodermal cells expressing hyGCaMP were observed most of the time randomly distributed, whereas less frequently spontaneous Ca²⁺ signals in form of a coordinate “Ca²⁺-wave” were observed (Fig 15B). Propagations of slow Ca²⁺ signals were recorded also within a single cell (Fig 15C). The molecular mechanism of the Ca²⁺ propagation in hydra is unknown either within a single cell or throughout a cellular network. One can speculated if such a slow Ca²⁺ signal within a cell used internal Ca²⁺ stores and propagates passively by diffusion or actively by mechanisms like Ca²⁺ induced Ca²⁺ release (Berridge et al., 2000). The Ca²⁺-wave propagation throughout the neighbouring cells based probably on gap junctions but also propagation via TNT might be a possible explanation (Rustom et al., 2004). Most of the time the Ca²⁺-waves started from a central point and spread out in all directions like concentric circles. Ca²⁺-waves were mostly observed in the foot region and sometimes in the head region, but never observed in the middle region (Fig 15G). These finding and the propagation in form of concentric circles might be depend on proceeding pacemaker neuronal activity. According to that Khalturin et al. observed that interstitial stem cell, after entering the neuron differentiation pathway migrate toward the head and foot region (Khalturin et al., 2007). Therefore, it could be possible that nerve cells innervate ectodermal cells and trigger such observed Ca²⁺-waves.

Spontaneous changes in Ca²⁺ concentrations observed in endodermal cells expressing hyGCaMP differed dramatically from the Ca²⁺ signals visualised in ectodermal cells. The Ca²⁺ signals were much faster and not restricted to a few cells rather

the entire foot region show fast oscillatory changes in fluorescents (Fig 15E and 15F). Such Ca^{2+} bursts were also observed throughout the whole animal, but again the foot and the head region seems to be more active than the middle region (Fig 15H). Therefore, it could be possible that neuronal cell activity trigger such Ca^{2+} bursts.

In 1963, Passano et al. described first time contraction of the body column as a result of ectodermal contraction burst pacemaker system. They could show that hydra undergoes series of longitudinal contractions each contraction is preceded by a large (30mV) but slow (250-500msec) compound potential. These ectodermal contractions bursts are similar to the observed endodermal Ca^{2+} bursts (Fig 15E). It is unclear if these signals are triggered by the same source e.g. nerve cells or activated each other. It is also unknown whether contraction bursts follow or precede endodermal Ca^{2+} bursts and whether contraction burst are really ectodermal origins.

6.10 Visualisation of nuclear Ca^{2+} signals in freshwater polyps using hyGCaMP NLS

The aim of my PhD thesis was to visualise nuclear Ca^{2+} signals *in vivo*. Using transgenic hydra expressing hyGCaMP NLS, changes in nuclear Ca^{2+} signals were observed *in vivo* (Fig. 16A and 16B). However, to differentiate between changes in fluorescent evoked by increase in Ca^{2+} concentration and changes in fluorescent caused purely by movement artefacts, a hydra optimised red fluorescent protein (mRFPmars) was attached to the C-terminus of the indicator (Muller-Taubenberger et al., 2006). Using transgenic hydra expressing hyGCaMP NLS mars in all ectodermal cells, comparable results were recorded. These suggest that the observed changes in fluorescent are indeed based on an increase in Ca^{2+} concentration (Fig. 16D and 16E). Surprisingly, only a few nuclei of hundreds showed spontaneous changes in fluorescent, but increase in Ca^{2+} concentration with the same frequency as ectodermal Ca^{2+} -wave were expected. Eder et al. reported that the nuclear envelope is unlikely to be a diffusion barrier for Ca^{2+} ions (Eder and Bading, 2007). Therefore, it is unclear why only a few nuclei show an increase in fluorescent. Perhaps, these differences depend on the indicator itself due to binding to endogenous binding partners, which was never observed other cell systems, but cannot be exclude. Another explanation could be that milieu in the nucleus is different compare to

the cytoplasm in Hydra (e.g. pH-value) and therefore kinetics and sensitivity of the indicator are changed with the consequence that small increases in nuclear Ca^{2+} concentration can not be detected anymore.

In general, not much is known about Ca^{2+} signalling in hydra, indeed it is the first time that changes in nuclear Ca^{2+} concentration are visualised in hydra. A proteomic study by Pauly et al. identified three Ca^{2+} binding proteins including calmodulin, which is a key player in the nuclear Ca^{2+} pathway described above (Pauly et al., 2007). Moreover, *Cnidaria* not only have about the same number of genes as human and share most of their genes with human (Miller et al., 2005) but their protein sequences are often more similar to human sequences than to those from fly and worm (Kortschak et al., 2003). One can speculate if such nuclear Ca^{2+} signals play a role in CREB dependent gene transcription. Signalling pathways might be evolutionary conserved and several groups have reported that CREB plays a role hydra head regeneration (Galliot et al., 1995; Kaloulis et al., 2004; Arvizu et al., 2006; Manuel et al., 2006; Chera et al., 2007). However, to determine the role of nuclear Ca^{2+} signals in hydra is an exciting question but could be answered here. Nevertheless, it is unlikely that nuclear Ca^{2+} signals have no function in hydra.

7 References

- Andersen P, Bliss TV, Skrede KK (1971) Unit analysis of hippocampal population spikes. *Exp Brain Res* 13:208-221.
- Arnold FJ, Hofmann F, Bengtson CP, Wittmann M, Vanhoutte P, Bading H (2005) Microelectrode array recordings of cultured hippocampal networks reveal a simple model for transcription and protein synthesis-dependent plasticity. *J Physiol* 564:3-19.
- Arvizu F, Aguilera A, Salgado LM (2006) Activities of the protein kinases STK, PI3K, MEK, and ERK are required for the development of the head organizer in *Hydra magnipapillata*. *Differentiation* 74:305-312.
- Aso, Y (2007) Activity dependent induction of Gadd45 family genes and promotion of survival in hippocampal neurons. Master Thesis
- Atchison RW (1970) The role of herpesviruses in adenovirus-associated virus replication in vitro. *Virology* 42:155-162.
- Bachevalier J, Alvarado MC, Malkova L (1999) Memory and socioemotional behavior in monkeys after hippocampal damage incurred in infancy or in adulthood. *Biol Psychiatry* 46:329-339.
- Bading H (2000) Transcription-dependent neuronal plasticity the nuclear calcium hypothesis. *Eur J Biochem* 267:5280-5283.
- Bading H, Greenberg ME (1991) Stimulation of protein tyrosine phosphorylation by NMDA receptor activation. *Science* 253:912-914.
- Bading H, Ginty DD, Greenberg ME (1993) Regulation of gene expression in hippocampal neurons by distinct calcium signaling pathways. *Science* 260:181-186.
- Bading H, Segal MM, Sucher NJ, Dudek H, Lipton SA, Greenberg ME (1995) N-methyl-D-aspartate receptors are critical for mediating the effects of glutamate on intracellular calcium concentration and immediate early gene expression in cultured hippocampal neurons. *Neuroscience* 64:653-664.
- Baird GS, Zacharias DA, Tsien RY (1999) Circular permutation and receptor insertion within green fluorescent proteins. *Proc Natl Acad Sci U S A* 96:11241-11246.

- Barria A, Muller D, Derkach V, Griffith LC, Soderling TR (1997) Regulatory phosphorylation of AMPA-type glutamate receptors by CaM-KII during long-term potentiation. *Science* 276:2042-2045.
- Bartlett JS, Wilcher R, Samulski RJ (2000) Infectious entry pathway of adeno-associated virus and adeno-associated virus vectors. *J Virol* 74:2777-2785.
- Becerra SP, Rose JA, Hardy M, Baroudy BM, Anderson CW (1985) Direct mapping of adeno-associated virus capsid proteins B and C: a possible ACG initiation codon. *Proc Natl Acad Sci U S A* 82:7919-7923.
- Berridge MJ (1993) Inositol trisphosphate and calcium signalling. *Nature* 361:315-325.
- Berridge MJ, Lipp P, Bootman MD (2000) The versatility and universality of calcium signalling. *Nat Rev Mol Cell Biol* 1:11-21.
- Bito H, Deisseroth K, Tsien RW (1996) CREB phosphorylation and dephosphorylation: a Ca(2+)- and stimulus duration-dependent switch for hippocampal gene expression. *Cell* 87:1203-1214.
- Bleker S, Sonntag F, Kleinschmidt JA (2005) Mutational analysis of narrow pores at the fivefold symmetry axes of adeno-associated virus type 2 capsids reveals a dual role in genome packaging and activation of phospholipase A2 activity. *J Virol* 79:2528-2540.
- Blinks JR, Prendergast FG, Allen DG (1976) Photoproteins as biological calcium indicators. *Pharmacol Rev* 28:1-93.
- Bliss TV, Lomo T (1973) Long-lasting potentiation of synaptic transmission in the dentate area of the anaesthetized rabbit following stimulation of the perforant path. *J Physiol* 232:331-356.
- Bliss TV, Collingridge GL (1993) A synaptic model of memory: long-term potentiation in the hippocampus. *Nature* 361:31-39.
- Blumenthal DK, Krebs EG (1987) Preparation and properties of the calmodulin-binding domain of skeletal muscle myosin light chain kinase. *Methods Enzymol* 139:115-126.
- Boehm J, Malinow R (2005) AMPA receptor phosphorylation during synaptic plasticity. *Biochem Soc Trans* 33:1354-1356.

- Bongers, M (2007) Analysis of expression of a nuclear calmodulin binding peptide in the *Drosophila melanogaster* brain. Bachelor Thesis
- Bootman MD, Lipp P (1999) Ringing changes to the 'bell-shaped curve'. *Curr Biol* 9:R876-878.
- Bosch TC (2007) Why polyps regenerate and we don't: towards a cellular and molecular framework for Hydra regeneration. *Dev Biol* 303:421-433.
- Bourtchuladze R, Frenguelli B, Blendy J, Cioffi D, Schutz G, Silva AJ (1994) Deficient long-term memory in mice with a targeted mutation of the cAMP-responsive element-binding protein. *Cell* 79:59-68.
- Brand AH, Perrimon N (1993) Targeted gene expression as a means of altering cell fates and generating dominant phenotypes. *Development* 118:401-415.
- Burger C, Gorbatyuk OS, Velardo MJ, Peden CS, Williams P, Zolotukhin S, Reier PJ, Mandel RJ, Muzyczka N (2004) Recombinant AAV viral vectors pseudotyped with viral capsids from serotypes 1, 2, and 5 display differential efficiency and cell tropism after delivery to different regions of the central nervous system. *Mol Ther* 10:302-317.
- Byers D, Davis RL, Kiger JA, Jr. (1981) Defect in cyclic AMP phosphodiesterase due to the dunce mutation of learning in *Drosophila melanogaster*. *Nature* 289:79-81.
- Campbell RD (1967) Tissue dynamics of steady state growth in *Hydra littoralis*. I. Patterns of cell division. *Dev Biol* 15:487-502.
- Cardenas M, Fabila YV, Yum S, Cerbon J, Bohmer FD, Wetzker R, Fujisawa T, Bosch TC, Salgado LM (2000) Selective protein kinase inhibitors block head-specific differentiation in hydra. *Cell Signal* 12:649-658.
- Cardenas MM, Salgado LM (2003) STK, the src homologue, is responsible for the initial commitment to develop head structures in Hydra. *Dev Biol* 264:495-505.
- Casto BC, Atchison RW, Hammon WM (1967) Studies on the relationship between adeno-associated virus type I (AAV-1) and adenoviruses. I. Replication of AAV-1 in certain cell cultures and its effect on helper adenovirus. *Virology* 32:52-59.
- Cetin A, Komai S, Eliava M, Seeburg PH, Osten P (2006) Stereotaxic gene delivery in the rodent brain. *Nat Protoc* 1:3166-3173.

- Chawla S, Bading H (2001) CREB/CBP and SRE-interacting transcriptional regulators are fast on-off switches: duration of calcium transients specifies the magnitude of transcriptional responses. *J Neurochem* 79:849-858.
- Chawla S, Hardingham GE, Quinn DR, Bading H (1998) CBP: a signal-regulated transcriptional coactivator controlled by nuclear calcium and CaM kinase IV. *Science* 281:1505-1509.
- Chen C, Tonegawa S (1997) Molecular genetic analysis of synaptic plasticity, activity-dependent neural development, learning, and memory in the mammalian brain. *Annu Rev Neurosci* 20:157-184.
- Chen L, Chetkovich DM, Petralia RS, Sweeney NT, Kawasaki Y, Wenthold RJ, Brecht DS, Nicoll RA (2000) Stargazin regulates synaptic targeting of AMPA receptors by two distinct mechanisms. *Nature* 408:936-943.
- Chen S, Kapturczak M, Loiler SA, Zolotukhin S, Glushakova OY, Madsen KM, Samulski RJ, Hauswirth WW, Campbell-Thompson M, Berns KI, Flotte TR, Atkinson MA, Tisher CC, Agarwal A (2005) Efficient transduction of vascular endothelial cells with recombinant adeno-associated virus serotype 1 and 5 vectors. *Hum Gene Ther* 16:235-247.
- Chera S, Kaloulis K, Galliot B (2007) The cAMP response element binding protein (CREB) as an integrative HUB selector in metazoans: clues from the hydra model system. *Biosystems* 87:191-203.
- Chiorini JA, Kim F, Yang L, Kotin RM (1999) Cloning and characterization of adeno-associated virus type 5. *J Virol* 73:1309-1319.
- Chiorini JA, Yang L, Liu Y, Safer B, Kotin RM (1997) Cloning of adeno-associated virus type 4 (AAV4) and generation of recombinant AAV4 particles. *J Virol* 71:6823-6833.
- Clapham DE (1995) Calcium signaling. *Cell* 80:259-268.
- Coan EJ, Collingridge GL (1987) Characterization of an N-methyl-D-aspartate receptor component of synaptic transmission in rat hippocampal slices. *Neuroscience* 22:1-8.

- Coan EJ, Saywood W, Collingridge GL (1987) MK-801 blocks NMDA receptor-mediated synaptic transmission and long term potentiation in rat hippocampal slices. *Neurosci Lett* 80:111-114.
- Collingridge GL, Kehl SJ, McLennan H (1983) Excitatory amino acids in synaptic transmission in the Schaffer collateral-commissural pathway of the rat hippocampus. *J Physiol* 334:33-46.
- Connolly JB, Roberts IJ, Armstrong JD, Kaiser K, Forte M, Tully T, O'Kane CJ (1996) Associative learning disrupted by impaired Gs signaling in *Drosophila* mushroom bodies. *Science* 274:2104-2107.
- Couto A, Alenius M, Dickson BJ (2005) Molecular, anatomical, and functional organization of the *Drosophila* olfactory system. *Curr Biol* 15:1535-1547.
- Crittenden JR, Skoulakis EM, Han KA, Kalderon D, Davis RL (1998) Tripartite mushroom body architecture revealed by antigenic markers. *Learn Mem* 5:38-51.
- Cruzalegui FH, Means AR (1993) Biochemical characterization of the multifunctional Ca²⁺/calmodulin-dependent protein kinase type IV expressed in insect cells. *J Biol Chem* 268:26171-26178.
- Daly KC, Christensen TA, Lei H, Smith BH, Hildebrand JG (2004) Learning modulates the ensemble representations for odors in primary olfactory networks. *Proc Natl Acad Sci U S A* 101:10476-10481.
- Davis RL (2004) Olfactory learning. *Neuron* 44:31-48.
- Davis RL (2005) Olfactory memory formation in *Drosophila*: from molecular to systems neuroscience. *Annu Rev Neurosci* 28:275-302.
- de Belle JS, Heisenberg M (1994) Associative odor learning in *Drosophila* abolished by chemical ablation of mushroom bodies. *Science* 263:692-695.
- Deutzmann R, Fowler S, Zhang X, Boone K, Dexter S, Boot-Handford RP, Rachel R, Sarras MP, Jr. (2000) Molecular, biochemical and functional analysis of a novel and developmentally important fibrillar collagen (Hcol-I) in hydra. *Development* 127:4669-4680.
- Diamond DM, Dunwiddie TV, Rose GM (1988) Characteristics of hippocampal primed burst potentiation in vitro and in the awake rat. *J Neurosci* 8:4079-4088.

- Didelot G, Molinari F, Tchenio P, Comas D, Milhiet E, Munnich A, Colleaux L, Preat T (2006) Tequila, a neurotrypsin ortholog, regulates long-term memory formation in *Drosophila*. *Science* 313:851-853.
- Diegelmann S, Fiala A, Leibold C, Spall T, Buchner E (2002) Transgenic flies expressing the fluorescence calcium sensor Cameleon 2.1 under UAS control. *Genesis* 34:95-98.
- Diez-Garcia J, Akemann W, Knopfel T (2007) In vivo calcium imaging from genetically specified target cells in mouse cerebellum. *Neuroimage* 34:859-869.
- Ditzel, D (2008) Imaging of spatially distinct calcium signals using recombinant Ca²⁺ probes. Diploma Thesis
- Duan D, Li Q, Kao AW, Yue Y, Pessin JE, Engelhardt JF (1999) Dynamin is required for recombinant adeno-associated virus type 2 infection. *J Virol* 73:10371-10376.
- Dubnau J, Grady L, Kitamoto T, Tully T (2001) Disruption of neurotransmission in *Drosophila* mushroom body blocks retrieval but not acquisition of memory. *Nature* 411:476-480.
- Dubnau J, Chiang AS, Grady L, Barditch J, Gossweiler S, McNeil J, Smith P, Buldoc F, Scott R, Certa U, Broger C, Tully T (2003) The staufen/pumilio pathway is involved in *Drosophila* long-term memory. *Curr Biol* 13:286-296.
- Dudai Y (1983) Mutations affect storage and use of memory differentially in *Drosophila*. *Proc Natl Acad Sci U S A* 80:5445-5448.
- Dudai Y, Jan YN, Byers D, Quinn WG, Benzer S (1976) dunce, a mutant of *Drosophila* deficient in learning. *Proc Natl Acad Sci U S A* 73:1684-1688.
- Eder A, Bading H (2007) Calcium signals can freely cross the nuclear envelope in hippocampal neurons: somatic calcium increases generate nuclear calcium transients. *BMC Neurosci* 8:57.
- Ehlers MD (2000) Reinsertion or degradation of AMPA receptors determined by activity-dependent endocytic sorting. *Neuron* 28:511-525.
- Engert F, Bonhoeffer T (1999) Dendritic spine changes associated with hippocampal long-term synaptic plasticity. *Nature* 399:66-70.

- Evanko DS, Haydon PG (2005) Elimination of environmental sensitivity in a cameleon FRET-based calcium sensor via replacement of the acceptor with Venus. *Cell Calcium* 37:341-348.
- Fabila Y, Navarro L, Fujisawa T, Bode HR, Salgado LM (2002) Selective inhibition of protein kinases blocks the formation of a new axis, the beginning of budding, in Hydra. *Mech Dev* 119:157-164.
- Feany MB, Quinn WG (1995) A neuropeptide gene defined by the Drosophila memory mutant amnesiac. *Science* 268:869-873.
- Fiala A, Spall T, Diegelmann S, Eisermann B, Sachse S, Devaud JM, Buchner E, Galizia CG (2002) Genetically expressed cameleon in Drosophila melanogaster is used to visualize olfactory information in projection neurons. *Curr Biol* 12:1877-1884.
- Fink CC, Meyer T (2002) Molecular mechanisms of CaMKII activation in neuronal plasticity. *Curr Opin Neurobiol* 12:293-299.
- Fischer-Fantuzzi L, Vesco C (1988) Cell-dependent efficiency of reiterated nuclear signals in a mutant simian virus 40 oncoprotein targeted to the nucleus. *Mol Cell Biol* 8:5495-5503.
- Fisher SK, Heacock AM, Agranoff BW (1992) Inositol lipids and signal transduction in the nervous system: an update. *J Neurochem* 58:18-38.
- Fishilevich E, Vosshall LB (2005) Genetic and functional subdivision of the Drosophila antennal lobe. *Curr Biol* 15:1548-1553.
- Fowler SJ, Jose S, Zhang X, Deutzmann R, Sarras MP, Jr., Boot-Handford RP (2000) Characterization of hydra type IV collagen. Type IV collagen is essential for head regeneration and its expression is up-regulated upon exposure to glucose. *J Biol Chem* 275:39589-39599.
- Fukazawa Y, Saitoh Y, Ozawa F, Ohta Y, Mizuno K, Inokuchi K (2003) Hippocampal LTP is accompanied by enhanced F-actin content within the dendritic spine that is essential for late LTP maintenance in vivo. *Neuron* 38:447-460.
- Fukunaga K, Stoppini L, Miyamoto E, Muller D (1993) Long-term potentiation is associated with an increased activity of Ca²⁺/calmodulin-dependent protein kinase II. *J Biol Chem* 268:7863-7867.

- Furuichi T, Mikoshiba K (1995) Inositol 1, 4, 5-trisphosphate receptor-mediated Ca²⁺ signaling in the brain. *J Neurochem* 64:953-960.
- Galliot B, Schummer M (1993) 'Guessmer' screening strategy applied to species with AT-rich coding sequences. *Trends Genet* 9:3-4.
- Galliot B, Welschof M, Schuckert O, Hoffmeister S, Schaller HC (1995) The cAMP response element binding protein is involved in hydra regeneration. *Development* 121:1205-1216.
- Gao GP, Alvira MR, Wang L, Calcedo R, Johnston J, Wilson JM (2002) Novel adeno-associated viruses from rhesus monkeys as vectors for human gene therapy. *Proc Natl Acad Sci U S A* 99:11854-11859.
- Gao Q, Yuan B, Chess A (2000) Convergent projections of *Drosophila* olfactory neurons to specific glomeruli in the antennal lobe. *Nat Neurosci* 3:780-785.
- Gierer A, Berking S, Bode H, David CN, Flick K, Hansmann G, Schaller H, Trenkner E (1972) Regeneration of hydra from reaggregated cells. *Nat New Biol* 239:98-101.
- Ginty DD, Bonni A, Greenberg ME (1994) Nerve growth factor activates a Ras-dependent protein kinase that stimulates c-fos transcription via phosphorylation of CREB. *Cell* 77:713-725.
- Goodwin SF, Del Vecchio M, Velinzon K, Hogel C, Russell SR, Tully T, Kaiser K (1997) Defective learning in mutants of the *Drosophila* gene for a regulatory subunit of cAMP-dependent protein kinase. *J Neurosci* 17:8817-8827.
- Green MR, Roeder RG (1980) Definition of a novel promoter for the major adenovirus-associated virus mRNA. *Cell* 22:231-242.
- Greenstein YJ, Pavlides C, Winson J (1988) Long-term potentiation in the dentate gyrus is preferentially induced at theta rhythm periodicity. *Brain Res* 438:331-334.
- Griesbeck O (2004) Fluorescent proteins as sensors for cellular functions. *Curr Opin Neurobiol* 14:636-641.
- Griesbeck O, Baird GS, Campbell RE, Zacharias DA, Tsien RY (2001) Reducing the environmental sensitivity of yellow fluorescent protein. Mechanism and applications. *J Biol Chem* 276:29188-29194.
- Grynkiewicz G, Poenie M, Tsien RY (1985) A new generation of Ca²⁺ indicators with greatly improved fluorescence properties. *J Biol Chem* 260:3440-3450.

- Hardingham GE, Bading H (1998) Nuclear calcium: a key regulator of gene expression. *Biometals* 11:345-358.
- Hardingham GE, Arnold FJ, Bading H (2001) Nuclear calcium signaling controls CREB-mediated gene expression triggered by synaptic activity. *Nat Neurosci* 4:261-267.
- Hardingham GE, Chawla S, Johnson CM, Bading H (1997) Distinct functions of nuclear and cytoplasmic calcium in the control of gene expression. *Nature* 385:260-265.
- Hasan MT, Friedrich RW, Euler T, Larkum ME, Giese G, Both M, Duebel J, Waters J, Bujard H, Griesbeck O, Tsien RY, Nagai T, Miyawaki A, Denk W (2004) Functional fluorescent Ca²⁺ indicator proteins in transgenic mice under TET control. *PLoS Biol* 2:e163.
- Hauck B, Chen L, Xiao W (2003) Generation and characterization of chimeric recombinant AAV vectors. *Mol Ther* 7:419-425.
- Heim N, Griesbeck O (2004) Genetically encoded indicators of cellular calcium dynamics based on troponin C and green fluorescent protein. *J Biol Chem* 279:14280-14286.
- Heim R, Tsien RY (1996) Engineering green fluorescent protein for improved brightness, longer wavelengths and fluorescence resonance energy transfer. *Curr Biol* 6:178-182.
- Heinemann U, Hahn M (1995) Circular permutation of polypeptide chains: implications for protein folding and stability. *Prog Biophys Mol Biol* 64:121-143.
- Heisenberg M (2003) Mushroom body memoir: from maps to models. *Nat Rev Neurosci* 4:266-275.
- Heisenberg M, Wolf R (1993) The sensory-motor link in motion-dependent flight control of flies. *Rev Oculomot Res* 5:265-283.
- Heisenberg M, Borst A, Wagner S, Byers D (1985) *Drosophila* mushroom body mutants are deficient in olfactory learning. *J Neurogenet* 2:1-30.
- Hermonat PL, Muzyczka N (1984) Use of adeno-associated virus as a mammalian DNA cloning vector: transduction of neomycin resistance into mammalian tissue culture cells. *Proc Natl Acad Sci U S A* 81:6466-6470.
- Hollmann M, Heinemann S (1994) Cloned glutamate receptors. *Annu Rev Neurosci* 17:31-108.

- Hu SC, Chrivia J, Ghosh A (1999) Regulation of CBP-mediated transcription by neuronal calcium signaling. *Neuron* 22:799-808.
- Ikura M, Clore GM, Gronenborn AM, Zhu G, Klee CB, Bax A (1992) Solution structure of a calmodulin-target peptide complex by multidimensional NMR. *Science* 256:632-638.
- Im DS, Muzyczka N (1989) Factors that bind to adeno-associated virus terminal repeats. *J Virol* 63:3095-3104.
- Im DS, Muzyczka N (1990) The AAV origin binding protein Rep68 is an ATP-dependent site-specific endonuclease with DNA helicase activity. *Cell* 61:447-457.
- Im DS, Muzyczka N (1992) Partial purification of adeno-associated virus Rep78, Rep52, and Rep40 and their biochemical characterization. *J Virol* 66:1119-1128.
- Impey S, Obrietan K, Wong ST, Poser S, Yano S, Wayman G, Deloulme JC, Chan G, Storm DR (1998) Cross talk between ERK and PKA is required for Ca²⁺ stimulation of CREB-dependent transcription and ERK nuclear translocation. *Neuron* 21:869-883.
- Isabel G, Pascual A, Preat T (2004) Exclusive consolidated memory phases in *Drosophila*. *Science* 304:1024-1027.
- Janson CG, McPhee SW, Leone P, Freese A, During MJ (2001) Viral-based gene transfer to the mammalian CNS for functional genomic studies. *Trends Neurosci* 24:706-712.
- Jefferis GS, Marin EC, Stocker RF, Luo L (2001) Target neuron prespecification in the olfactory map of *Drosophila*. *Nature* 414:204-208.
- Ji G, Feldman ME, Deng KY, Greene KS, Wilson J, Lee JC, Johnston RC, Rishniw M, Tallini Y, Zhang J, Wier WG, Blaustein MP, Xin HB, Nakai J, Kotlikoff MI (2004) Ca²⁺-sensing transgenic mice: postsynaptic signaling in smooth muscle. *J Biol Chem* 279:21461-21468.
- Johanning FW, Holthoff K (2006) Nuclear calcium signals during L-LTP induction do not predict the degree of synaptic potentiation. *Cell Calcium*.
- Kahn-Kirby AH, Dantzker JL, Apicella AJ, Schafer WR, Browse J, Bargmann CI, Watts JL (2004) Specific polyunsaturated fatty acids drive TRPV-dependent sensory signaling in vivo. *Cell* 119:889-900.

- Kaloulis K, Chera S, Hassel M, Gauchat D, Galliot B (2004) Reactivation of developmental programs: the cAMP-response element-binding protein pathway is involved in hydra head regeneration. *Proc Natl Acad Sci U S A* 101:2363-2368.
- Kandel ER (2001) The molecular biology of memory storage: a dialogue between genes and synapses. *Science* 294:1030-1038.
- Kashiwakura Y, Tamayose K, Iwabuchi K, Hirai Y, Shimada T, Matsumoto K, Nakamura T, Watanabe M, Oshimi K, Daida H (2005) Hepatocyte growth factor receptor is a coreceptor for adeno-associated virus type 2 infection. *J Virol* 79:609-614.
- Kauer JA, Malenka RC (2007) Synaptic plasticity and addiction. *Nat Rev Neurosci* 8:844-858.
- Keene AC, Waddell S (2007) Drosophila olfactory memory: single genes to complex neural circuits. *Nat Rev Neurosci* 8:341-354.
- Keene AC, Krashes MJ, Leung B, Bernard JA, Waddell S (2006) Drosophila dorsal paired medial neurons provide a general mechanism for memory consolidation. *Curr Biol* 16:1524-1530.
- Keene AC, Stratmann M, Keller A, Perrat PN, Vosshall LB, Waddell S (2004) Diverse odor-conditioned memories require uniquely timed dorsal paired medial neuron output. *Neuron* 44:521-533.
- Kern A, Schmidt K, Leder C, Muller OJ, Wobus CE, Bettinger K, Von der Lieth CW, King JA, Kleinschmidt JA (2003) Identification of a heparin-binding motif on adeno-associated virus type 2 capsids. *J Virol* 77:11072-11081.
- Khalturin K, Anton-Erxleben F, Milde S, Plotz C, Wittlieb J, Hemmrich G, Bosch TC (2007) Transgenic stem cells in Hydra reveal an early evolutionary origin for key elements controlling self-renewal and differentiation. *Dev Biol* 309:32-44.
- Klein RL, Meyer EM, Peel AL, Zolotukhin S, Meyers C, Muzyczka N, King MA (1998) Neuron-specific transduction in the rat septohippocampal or nigrostriatal pathway by recombinant adeno-associated virus vectors. *Exp Neurol* 150:183-194.
- Klein RL, Hamby ME, Gong Y, Hirko AC, Wang S, Hughes JA, King MA, Meyer EM (2002) Dose and promoter effects of adeno-associated viral vector for green fluorescent protein expression in the rat brain. *Exp Neurol* 176:66-74.

- Klugmann M, Symes CW, Leichtlein CB, Klausner BK, Dunning J, Fong D, Young D, During MJ (2005) AAV-mediated hippocampal expression of short and long Homer 1 proteins differentially affect cognition and seizure activity in adult rats. *Mol Cell Neurosci* 28:347-360.
- Kortschak RD, Samuel G, Saint R, Miller DJ (2003) EST analysis of the cnidarian *Acropora millepora* reveals extensive gene loss and rapid sequence divergence in the model invertebrates. *Curr Biol* 13:2190-2195.
- Kotlikoff MI (2007) Genetically encoded Ca²⁺ indicators: using genetics and molecular design to understand complex physiology. *J Physiol* 578:55-67.
- Krashes MJ, Keene AC, Leung B, Armstrong JD, Waddell S (2007) Sequential use of mushroom body neuron subsets during *Drosophila* odor memory processing. *Neuron* 53:103-115.
- Kuznetsov SG, Anton-Erxleben F, Bosch TC (2002) Epithelial interactions in *Hydra*: apoptosis in interspecies grafts is induced by detachment from the extracellular matrix. *J Exp Biol* 205:3809-3817.
- Kyostio SR, Owens RA, Weitzman MD, Antoni BA, Chejanovsky N, Carter BJ (1994) Analysis of adeno-associated virus (AAV) wild-type and mutant Rep proteins for their abilities to negatively regulate AAV p5 and p19 mRNA levels. *J Virol* 68:2947-2957.
- Lamprecht R, LeDoux J (2004) Structural plasticity and memory. *Nat Rev Neurosci* 5:45-54.
- Laroche S, Davis S, Jay TM (2000) Plasticity at hippocampal to prefrontal cortex synapses: dual roles in working memory and consolidation. *Hippocampus* 10:438-446.
- Larson J, Wong D, Lynch G (1986) Patterned stimulation at the theta frequency is optimal for the induction of hippocampal long-term potentiation. *Brain Res* 368:347-350.
- Lessing D, Carlson JR (1999) Chemosensory behavior: the path from stimulus to response. *Curr Opin Neurobiol* 9:766-771.
- Limback-Stokin K, Korzus E, Nagaoka-Yasuda R, Mayford M (2004) Nuclear calcium/calmodulin regulates memory consolidation. *J Neurosci* 24:10858-10867.

- Livingstone MS, Sziber PP, Quinn WG (1984) Loss of calcium/calmodulin responsiveness in adenylate cyclase of rutabaga, a *Drosophila* learning mutant. *Cell* 37:205-215.
- Lu YM, Jia Z, Janus C, Henderson JT, Gerlai R, Wojtowicz JM, Roder JC (1997) Mice lacking metabotropic glutamate receptor 5 show impaired learning and reduced CA1 long-term potentiation (LTP) but normal CA3 LTP. *J Neurosci* 17:5196-5205.
- Lynch MA (2004) Long-term potentiation and memory. *Physiol Rev* 84:87-136.
- Malenka RC (2003) The long-term potential of LTP. *Nat Rev Neurosci* 4:923-926.
- Malenka RC, Nicoll RA (1999) Long-term potentiation--a decade of progress? *Science* 285:1870-1874.
- Malenka RC, Bear MF (2004) LTP and LTD: an embarrassment of riches. *Neuron* 44:5-21.
- Malenka RC, Kauer JA, Perkel DJ, Mauk MD, Kelly PT, Nicoll RA, Waxham MN (1989) An essential role for postsynaptic calmodulin and protein kinase activity in long-term potentiation. *Nature* 340:554-557.
- Malinow R, Schulman H, Tsien RW (1989) Inhibition of postsynaptic PKC or CaMKII blocks induction but not expression of LTP. *Science* 245:862-866.
- Mammen AL, Kameyama K, Roche KW, Huganir RL (1997) Phosphorylation of the alpha-amino-3-hydroxy-5-methylisoxazole-4-propionic acid receptor GluR1 subunit by calcium/calmodulin-dependent kinase II. *J Biol Chem* 272:32528-32533.
- Mank M, Reiff DF, Heim N, Friedrich MW, Borst A, Griesbeck O (2006) A FRET-based calcium biosensor with fast signal kinetics and high fluorescence change. *Biophys J* 90:1790-1796.
- Manuel GC, Reynoso R, Gee L, Salgado LM, Bode HR (2006) PI3K and ERK 1-2 regulate early stages during head regeneration in hydra. *Dev Growth Differ* 48:129-138.
- Marin EC, Jefferis GS, Komiyama T, Zhu H, Luo L (2002) Representation of the glomerular olfactory map in the *Drosophila* brain. *Cell* 109:243-255.

- Matsuzaki M, Honkura N, Ellis-Davies GC, Kasai H (2004) Structural basis of long-term potentiation in single dendritic spines. *Nature* 429:761-766.
- Matthews RP, Guthrie CR, Wailes LM, Zhao X, Means AR, McKnight GS (1994) Calcium/calmodulin-dependent protein kinase types II and IV differentially regulate CREB-dependent gene expression. *Mol Cell Biol* 14:6107-6116.
- Mayr B, Montminy M (2001) Transcriptional regulation by the phosphorylation-dependent factor CREB. *Nat Rev Mol Cell Biol* 2:599-609.
- McGuire SE, Le PT, Davis RL (2001) The role of *Drosophila* mushroom body signaling in olfactory memory. *Science* 293:1330-1333.
- McGuire SE, Le PT, Osborn AJ, Matsumoto K, Davis RL (2003) Spatiotemporal rescue of memory dysfunction in *Drosophila*. *Science* 302:1765-1768.
- McLaughlin SK, Collis P, Hermonat PL, Muzyczka N (1988) Adeno-associated virus general transduction vectors: analysis of proviral structures. *J Virol* 62:1963-1973.
- Mendelson E, Trempe JP, Carter BJ (1986) Identification of the trans-acting Rep proteins of adeno-associated virus by antibodies to a synthetic oligopeptide. *J Virol* 60:823-832.
- Miller DJ, Ball EE, Technau U (2005) Cnidarians and ancestral genetic complexity in the animal kingdom. *Trends Genet* 21:536-539.
- Minta A, Tsien RY (1989) Fluorescent indicators for cytosolic sodium. *J Biol Chem* 264:19449-19457.
- Miyawaki A, Griesbeck O, Heim R, Tsien RY (1999) Dynamic and quantitative Ca²⁺ measurements using improved cameleons. *Proc Natl Acad Sci U S A* 96:2135-2140.
- Miyawaki A, Llopis J, Heim R, McCaffery JM, Adams JA, Ikura M, Tsien RY (1997) Fluorescent indicators for Ca²⁺ based on green fluorescent proteins and calmodulin. *Nature* 388:882-887.
- Mizuno H, Sawano A, Eli P, Hama H, Miyawaki A (2001) Red fluorescent protein from *Discosoma* as a fusion tag and a partner for fluorescence resonance energy transfer. *Biochemistry* 40:2502-2510.

- Mori M, Konno T, Ozawa T, Murata M, Imoto K, Nagayama K (2000) Novel interaction of the voltage-dependent sodium channel (VDSC) with calmodulin: does VDSC acquire calmodulin-mediated Ca²⁺-sensitivity? *Biochemistry* 39:1316-1323.
- Morris RG, Anderson E, Lynch GS, Baudry M (1986) Selective impairment of learning and blockade of long-term potentiation by an N-methyl-D-aspartate receptor antagonist, AP5. *Nature* 319:774-776.
- Muller WA (1996) Pattern formation in the immortal Hydra. *Trends Genet* 12:91-96.
- Muller-Taubenberger A, Vos MJ, Bottger A, Lasi M, Lai FP, Fischer M, Rottner K (2006) Monomeric red fluorescent protein variants used for imaging studies in different species. *Eur J Cell Biol* 85:1119-1129.
- Muralidhar S, Becerra SP, Rose JA (1994) Site-directed mutagenesis of adeno-associated virus type 2 structural protein initiation codons: effects on regulation of synthesis and biological activity. *J Virol* 68:170-176.
- Nagai T, Sawano A, Park ES, Miyawaki A (2001) Circularly permuted green fluorescent proteins engineered to sense Ca²⁺. *Proc Natl Acad Sci U S A* 98:3197-3202.
- Nagai T, Yamada S, Tominaga T, Ichikawa M, Miyawaki A (2004) Expanded dynamic range of fluorescent indicators for Ca(2+) by circularly permuted yellow fluorescent proteins. *Proc Natl Acad Sci U S A* 101:10554-10559.
- Nagai T, Ibata K, Park ES, Kubota M, Mikoshiba K, Miyawaki A (2002) A variant of yellow fluorescent protein with fast and efficient maturation for cell-biological applications. *Nat Biotechnol* 20:87-90.
- Nakai J, Ohkura M, Imoto K (2001) A high signal-to-noise Ca(2+) probe composed of a single green fluorescent protein. *Nat Biotechnol* 19:137-141.
- Neves G, Cooke SF, Bliss TV (2008) Synaptic plasticity, memory and the hippocampus: a neural network approach to causality. *Nat Rev Neurosci* 9:65-75.
- Nicoll RA, Malenka RC (1999) Expression mechanisms underlying NMDA receptor-dependent long-term potentiation. *Ann N Y Acad Sci* 868:515-525.
- O'Keefe J, Dostrovsky J (1971) The hippocampus as a spatial map. Preliminary evidence from unit activity in the freely-moving rat. *Brain Res* 34:171-175.

- Ohkura M, Matsuzaki M, Kasai H, Imoto K, Nakai J (2005) Genetically encoded bright Ca²⁺ probe applicable for dynamic Ca²⁺ imaging of dendritic spines. *Anal Chem* 77:5861-5869.
- Opie SR, Warrington KH, Jr., Agbandje-McKenna M, Zolotukhin S, Muzyczka N (2003) Identification of amino acid residues in the capsid proteins of adeno-associated virus type 2 that contribute to heparan sulfate proteoglycan binding. *J Virol* 77:6995-7006.
- Ouyang Y, Kantor D, Harris KM, Schuman EM, Kennedy MB (1997) Visualization of the distribution of autophosphorylated calcium/calmodulin-dependent protein kinase II after tetanic stimulation in the CA1 area of the hippocampus. *J Neurosci* 17:5416-5427.
- Palmer AE, Giacomello M, Kortemme T, Hires SA, Lev-Ram V, Baker D, Tsien RY (2006) Ca²⁺ indicators based on computationally redesigned calmodulin-peptide pairs. *Chem Biol* 13:521-530.
- Papadia S, Stevenson P, Hardingham NR, Bading H, Hardingham GE (2005) Nuclear Ca²⁺ and the cAMP response element-binding protein family mediate a late phase of activity-dependent neuroprotection. *J Neurosci* 25:4279-4287.
- Pascalis O, Bachevalier J (1999) Neonatal aspiration lesions of the hippocampal formation impair visual recognition memory when assessed by paired-comparison task but not by delayed nonmatching-to-sample task. *Hippocampus* 9:609-616.
- Pauly B, Lasi M, MacKintosh C, Morrice N, Imhof A, Regula J, Rudd S, David CN, Bottger A (2007) Proteomic screen in the simple metazoan Hydra identifies 14-3-3 binding proteins implicated in cellular metabolism, cytoskeletal organisation and Ca²⁺ signalling. *BMC Cell Biol* 8:31.
- Pokorska A, Vanhoutte P, Arnold FJ, Silvagno F, Hardingham GE, Bading H (2003) Synaptic activity induces signalling to CREB without increasing global levels of cAMP in hippocampal neurons. *J Neurochem* 84:447-452.
- Pologruto TA, Yasuda R, Svoboda K (2004) Monitoring neural activity and [Ca²⁺] with genetically encoded Ca²⁺ indicators. *J Neurosci* 24:9572-9579.

- Qing K, Mah C, Hansen J, Zhou S, Dwarki V, Srivastava A (1999) Human fibroblast growth factor receptor 1 is a co-receptor for infection by adeno-associated virus 2. *Nat Med* 5:71-77.
- Quinn WG, Sziber PP, Booker R (1979) The *Drosophila* memory mutant amnesiac. *Nature* 277:212-214.
- Rabinowitz JE, Samulski RJ (2000) Building a better vector: the manipulation of AAV virions. *Virology* 278:301-308.
- Raymond CR, Redman SJ (2006) Spatial segregation of neuronal calcium signals encodes different forms of LTP in rat hippocampus. *J Physiol* 570:97-111.
- Reiff DF, Ihring A, Guerrero G, Isacoff EY, Joesch M, Nakai J, Borst A (2005) In vivo performance of genetically encoded indicators of neural activity in flies. *J Neurosci* 25:4766-4778.
- Rhoads AR, Friedberg F (1997) Sequence motifs for calmodulin recognition. *Faseb J* 11:331-340.
- Richardson WD, Westphal H (1984) Requirement for either early region 1a or early region 1b adenovirus gene products in the helper effect for adeno-associated virus. *J Virol* 51:404-410.
- Riemensperger T, Voller T, Stock P, Buchner E, Fiala A (2005) Punishment prediction by dopaminergic neurons in *Drosophila*. *Curr Biol* 15:1953-1960.
- Romoser VA, Hinkle PM, Persechini A (1997) Detection in living cells of Ca²⁺-dependent changes in the fluorescence emission of an indicator composed of two green fluorescent protein variants linked by a calmodulin-binding sequence. A new class of fluorescent indicators. *J Biol Chem* 272:13270-13274.
- Rose GM, Dunwiddie TV (1986) Induction of hippocampal long-term potentiation using physiologically patterned stimulation. *Neurosci Lett* 69:244-248.
- Rosenmund C, Stern-Bach Y, Stevens CF (1998) The tetrameric structure of a glutamate receptor channel. *Science* 280:1596-1599.
- Rustom A, Saffrich R, Markovic I, Walther P, Gerdes HH (2004) Nanotubular highways for intercellular organelle transport. *Science* 303:1007-1010.

- Samulski RJ, Chang LS, Shenk T (1989) Helper-free stocks of recombinant adeno-associated viruses: normal integration does not require viral gene expression. *J Virol* 63:3822-3828.
- Sanlioglu S, Benson PK, Yang J, Atkinson EM, Reynolds T, Engelhardt JF (2000) Endocytosis and nuclear trafficking of adeno-associated virus type 2 are controlled by rac1 and phosphatidylinositol-3 kinase activation. *J Virol* 74:9184-9196.
- Sarras MP, Jr., Deutzmann R (2001) Hydra and Niccolo Paganini (1782-1840)--two peas in a pod? The molecular basis of extracellular matrix structure in the invertebrate, Hydra. *Bioessays* 23:716-724.
- Sarras MP, Jr., Yan L, Leontovich A, Zhang JS (2002) Structure, expression, and developmental function of early divergent forms of metalloproteinases in hydra. *Cell Res* 12:163-176.
- Schlüter, J (2008) Ca²⁺ signalling in *H. vulgaris*. Diploma Thesis
- Schnell E, Sizemore M, Karimzadegan S, Chen L, Brecht DS, Nicoll RA (2002) Direct interactions between PSD-95 and stargazin control synaptic AMPA receptor number. *Proc Natl Acad Sci U S A* 99:13902-13907.
- Schwaerzel M, Heisenberg M, Zars T (2002) Extinction antagonizes olfactory memory at the subcellular level. *Neuron* 35:951-960.
- Segal M, Murphy DD (1998) CREB activation mediates plasticity in cultured hippocampal neurons. *Neural Plast* 6:1-7.
- Seymour-Laurent KJ, Barish ME (1995) Inositol 1,4,5-trisphosphate and ryanodine receptor distributions and patterns of acetylcholine- and caffeine-induced calcium release in cultured mouse hippocampal neurons. *J Neurosci* 15:2592-2608.
- Shaner NC, Campbell RE, Steinbach PA, Giepmans BN, Palmer AE, Tsien RY (2004) Improved monomeric red, orange and yellow fluorescent proteins derived from *Discosoma* sp. red fluorescent protein. *Nat Biotechnol* 22:1567-1572.
- Shang Y, Claridge-Chang A, Sjulson L, Pypaert M, Miesenböck G (2007) Excitatory local circuits and their implications for olfactory processing in the fly antennal lobe. *Cell* 128:601-612.

- Sheng M, Thompson MA, Greenberg ME (1991) CREB: a Ca(2+)-regulated transcription factor phosphorylated by calmodulin-dependent kinases. *Science* 252:1427-1430.
- Sheng M, Dougan ST, McFadden G, Greenberg ME (1988) Calcium and growth factor pathways of c-fos transcriptional activation require distinct upstream regulatory sequences. *Mol Cell Biol* 8:2787-2796.
- Shimizu H, Zhang X, Zhang J, Leontovich A, Fei K, Yan L, Sarras MP, Jr. (2002) Epithelial morphogenesis in hydra requires de novo expression of extracellular matrix components and matrix metalloproteinases. *Development* 129:1521-1532.
- Shimozono S, Fukano T, Kimura KD, Mori I, Kirino Y, Miyawaki A (2004) Slow Ca²⁺ dynamics in pharyngeal muscles in *Caenorhabditis elegans* during fast pumping. *EMBO Rep* 5:521-526.
- Siegmund T, Korge G (2001) Innervation of the ring gland of *Drosophila melanogaster*. *J Comp Neurol* 431:481-491.
- Sigrist SJ, Thiel PR, Reiff DF, Lachance PE, Lasko P, Schuster CM (2000) Postsynaptic translation affects the efficacy and morphology of neuromuscular junctions. *Nature* 405:1062-1065.
- Skoulakis EM, Kalderon D, Davis RL (1993) Preferential expression in mushroom bodies of the catalytic subunit of protein kinase A and its role in learning and memory. *Neuron* 11:197-208.
- Srivastava A, Lusby EW, Berns KI (1983) Nucleotide sequence and organization of the adeno-associated virus 2 genome. *J Virol* 45:555-564.
- Steele RE (2002) Developmental signaling in Hydra: what does it take to build a "simple" animal? *Dev Biol* 248:199-219.
- Stewart BA, Atwood HL, Renger JJ, Wang J, Wu CF (1994) Improved stability of *Drosophila* larval neuromuscular preparations in haemolymph-like physiological solutions. *J Comp Physiol [A]* 175:179-191.
- Stocker RF, Heimbeck G, Gendre N, de Belle JS (1997) Neuroblast ablation in *Drosophila* P[GAL4] lines reveals origins of olfactory interneurons. *J Neurobiol* 32:443-456.
- Stopfer M, Laurent G (1999) Short-term memory in olfactory network dynamics. *Nature* 402:664-668.

- Stoppini L, Buchs PA, Muller D (1991) A simple method for organotypic cultures of nervous tissue. *J Neurosci Methods* 37:173-182.
- Summerford C, Samulski RJ (1998) Membrane-associated heparan sulfate proteoglycan is a receptor for adeno-associated virus type 2 virions. *J Virol* 72:1438-1445.
- Summerford C, Bartlett JS, Samulski RJ (1999) AlphaVbeta5 integrin: a co-receptor for adeno-associated virus type 2 infection. *Nat Med* 5:78-82.
- Sun P, Enslen H, Myung PS, Maurer RA (1994) Differential activation of CREB by Ca²⁺/calmodulin-dependent protein kinases type II and type IV involves phosphorylation of a site that negatively regulates activity. *Genes Dev* 8:2527-2539.
- Takahashi A, Camacho P, Lechleiter JD, Herman B (1999) Measurement of intracellular calcium. *Physiol Rev* 79:1089-1125.
- Tallini YN, Ohkura M, Choi BR, Ji G, Imoto K, Doran R, Lee J, Plan P, Wilson J, Xin HB, Sanbe A, Gulick J, Mathai J, Robbins J, Salama G, Nakai J, Kotlikoff MI (2006) Imaging cellular signals in the heart in vivo: Cardiac expression of the high-signal Ca²⁺ indicator GCaMP2. *Proc Natl Acad Sci U S A* 103:4753-4758.
- Technau U, Cramer von Laue C, Rentzsch F, Luft S, Hobmayer B, Bode HR, Holstein TW (2000) Parameters of self-organization in Hydra aggregates. *Proc Natl Acad Sci U S A* 97:12127-12131.
- Tempel BL, Livingstone MS, Quinn WG (1984) Mutations in the dopa decarboxylase gene affect learning in *Drosophila*. *Proc Natl Acad Sci U S A* 81:3577-3581.
- Tramier M, Zahid M, Mevel JC, Masse MJ, Coppey-Moisan M (2006) Sensitivity of CFP/YFP and GFP/mCherry pairs to donor photobleaching on FRET determination by fluorescence lifetime imaging microscopy in living cells. *Microsc Res Tech* 69:933-939.
- Tratschin JD, Miller IL, Carter BJ (1984) Genetic analysis of adeno-associated virus: properties of deletion mutants constructed in vitro and evidence for an adeno-associated virus replication function. *J Virol* 51:611-619.
- Trempe JP, Carter BJ (1988) Alternate mRNA splicing is required for synthesis of adeno-associated virus VP1 capsid protein. *J Virol* 62:3356-3363.

- Trempe JP, Mendelson E, Carter BJ (1987) Characterization of adeno-associated virus rep proteins in human cells by antibodies raised against rep expressed in *Escherichia coli*. *Virology* 161:18-28.
- Tsien RY (1998) The green fluorescent protein. *Annu Rev Biochem* 67:509-544.
- Tully T, Quinn WG (1985) Classical conditioning and retention in normal and mutant *Drosophila melanogaster*. *J Comp Physiol [A]* 157:263-277.
- Tully T, Preat T, Boynton SC, Del Vecchio M (1994) Genetic dissection of consolidated memory in *Drosophila*. *Cell* 79:35-47.
- Vosshall LB, Wong AM, Axel R (2000) An olfactory sensory map in the fly brain. *Cell* 102:147-159.
- Waddell S, Quinn WG (2001) What can we teach *Drosophila*? What can they teach us? *Trends Genet* 17:719-726.
- Waddell S, Armstrong JD, Kitamoto T, Kaiser K, Quinn WG (2000) The amnesiac gene product is expressed in two neurons in the *Drosophila* brain that are critical for memory. *Cell* 103:805-813.
- Wang J, Campos B, Jamieson GA, Jr., Kaetzel MA, Dedman JR (1995) Functional elimination of calmodulin within the nucleus by targeted expression of an inhibitor peptide. *J Biol Chem* 270:30245-30248.
- Wang J, Moreira KM, Campos B, Kaetzel MA, Dedman JR (1996) Targeted neutralization of calmodulin in the nucleus blocks DNA synthesis and cell cycle progression. *Biochim Biophys Acta* 1313:223-228.
- Wang JW, Wong AM, Flores J, Vosshall LB, Axel R (2003) Two-photon calcium imaging reveals an odor-evoked map of activity in the fly brain. *Cell* 112:271-282.
- Wang Y, Guo HF, Pologruto TA, Hannan F, Hakker I, Svoboda K, Zhong Y (2004) Stereotyped odor-evoked activity in the mushroom body of *Drosophila* revealed by green fluorescent protein-based Ca^{2+} imaging. *J Neurosci* 24:6507-6514.
- Weislogel, JM (2003) Calcium imaging using recombinant Ca^{2+} probes in primary hippocampal neurons. Diploma Thesis

- Weitzman MD, Kyostio SR, Kotin RM, Owens RA (1994) Adeno-associated virus (AAV) Rep proteins mediate complex formation between AAV DNA and its integration site in human DNA. *Proc Natl Acad Sci U S A* 91:5808-5812.
- Westfall IA (1996) Ultrastructure of synapses in the first-evolved nervous systems. *J Neurocytol* 25:735-746.
- Wilson RI, Laurent G (2005) Role of GABAergic inhibition in shaping odor-evoked spatiotemporal patterns in the *Drosophila* antennal lobe. *J Neurosci* 25:9069-9079.
- Wittlieb J, Khalturin K, Lohmann JU, Anton-Erxleben F, Bosch TC (2006) Transgenic Hydra allow in vivo tracking of individual stem cells during morphogenesis. *Proc Natl Acad Sci U S A* 103:6208-6211.
- Wong AM, Wang JW, Axel R (2002) Spatial representation of the glomerular map in the *Drosophila* protocerebrum. *Cell* 109:229-241.
- Wu CL, Xia S, Fu TF, Wang H, Chen YH, Leong D, Chiang AS, Tully T (2007) Specific requirement of NMDA receptors for long-term memory consolidation in *Drosophila* ellipsoid body. *Nat Neurosci*.
- Wu Z, Asokan A, Samulski RJ (2006) Adeno-associated virus serotypes: vector toolkit for human gene therapy. *Mol Ther* 14:316-327.
- Xia S, Miyashita T, Fu TF, Lin WY, Wu CL, Pyzocha L, Lin IR, Saitoe M, Tully T, Chiang AS (2005) NMDA receptors mediate olfactory learning and memory in *Drosophila*. *Curr Biol* 15:603-615.
- Xiao W, Warrington KH, Jr., Hearing P, Hughes J, Muzyczka N (2002) Adenovirus-facilitated nuclear translocation of adeno-associated virus type 2. *J Virol* 76:11505-11517.
- Xiao W, Chirmule N, Berta SC, McCullough B, Gao G, Wilson JM (1999) Gene therapy vectors based on adeno-associated virus type 1. *J Virol* 73:3994-4003.
- Xing J, Ginty DD, Greenberg ME (1996) Coupling of the RAS-MAPK pathway to gene activation by RSK2, a growth factor-regulated CREB kinase. *Science* 273:959-963.
- Xu R, Janson CG, Mastakov M, Lawlor P, Young D, Mouravlev A, Fitzsimons H, Choi KL, Ma H, Dragunow M, Leone P, Chen Q, Dicker B, During MJ (2001)

- Quantitative comparison of expression with adeno-associated virus (AAV-2) brain-specific gene cassettes. *Gene Ther* 8:1323-1332.
- Yin JC, Tully T (1996) CREB and the formation of long-term memory. *Curr Opin Neurobiol* 6:264-268.
- Yin JC, Del Vecchio M, Zhou H, Tully T (1995) CREB as a memory modulator: induced expression of a dCREB2 activator isoform enhances long-term memory in *Drosophila*. *Cell* 81:107-115.
- Yin JC, Wallach JS, Del Vecchio M, Wilder EL, Zhou H, Quinn WG, Tully T (1994) Induction of a dominant negative CREB transgene specifically blocks long-term memory in *Drosophila*. *Cell* 79:49-58.
- Yu D, Ponomarev A, Davis RL (2004) Altered representation of the spatial code for odors after olfactory classical conditioning; memory trace formation by synaptic recruitment. *Neuron* 42:437-449.
- Yu D, Keene AC, Srivatsan A, Waddell S, Davis RL (2005) *Drosophila* DPM neurons form a delayed and branch-specific memory trace after olfactory classical conditioning. *Cell* 123:945-957.
- Yuste R, Bonhoeffer T (2001) Morphological changes in dendritic spines associated with long-term synaptic plasticity. *Annu Rev Neurosci* 24:1071-1089.
- Zacharias DA, Violin JD, Newton AC, Tsien RY (2002) Partitioning of lipid-modified monomeric GFPs into membrane microdomains of live cells. *Science* 296:913-916.
- Zhang SJ, Steijaert MN, Lau D, Schutz G, Delucinge-Vivier C, Descombes P, Bading H (2007) Decoding NMDA Receptor Signaling: Identification of Genomic Programs Specifying Neuronal Survival and Death. *Neuron* 53:549-562.
- Zhou X, Muzyczka N (1998) In vitro packaging of adeno-associated virus DNA. *J Virol* 72:3241-3247.
- Zola SM, Squire LR, Teng E, Stefanacci L, Buffalo EA, Clark RE (2000) Impaired recognition memory in monkeys after damage limited to the hippocampal region. *J Neurosci* 20:451-463.